UNIVERSITY OF OKLAHOMA
GRADUATE COLLEGE

TROPICAL CLIMATE STABILITY, HADLEY CIRCULATION, AND DEEP CUMULUS CONVECTION: VITAL SYNERGISM ON A WET PLANET

A Dissertation
SUBMITTED TO THE GRADUATE FACULTY
in partial fulfillment of the requirements for the
degree of
Doctor of Philosophy

By
LUCIANO FLEISCHFRESSER
Norman, Oklahoma
2000

UMI Number: 9975794

Bell & Howell Information and Learning Company
300 North Zeeb Road
P.O. Box 1346
Ann Arbor, MI 48106-1346

TROPICAL CLIMATE STABILITY, HADLEY CIRCULATION, AND DEEP CUMULUS CONVECTION: VITAL SYNERGISM ON A WET PLANET

A Dissertation APPROVED FOR THE
SCHOOL OF METEOROLOGY

By

Brian Fiedler

[illegible]

Susan Postawko

[illegible]

Dedication

To the memory of my maternal grandfather, Antonio Paulino, and to the memory of my father-in-law, Ernesto Taborda. These men, in their own ways, were examples of how to live a truly free life while contributing to society.

Acknowledgements

Many thanks go to Dr. Susan Postawko for being supportive during the most critical part of my student career. Not only she funded me during the last three months, but also she listened to my concerns and provided expert academic advice during the past year or so. She was the first person who emphasized that my results are better viewed as bounds for the results of more complex models and/or observations. Such remark significantly helped me in writing up this dissertation in a more intelligible way.

There have been a lot of great people that, in one way or another, have helped me throughout my studies at the University of Oklahoma. I'd like to acknowledge the current (well, not anymore) staff of the School of Meteorology — Ginger Hunt, Marcia Pallutto, Celia Jones and Nancy Agrawal — for their help with clerical matters and many other ways that no one would understand if I tried to explain. A little further away, in the Oklahoma Memorial Union, Mrs. Olga Baumgardner has been key with all those little things that only "aliens" must worry about. Faculty in the College of Geosciences that I am especially grateful include the following: Dr. Joshua Wurman, for reducing my financial debt while providing an experience of a lifetime with the operation of the "Doppler on Wheels" in Alaska and Utah; Dr. Bill Beasley, who, when director of the SoM, got to know about my weaknesses, and he was still willing to hear me during certain difficult times; Dr. David Deming, the external member of my committee, who helped me put my feet on the ground, and walk one step at a time; Dr. Mark Reeder, the original external member of my committee, a pure mathematician who once said that Physics, for him, was only a manifestation of mathematical principles. That statement had an influence on me, but I don't agree completely with it: for me, Physics can be more than a manifestation of mathematical principles. But I am convinced that the Physics represented in numerical models of natural systems (atmosphere, oceans, etc.) is nothing more that a manifestation of such principles. This modified conviction has been formed with the influence of Dr. Brian Fiedler, the chair of my doctoral committee, with whom I had invaluable exchanges. He also funded me for about a year, for which I am very grateful, and he gave me the opportunity to teach in one of his classes, another very important experience. The use of the NCAR radiation schemes was his suggestion, and the incorporation of another deep cumulus parameterization, his demand. I also won't forget his short e-mails giving me references on my research topic during the past few months, when I was trying to find something to keep me busy. He, as I understand it, was attempting to show some compassion. At last but not least, for all my computing needs during the past years, the help and professionalism of Tom Condo, Tim Kwiatkowski, Courtney Garrison and Mark Laufersweiler are greatly appreciated. I think there are more people that should be acknowledged here as being helpful in one way or another, but I don't know who they are, or I may have forgotten. For those, please accept my empathy and thanks.

Outside Oklahoma I am specially thankful to Dr. Arthur Hou, my mentor during a summer internship at NASA Goddard Space Flight Center. He kindly gave me access to some still to be published research (at that time) that helped me in forming the backbone of this work. Back in Brazil, the financial support provided by CAPES, a sponsoring agency from the Brazilian government, is also greatly acknowledged.

On a personal level, I am very thankful to my parents, Marcos Germano and Maria Isabel, for being just who they are. Marin and Jan Ceballo provided sympathy, friendship and great barbecue dinners for me and my family for as long as I can remember we've been in Norman. Finally, Joséli de Cássia and Christopher, wife and son, should be the ones to be awarded a degree. They are the only human beings who really know what this has been about...

Contents

List Of Tables

List Of Figures

Abstract

This research is about developing a more internally consistent formulation of cumulus convection and the atmospheric branch of the hydrological cycle in a newly developed Hadley circulation model. The ultimate goal is to analyze the climate equilibrium of a symmetric tropical hydrostatic atmosphere, particularly studying cause and effect relations determining the magnitude of water vapor-related feedbacks in climate sensitivity experiments.

Important features of the proposed formulation for precipitating deep turbulent clouds include the ability to calculate precipitation efficiencies, a new postulation relating cumulus buoyancy to solar radiation, and the implicit account of latent heat release that manifest itself by scaling cumulus drafts to observed magnitudes. The Hadley model is based on primitive equations, and it incorporates the NCAR column radiation scheme. To calculate climatic feedbacks, the inverse simulation approach is used. An interrelationship technique is applied to diagnose feedback factors associated with changes of water vapor amount and distribution, of lapse-rate, and of deep cumulus cloud cover. The aim is to contrast the novel model for deep clouds with a mass flux deep cumulus parameterization when a thermally direct circulation (Hadley cell) is present.

When only a lapse-rate adjustment is used to crudely represent tropical convection, the calculated climate sensitivity lies in the typical range of equatorial sensitivities given by global circulation models (GCMs). This result suggests that the Hadley model is capturing the essential physics of these models as far as these sensitivities are concerned. In the comparison analyses, the climate equilibrium is stable and effected by net positive feedback when the new cumulus model is used. Moreover, the calculated tropical climate sensitivities are consistently lower than the aforementioned typical range, bringing them closer to sensitivities suggested by observed data. Interestingly, the tropical climate equilibrium is unstable with the mass flux scheme. It is shown quantitatively that relative humidity changes in the model upper-troposphere determine the sign of the water vapor feedback. Recommendations to narrow humidity uncertainties in climate change simulations are presented.

Chapter 1

Introduction

1.1 The Problem

To the extent that different climate regimes are associated with the meridional thermal contrast between equatorial and polar regions, symmetric models of the atmosphere become relevant tools for climate change studies. In this context, at least two major regions associated with distinct general circulation patterns should be identified: the tropics, where the relevant dynamical heat transport mechanism is associated with the Hadley cell; and the extra-tropics, where baroclinic eddies are responsible for transporting the surplus of energy from equatorial to polar regions. Figure 1.1 schematically depicts such regions. The energy budget of the axisymmetric tropical region needs to account for the imbalance of short and longwave radiation at the top of its atmosphere, and for the above-mentioned meridional heat fluxes, as shown in figure 1.2. In this study, however, the later cannot be explicitly calculated since lateral boundaries with no flux conditions are required to satisfy the conservation laws forming the basis of the Hadley circulation model. This is not to say that, in the symmetric context under consideration here, the Hadley cell is not strictly observed since averaging with respect to seasons and longitudes is required to produce it. Thus, limitations are imposed on the comparability of the modeled tropical atmospheric structure and the observed one. On the other hand, a sensitivity analyses can be accomplished, if one keeps in mind that what can be obtained from the axisymmetric model is a *bound* for the tropical climate sensitivity. It will be argued in a later chapter that, in the context of an equilibrium analyses, such will be a lower bound for the equatorial sensitivity that can be calculated from GCMs in a "warmer" equilibrium response.

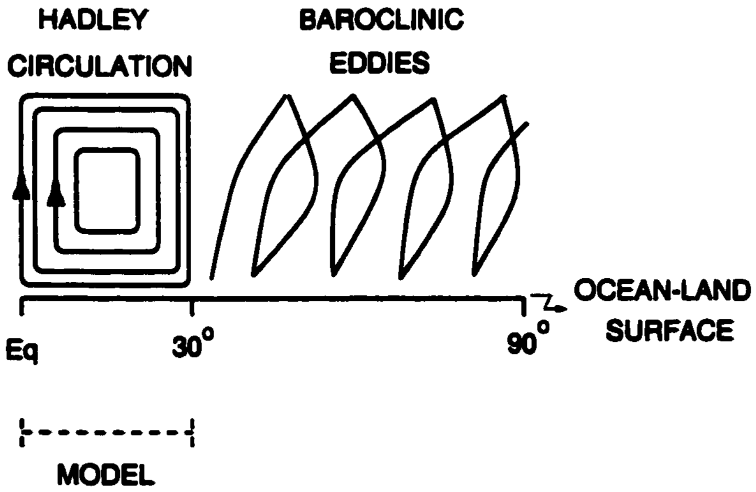

Figure 1.1: Conceptual idealization of axisymmetric tropospheric motions.

So far, the bulk of observational analyses aiming at this issue can only address tropical sensitivities that are associated with time-scales ranging from weeks to a few years [Soden and Fu (1995), Sun and Held (1996), Yang and Tung (1998)]. Such sensitivities, as noted in Lindzen (1997), are primarily

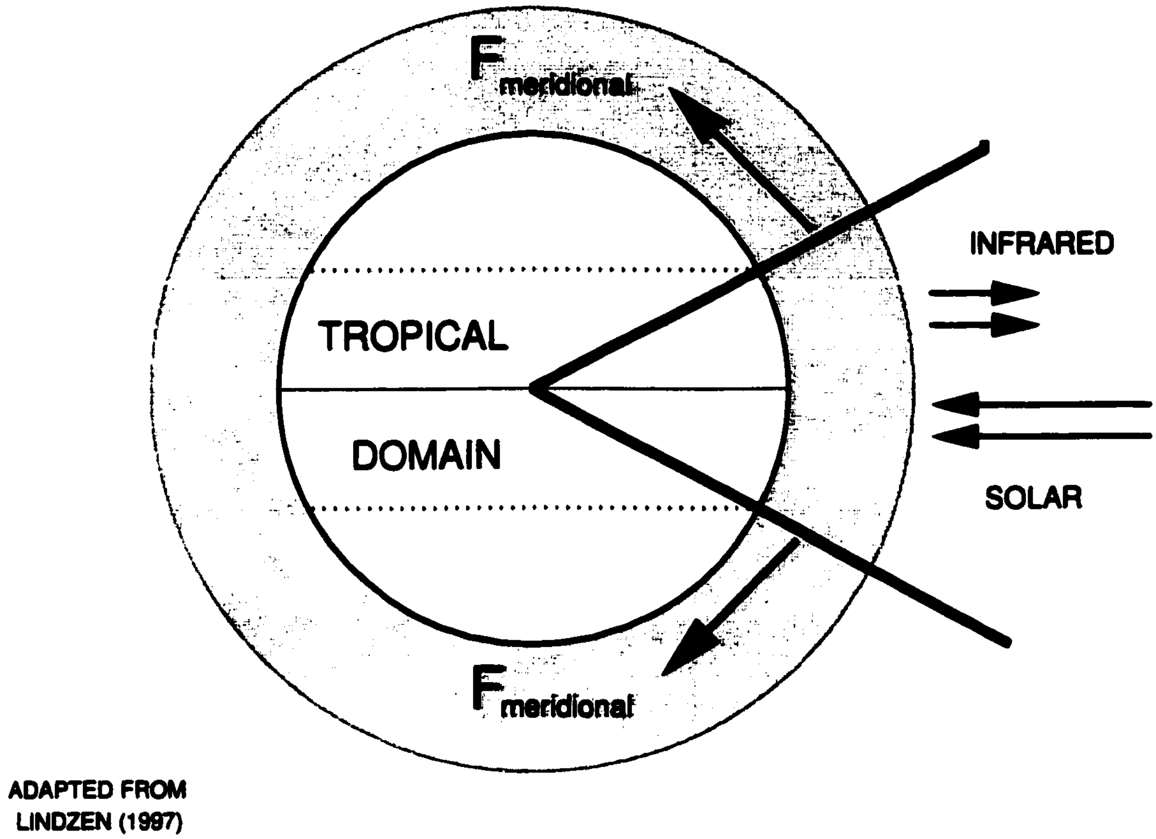

Figure 1.2: Schematic depiction of tropical energy budget.

related to the rearrangement of regional climatic patterns, but they are not necessarily relevant to different climatic regimes of the sort associated with distinct temperature gradients between the equator and the poles. Paleoclimate data are more appealing in this regard, and they have indicated a certain degree of stability for the tropics [Lindzen (1994)]. That is, it appears that the tropical climate sensitivity is smaller than the climate sensitivity of the extra-tropics — a result that has also been suggested by low order models [Held (1978), Lindzen et al. (1982)].

The reasoning for such equatorial stability inevitably leads one to consider compensative effects that must be operating in this region. On one hand, the Hadley cell appears as the major dynamical mechanism for reducing any meridional thermal contrast that would exist in its absence. In addition, the possibility of negative feedbacks arises as another cause for maintaining such tropical stability. The later brings water vapor to the forefront of scientific speculations, since it is the most important greenhouse gas in the earth's atmosphere. In this connection, it is interesting to note that the understanding of what actually constitutes the water vapor feedback has only recently being established. Figure 1.3 illustrates this point. Concentrating in the region from 30° S to 30° N, this figure shows very narrow moist regions in the upper-troposphere associated with deep cumulus towers surrounded by broad expanses of dry air over the sub-tropical oceans. Thus, the climatic feedback due to water vapor depends on how the moist/dry areas in the upper-tropical troposphere change relatively one to another, and on the degree of moistening/drying of these regions [Sinha and Allen (1994), Pierrehumbert (1995)]. Suppose that a positive tropical mean SST perturbation results in drier sub-tropical air and broader dry regions in an equilibrium response. One can intuitively argue that such behavior would imply a negative feedback due to water vapor. The reason is that drier sub-tropical air and broader dry regions would result in more infrared cooling to compensate for the imposed warming at the surface. The reverse situation would then imply a positive water vapor feedback. As suggested earlier, the transient behavior of such mechanism has been actively investigated from the observational standpoint. But there is no guarantee that the assertion of this feedback with seasonal datasets, for example, will imply the same result in a different climatic regime, as apparently is the belief of Goody et al. (1998). Moreover, it seems to be common sense that paleoclimate data — a natural choice to bound the *equilibrium* climate feedback — is not reliable to estimate global patterns yet. Wigley et al. (1997) have also stated that global, near-surface temperature data sets are still not accurate enough to narrow the uncertainty range in the climate sensitivity below that estimated from climate models. As a consequence, the numerical approach is currently the best way in estimating the *equilibrium* tropical climate sensitivity.

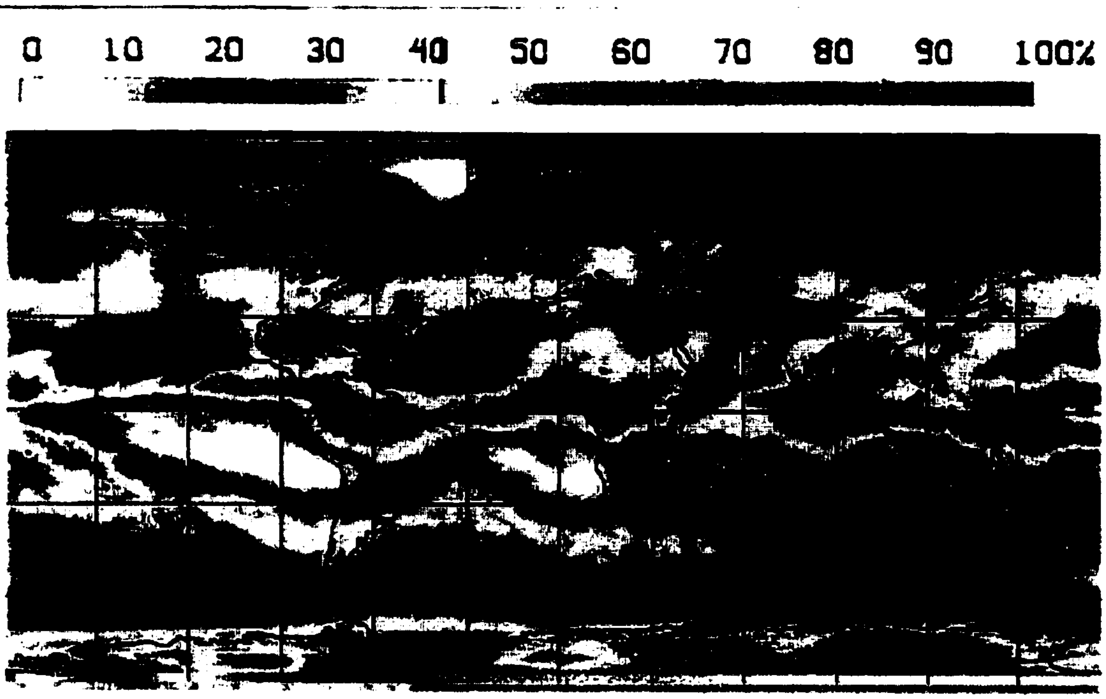

Figure 1.3: Relative humidities in the layer 500 - 300 mb derived from 183 GHz soundings from SSM/T-2 averaged over all of May 1995. The color scale for relative humidity is shown above the figure. Panel provided by Dr. Arthur Hou, NASA/Greenbelt (personal communication).

General circulation models have produced no apparent distinction between tropical and extra-tropical climate sensitivities. In addition, the water vapor feedback in such models is positive and the most dominant, largely determining the equilibrium temperature response associated with radiative perturbations. It has been argued that the quantification of tropical upper-tropospheric water vapor is the major problem producing the above-mentioned results — being apparently in disagreement with current observations. The relevant process in this discussion is the upper-level moistening by cumulus towers, which puts emphasis on the parameterization of tropical deep cumulus convection [Spencer and Braswell (1997)]. Given these apparent discrepancies between models and observations, it becomes relevant to study cause and effect relations that are connected with the models' limitations. These analyses are better accomplished with low order models that isolate the relevant physical processes under consideration.

In this study, the analysis of a Hadley circulation model that largely reproduces the equilibrium equatorial climate sensitivity and tropical water vapor feedback calculated by GCMs is proposed to identify cause and effect relationships. It is the aim of this research to incorporate a more internally consistent treatment of water vapor and tropical deep cumulus convection than is currently done in global models. Moreover, the dependence of outgoing infrared fluxes on water vapor is accounted for in the Hadley model by the inclusion of an explicit hydrological cycle and the NCAR column radiation scheme [Kiehl et al. (1996)]. Thus, some of the most important physical processes responsible for the alleged tropical climate stability are taken into account in this model. It is hoped that this investigation will point directions and implications for the improvement of GCMs.

In conclusion, the notion of equilibrium should be clarified. It generally refers to the response of a system due to some perturbation over an infinite time-scale. Another way of viewing the notion of equilibrium is depicted in figure 1.4, adapted from Lewis and Prinn (1984). The equilibrium concept, which is somewhat distinct from the steady-state one, has to do with variables that are time invariant without gradients or fluxes maintaining such invariance. Thus, in the context of the Hadley model, *equilibrium* refers to the tropical mean sea-surface temperature being specified as an input parameter. The perturbation experiments that will be discussed in the following chapters are changes from one equilibrium tropical mean sea-surface temperature to another one. It is not a time evolution approach from an observed state to a future one. As a consequence, the equilibrium solution provides the *background* state. To get closer to observed behavior, higher levels of complexity must be included in the model. They are the steady-state, the cyclic and the evolutionary levels of complexity. Equilibrium and steady-state levels of sophistication are accounted in this study, but not cyclic and evolutionary ones. The steady-state achieved in a numerical simulation is the prerequisite for the validity of the equilibrium analyses. Such steady-state is attained with the equalization of rates naturally produced in a simulation.

1.2 Importance of Research

From a political perspective, policy formulation based on global warming has been an active topic on governments' agendas worldwide. The subject transcends even that domain, reaching theological and philosophical circles of debate. Such popularity of the issue in question relates to the more fundamental question of whether humanity can or cannot modify the earth's climate; and if it can, which people (nation) is contributing more and less for

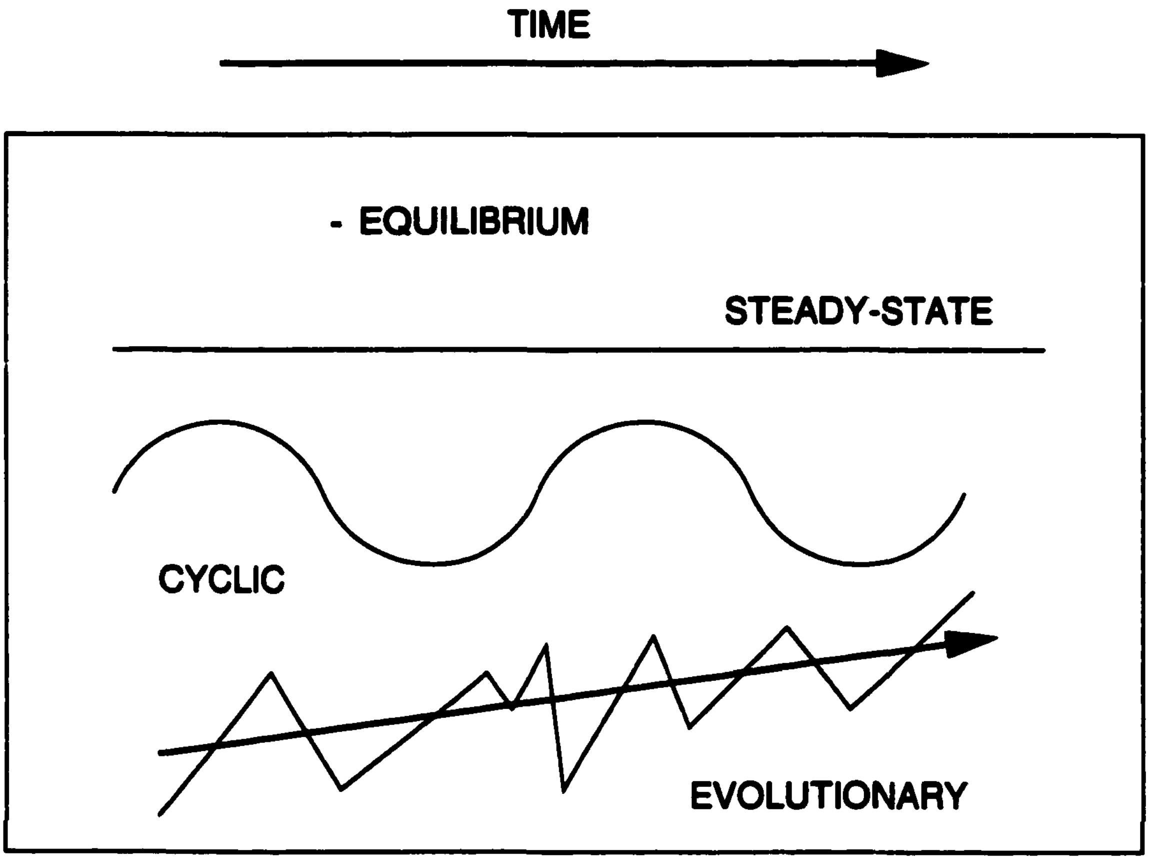

ADAPTED FROM LEWIS AND PRINN (1984)

Figure 1.4: Depiction of different levels of complexity in modeling natural systems like the atmosphere.

such alleged "threat". Thus, the popular interest can be easily argued for without even stating the scientific interest for further research.

Figure 1.5, adapted from the U.S. Senate (1996), summarizes the current problems with models used to forecast global warming. One sees that, with such order of magnitude of the uncertainties when compared with the commonly accepted CO_2 radiative forcing, the predictions are unreliable at best. Even though the uncertainty associated with the humidity bar chart is the lowest one, its order of magnitude is still five (5) times greater than the usual CO_2 radiative forcing of 4 W/m^2. In addition, due to the recognition of the water vapor feedback as crucial in determining greenhouse warming scenarios, the interest in the question here proposed is justified.

More recently, there has been many studies, either model-based and observational, trying to address the problem. Global climate models are powerful tools despite the deficiencies mentioned above. Invariably, almost all of the current generation of these global models produces a positive water vapor feedback. It seems hard to contest such "consensus", but satellite observations provide some clues that GCMs' results might be overamplified. Spencer and Braswell (1997) showed some evidence of the dryness of upper-tropospheric regions based on the SSM/T-2 instrument. Such evidence supports the possibility of a physically acceptable greenhouse process proposed in Lindzen (1997), which might be very close to what is encountered in the earth's atmosphere. Thus, it opens the option for a water vapor feedback much less dominant than the one defended by models. In point of fact, it allows the possibility of a negative feedback due to water vapor that can easily amount to cooling of the planet under an increased concentration of CO_2.

These are all speculative assertions without any quantitative backing so far, and they are mainly provided to "stir" the reader's curiosity on the topic; at the same time, they illustrate why the question is interesting. But at least one point must be taken at face value: the recorded history of global mean air-surface temperatures does not convincingly establish a correspondence between increasing concentration of carbon dioxide in the atmosphere and

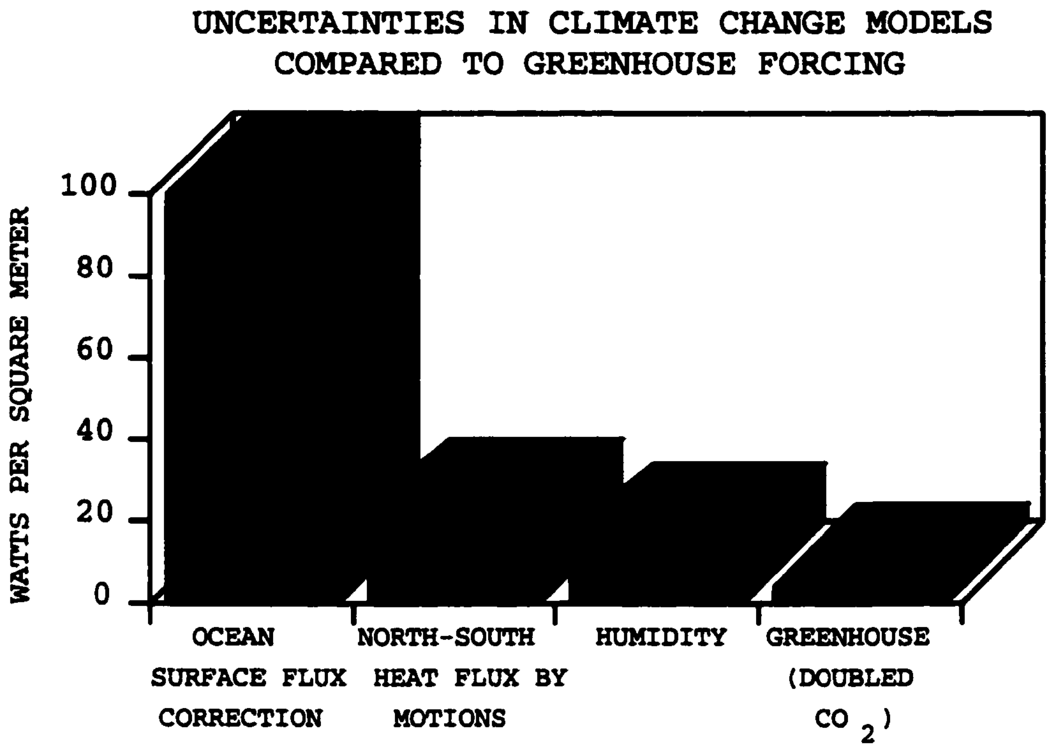

Figure 1.5: Plot adapted from testimony by Salie Baliunas to the 104th U.S. Congress.

warming of the planet. That fact, *per se*, raises a reasonable concern about model predictions, warranting an interest for further investigation.

In conclusion, the importance of the research can be stated either based on the popular concern or on the uncertainties in the numerical models used to address climate change issues. I have provided both for better appreciation of how science and society are closely interleaved.

1.3 Previous Related Studies

The current interest in the earth's Hadley circulation was re-born, I believe, with the publication of two papers reporting results of a doctoral dissertation [Schneider and Lindzen (1977) and Schneider (1977)], following the seminal work of Eliassen (1951). The first two papers debunked some of the skepticism on symmetric models by demonstrating that important features of the tropical general circulation can be qualitatively captured. In particular, it was shown that surface easterlies and westerlies were placed at about the right locations, as well as the upper-tropospheric zonal jet stream. Quantitatively, the jet obtained did not agree well with the observed one, being about four (4) times stronger. Moreover, the simulated surface winds were a bit too weak when compared to available observations. Nevertheless, this symmetric model was successful in establishing the importance of the Hadley cell in the tropics. As a tool for climate stability studies, however, it was not a suitable one. Two crucial approximations — the use of a Newtonian cooling law and the lack of an explicit hydrological cycle — are important drawbacks in addressing climate issues.

After Schneider's landmark study, the interest in the Hadley circulation was revived, and subsequent investigations focused mainly on theoretical dynamical aspects of the Hadley cell [Held and Hou (1980) ; Magalhães (1985); Fang (1995); Cessi (1998)]. All above-mentioned studies dealt with analytical and numerical solutions without incorporating explicit moist processes and detailed radiation models. Satoh (1994, 1995) managed to include an explicit hydrological cycle and a more sophisticated treatment of radiative transfer. A few important remarks should be noted from Satoh's results:

the zonal jet obtained was much more reasonable in magnitude (a factor of only 1.5 greater than the observed one); convective adjustments were incorporated to represent the effects of gravitational convection and; the good point was made that the Newtonian cooling employed in previous symmetric models effectively ensured a stable stratification of the model atmosphere, by-passing the need to represent convection more accurately.

A short and insightful account of the evolution of knowledge regarding the role of water vapor in greenhouse warming predictions is provided in Lindzen (1997). At least two points should be understood for the purposes of this study:

1. When a convective adjustment is incorporated in a radiation column model, it reduces the greenhouse effect by about 75% as compared to a pure radiative equilibrium solution. This result highlights the importance of convective motions as efficient heat conveyors where radiative opacity is high, as in the tropics at low levels.

2. The water vapor concentration decreases sharply when one moves away from the equator either upward or meridionally. The dryness of upper-levels provides a "window" where radiative cooling is an efficient process for transporting heat.

In this connection, the handling of tropical deep cumulus convection is one of the most prominent deficiencies hampering a better quantification of the water vapor feedback. Ellsaesser (1990) noted that the physical mechanism of the ascending motion of the Hadley cell is not the same as for tropical deep cumuli drafts. Such remark was partially based on observational studies by Riehl and Malkus (1958), which indicated that drafts in cumulus clouds are at least twice the magnitude of the mean ascending motion associated with the Hadley cell. It was postulated that buoyancy would be the relevant mechanism in providing the additional energy needed to accomplish the cleavage of the above two ascending motions. Such postulation led, at least partially, to the development of two major approaches in parameterizing deep cumulus convection — the one due to Kuo (1974), and the approach developed by Arakawa and Schubert (1974) (hereafter A&S).

According to Sun and Lindzen (1993), the fundamental difference between the two approaches relates to the assumptions about the large-scale flow in which cumulus clouds are embedded. They stated that Kuo's approach does not enforce an explicit scale separation between the cumulus convection and the surrounding environment while Arakawa-Schubert's approach does. In point of fact, the starting point for both parameterizations is the application of the top-hat method to distinguish between a cloudy and a non-cloudy (clear-sky) region in a certain area. A&S's method begins to deviate from Kuo's when it attempts to account for entrainment in and detrainment out of cumulus clouds, culminating in the quasi-equilibrium closure assumption. It also emphasizes the concept of a cumulus mass flux which is intimately tied to in-cloud updrafts, the latter being an important variable in Kuo's scheme as well. The key difference is that A&S's scheme employs a *spectral* representation of the cumulus ensemble with cloud types distinguished by their detrainment levels. Kuo's model uses the concept of a *bulk* cloud ensemble — an idea being used in some more recent mass flux schemes as well [e.g., Tiedtke (1989)]. The closure of A&S's scheme is based on convective available potential energy. In Kuo's method, it is based on low-level moisture convergence and conditionally unstable stratification.

The two approaches diverge drastically from each other in treating the quantification of precipitation production. Kuo's model employs a moisture partition parameter to ascertain how much of the water vapor converged in a column precipitates out, and how much stays in the air. A&S's model uses a budget equation for in-cloud liquid water and empirical relationships for cloud water/rain conversion to estimate precipitation production profiles. Thus, it appears that the distinction between "Kuo-type" and "A&S-type" schemes is related to two typical aspects of the parameterization of cumulus clouds — the closure assumption and the quantification of precipitation. In what follows, a critical assessment of these issues for each parameterization category is attempted with remarks on subsequent developments of the problem.

CLOSURE ASSUMPTIONS

1- A&S-type closure:

In A&S-type schemes, it is usually assumed that a cumulus ensemble is in equilibrium (in a statistical sense) with the large-scale flow in which it is embedded. That is, the energy available for cumulus convection is provided by the instability of the large-scale flow with an almost instantaneous response when compared with the time-scale for adjustment of the surrounding environment [Emanuel (1994)]. Arakawa and Schubert (1974) introduced the concept of the cloud work function, which is a measure of CAPE (Convective Available Potential Energy). Subsequent improvements of the A&S scheme used only the concept of CAPE without referring explicitly to cloud work functions [e.g., Zhang and McFarlane (1995)]. Although it has been argued that this closure is feasible, since it deals with the essential aspects of the parameterization problem, some room for uneasiness is left in utilizing energy as a criteria. In practical terms, schemes based on such closures will only affect the large-scale flow when CAPE is present.

The point here is simply that, as stated in Lindzen (1990), energy is, at best, a tool to establish consistency rather than causality. Thus, it does not seem appropriate to use CAPE as a closure assumption in the cumulus parameterization problem. Another aspect of the use of CAPE as a closure is the fact that it leads to a mathematically ill-posed problem for the determination of cumulus-base mass fluxes. Such determination is based on the solution of an integral equation. The problem lies in the fact that the formal solution of this equation under the quasi-equilibrium assumption results in negative cloud-base mass fluxes. A&S introduced inequalities to constrain the possible solutions. These constraints allow for the possibility that either no mass flux can be a solution, or that multiple positive values can become a solution. Some attempts to alleviate this situation have been proposed [Moorthi and Suarez (1992); Zhang and McFarlane (1995)], and they apparently make the problem more tractable and computationally more efficient. Recently, Pan and Randall (1998) have replaced the use of CAPE by CKE (Cumulus Kinetic Energy) in analogy with TKE (Turbulent Kinetic Energy), to establish the closure assumption. This modification hardly seems to be a significant improvement given that energy is still being used to establish a causal relation between parameterized cumulus and the resolved atmospheric flow.

2- Kuo-type closure:

The problems with Kuo-type closures, in particular the concept of moisture convergence, do not need much elaboration since critical opinions about them are abundant in the literature [e.g., Emanuel (1994)]. The second part of Kuo-type closures — the establishment of conditionally unstable stratification — is, however, a physically sound criteria at least for deep cumulus regimes. Most of tropical deep cumulus clouds and mid-latitude deep cumuli during summertime are invariably associated with conditionally unstable layers. Such criteria is not prone of the deficiencies in using some energy quantity as a closure, since conditionally unstable stratification can be ascertained by calculating moist and dry adiabatic lapse-rates only [e.g., Wallace and Hobbs (1977)]. In sum, it seems that the use of moisture convergence as a closure [Kuo (1965, 1974); Tiedtke (1989)] is not appropriate due to its relation to CISK (Conditional Instability of Second Kind). According to Raymond and Emanuel (1993), this closure is wrong since it promotes a statistical equilibrium between water substance and the large-scale flow. On the other hand, the use of plain conditional instability as a closure in deep cumulus regimes does seem to be appropriate for the reasons stated above.

From what has been described, it appears that the requirement of *quasi-universality*, as described in Arakawa (1993), is best met by a closure based on conditional instability during tropical deep cumulus regimes. Moisture convergence and CAPE closures suffer from the aforementioned drawbacks that are hardly justifiable. The other requirement — *maintenance of the* *predictability of large-scale fields* — is better framed in terms of how parameterization schemes deal with precipitation production and efficiencies. These issues are described next.

PRECIPITATION QUANTIFICATION

The way current cumulus parameterizations deal with precipitation is perhaps the most vexing problem they face. In short, the majority of the parameterizations proposed so far suffer from not being able to maintain the predictability of water vapor fields. A start towards understanding the source of this issue can be obtained by recalling basic requirements for the conservation laws of continuum mechanics.

The fundamental requisite that a continuity equation for water vapor mixing ratio (or specific humidity) must obey is that water vapor and air form an inter-penetrating continua [Aris (1962)]. A consequence of this requisite is that phase transitions and the subsequent release of latent heat must be treated as discontinuities that cannot be explicitly represented. In practice, the formulation of the water vapor budget in schemes that make the aforementioned representation explicit leads one to employ tuning parameters and/or empirical relations that ultimately pose a severe constraint on its predictability. Kuo-type and A&S-type parameterizations have this kind of problem. The scheme introduced in Emanuel (1991) does also lie in this category by specifying in-cloud precipitation efficiencies. Kuo-type schemes employ the concept of a moisture partition parameter already described. Subsequent attempts to improve upon the concept of moisture partition used different arguments to justify its utilization [Anthes (1977); Molinari (1982)], or slightly modified the original mathematical expression for it [Krishnamurti et al. (1980)]. But they all still used the b parameter as a tuning or empirical number.

In A&S-type methods, it is postulated that precipitation production is a specified fraction of the cumulus liquid water mass flux — posing a predictability limitation as well. The argument used for such specification is that it reproduces tropical precipitation production profiles reasonably well [Lord (1982); Tiedtke (1989); Moorthi and Suarez (1992); Zhang and McFarlane (1995)]. If one views these aspects as part of the closure problem, they are all doing poorly in attempting to maintain the predictability of water vapor fields. As a result, alternative approaches are needed to overcome these deficiencies.

In this study, a formulation for deep cumulus convection is proposed with the intention to overcome these predictability problems. The scheme only accounts for phase transitions and latent heat effects implicitly in the water vapor and in the energy budgets. The above discussion sets the context for the research proposed here. The tool, to be described in the following chapter, is a Hadley circulation model that includes the atmospheric branch of the hydrological cycle, and it also has a state-of-the-art radiation scheme. This tool is described next.

Chapter 2

Method

2.1 Hadley Model Description

The tool of this proposed research is a symmetric model of a tropical hydrostatic atmosphere[1]. The model is formulated in sigma-pressure coordinates with the lower boundary at $\sigma = 1$ and the upper-boundary at $\sigma = 10^{-4}$. Meridionally, the domain ranges from the equator to 30° N. Lateral no-flux conditions are employed at these boundaries, and a "swamp" with no heat capacity and infinite supply of moisture is used at the surface. The reason to use such lower boundary condition lies on the interest in analyzing the tropical climate equilibrium solution in the model. Such equilibrium solution is achieved after the model reaches a steady-state in an experiment, and thus the "swamp" is the only representation needed to simulate surface fluxes. Figure 2.1 schematically depicts what the symmetric model is aiming to resolve.

[1]A derivation of the model equations can be found in appendix A.

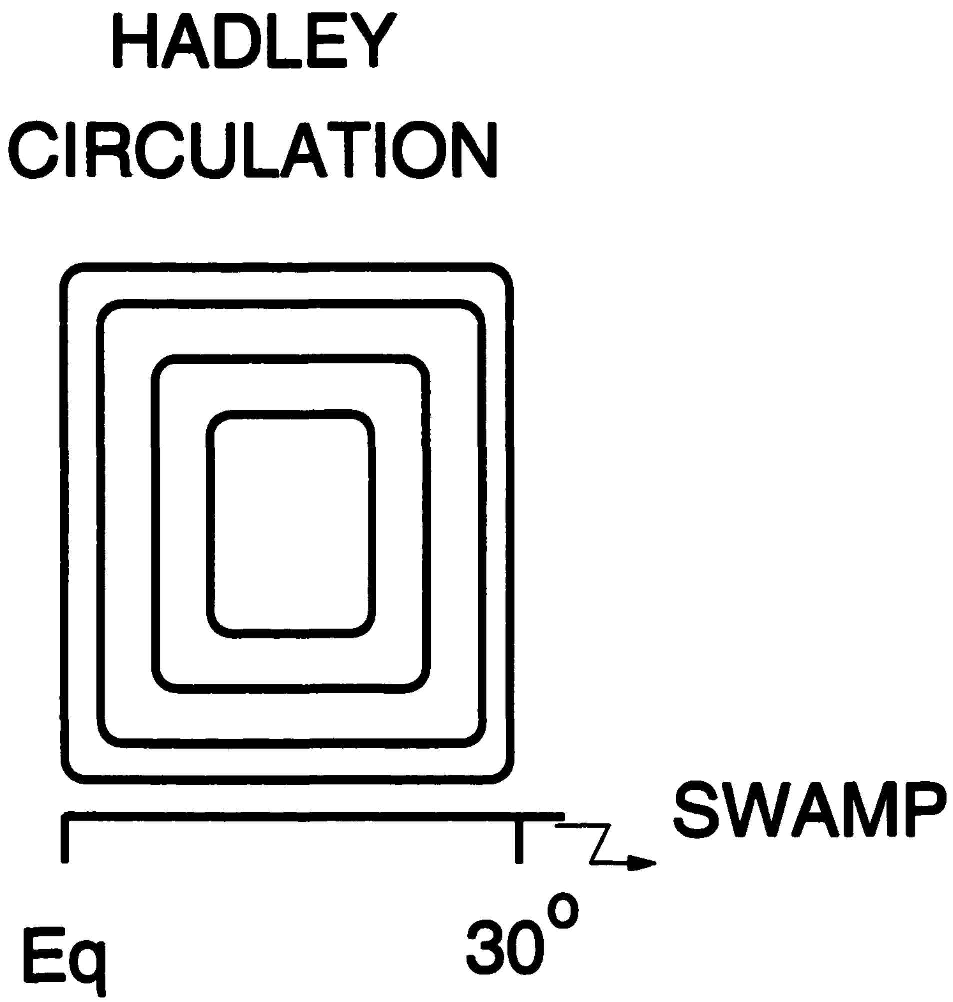

Figure 2.1: Schematic depiction of the symmetric model domain.

The grid resolution is uniform in the meridional direction and variable in the vertical. The vertical grid structure establishes a higher resolution in the troposphere than above it. This is an important feature to simulate the atmospheric branch of the hydrological cycle adequately, since the scale height of water vapor in the tropics is small compared to the depth of the troposphere [Lindzen (1991), Lindzen (1994)]. Figure 2.2 illustrates a set up of the grid with 11 points in the meridional direction and 51 points in the vertical.

Fluxes, meridional wind speed and the vertical "omega" motion variables are specified at such grid points. The other variables prognosticated by the model, i.e., angular momentum, dry-static energy, and specific humidity are specified at grid points half-way between the points depicted in the figure.

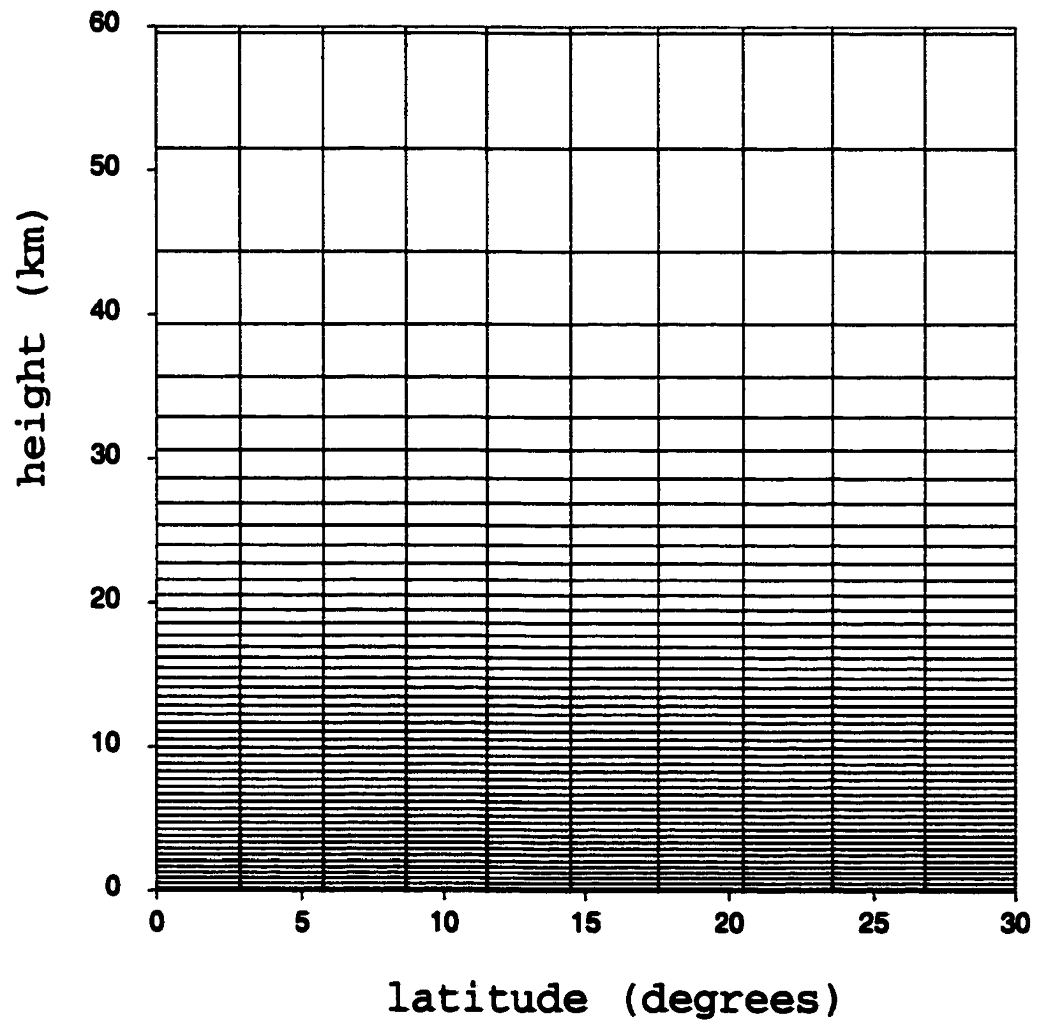

Figure 2.2: Model grid structure showing variable vertical resolution.

The initial conditions are a motionless atmosphere, and mean tropical profiles of temperature, specific humidity and ozone according to McClatchey et al. (1972). The ozone profile is taken for the sole purpose of serving as input for the radiation calculations. Such profiles are linearly interpolated to the model grid. The conservation laws for angular momentum, dry-static energy and specific humidity are discretized in flux form to ensure that sources and sinks are coming only from the model boundaries. Stresses in the angular momentum and meridional wind equations are parameterized based on a constant eddy *dynamic* viscosity of 10 kg m^{-1} s^{-1}. Tropical convection is generally represented by a convective adjustment procedure that employs the moist-adiabatic lapse-rate as the critical value for adjustment. Whenever the lapse-rate computed by the model becomes supercritical in any given layer, the adjustment procedure brings its value to the critical one, removing the convective instability and accounting locally for the heating due to the change of temperature. The lapse-rate adjustment procedure is an incomplete but efficient method to account for convection in the Hadley model. It is incomplete because it does not account for cloud cover and the redistribution of humidity resultant from moist convection. Its efficiency lies in effectively maintaining a stable stratification of the model atmosphere. When used without any other parameterization, the convective adjustment is meant to represent all imaginable types of convective motions with exception of the large-scale thermally direct circulation associated with the Hadley cell. Grid-scale condensation is also checked at each time-step whenever the predicted specific humidity value overcomes saturation.

2.2 Radiation Scheme

The NCAR column radiation scheme is a stand-alone version of the radiation parameterizations employed in the Community Climate Model. The formulation of the solar radiation is described in Briegleb (1992). The method uses the delta-Eddington approximation which is known for simulating the effects of multiple scattering with good accuracy. The solar spectrum is divided into 18 discrete spectral intervals from 0.2 to 5 μm. From these, there are seven bands for ozone, seven for water vapor, three for carbon dioxide and one for visible. Absorption due to O_2 is represented in two bands and the overlap between H_2O and CO_2 is ignored. A parameterization for water droplet clouds [Slingo (1989)] is incorporated. The scheme relates the extinction optical depth, the single-scattering albedo, and the asymmetry parameter to the cloud liquid water path and cloud drop effective radius. In-cloud liquid water paths are evaluated from a prescribed, meridionally and height varying, but time independent, cloud liquid water density profile, $\rho_l(z)$, given by

$$\rho_l = \rho_l^0 \cdot \exp\left(-z/h_l\right) \tag{2.1}$$

where the reference value ρ_l^0 is equal to $0.21 \mathrm{gm}^{-3}$. Instead of specifying a zonally symmetric meridional dependence for the cloud water scale height, h_l, it is locally diagnosed as a function of the vertically integrated water vapor (precipitable water) as:

$$h_l = 700 \cdot \ln(1.0 + \frac{1}{g} \cdot \int_{p_T}^{p_S} q \cdot dp) \tag{2.2}$$

The cloud water path is then determined by integrating the liquid water concentration using

$$CWP = \int \rho_l \cdot dz \tag{2.3}$$

which can be analytically evaluated for an arbitrary layer k as

$$CWP(k) = \rho_l^0 \cdot h_l \cdot [\exp(-z_{k+1/2}/h_l) - \exp(-z_{k-1/2}/h_l)] \tag{2.4}$$

where $z_{k+1/2}$ and $z_{k-1/2}$ are the heights of the k^{th} layer interfaces.

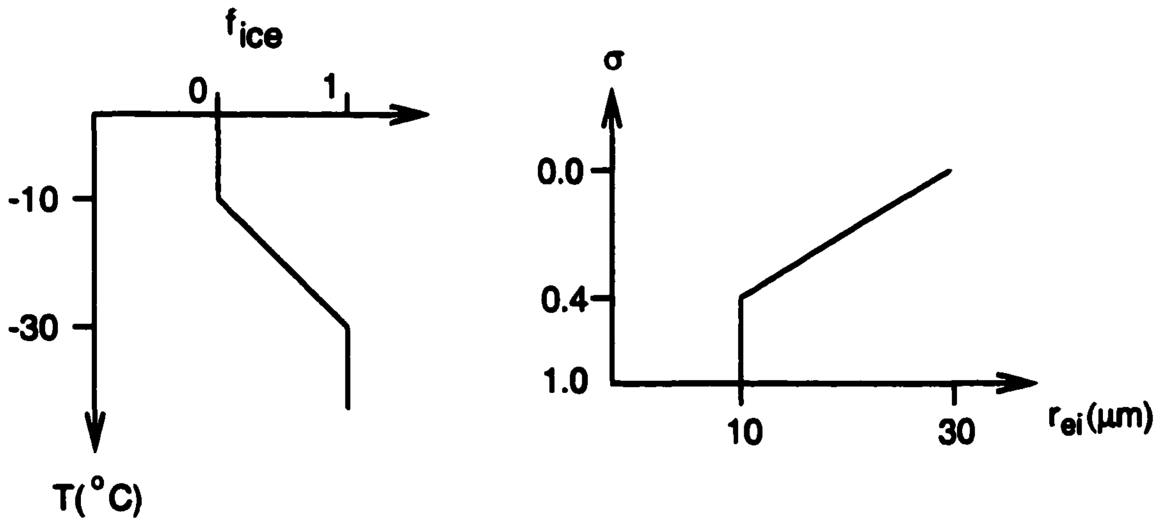

Figure 2.3: Plots showing how the fraction of the total cloud water in the form of ice and the cloud drop effective radius for ice are specified in the NCAR CRM.

Cloud drop effective radius for liquid water clouds, r_{el}, is specified to be 10 μm over oceans. For clouds containing ice, figure 2.3 illustrates how the cloud drop effective radius, r_{ei}, is specified. The way the fraction of the total cloud water in the form of ice is obtained is illustrated in the same figure.

After these quantities are evaluated, cloud optical properties for each spectral interval (extinction optical depth, single scattering albedo, asymmetry parameter and forward scattering parameter) are computed. Moreover, the cloud extinction optical depth τ_c in each model layer is modified as

$$\tau_c' = \tau_c \cdot a^{3/2} \tag{2.5}$$

where a is the fractional cloud cover in the layer; the power 3/2 is necessary to give results approximately the same as the random overlap assumption.

When used in the CCM, it has been reported that the solar radiation parameterization underestimates the climate sensitivity for increases in the CO_2 concentration [Briegleb (1992)]. This deficiency, however, does not affect the sensitivity experiments performed with the Hadley model, since carbon dioxide concentration is kept fixed at the baseline concentration of 300 ppmv.

The longwave radiation parameterization is the most important from the standpoint of the proposed analyses. The prominent feature of the longwave radiation calculation is the non-isothermal emissivity formulation for water vapor [Ramanathan and Downey (1986)]. In practice, such formulation resumes to the following expression:

$$F = B(T_s) - \int_0^1 A(\sigma) \cdot \partial B/\partial\sigma \cdot d\sigma \tag{2.6}$$

where F is the outgoing infrared flux at the top of the atmosphere. $B(T_s)$ is the Planck function evaluated at the surface temperature, $A(\sigma)$ is the absorptivity as a function of σ-pressure, and $\partial B/\partial\sigma$ is the derivative with respect to σ of the Planck function. The product of $A(\sigma)$ and $\partial B/\partial\sigma$ represents the interaction of two nonlinear functions — $A(\sigma)$ being dependent on the water vapor content of the atmosphere. In section 2.3, some results will demonstrate the effects of such nonlinearity in determining the model climate sensitivity. The use of the non-isothermal emissivity in the CRM is extended for carbon dioxide, nitrous oxide, methane and ozone. Chlorofluorocarbons (CFC11 and CFC12) are represented by an exponential transmission approximation. There are 8 broad-bands where the above constituents are represented, ranging from 500 to 1500 cm^{-1}.

Cloud emissivity is accounted for by defining an effective cloud amount for each model layer

$$a' = \epsilon_{cld} \cdot a \tag{2.7}$$

the cloud emissivity is defined as,

$$\epsilon_{cld} = 1 - \exp\left(-D\kappa_{abs} \cdot CWP\right) \tag{2.8}$$

where D is a diffusivity factor set to 1.66, κ_{abs} is the longwave absorption coefficient (m^2g^{-1}), and CWP is the cloud water path (gm^{-2}). The absorption coefficient is defined as,

$$\kappa_{abs} = \kappa_l \cdot (1 - f_{ice}) + \kappa_i \cdot f_{ice} \tag{2.9}$$

where κ_l is the longwave absorption coefficient for liquid cloud water, specified in a way such that $D\kappa_l$ is 0.15. κ_i is the absorption coefficient for the ice phase and is based on a broad band fit to the emissivity given by:

$$\kappa_i = 0.005 + \frac{1}{r_{ei}} \tag{2.10}$$

More details can be found in Kiehl et al. (1996).

2.3 Research Approach

The so-called inverse climate simulation is the method used in this research. It was formally introduced by Cess and Potter (1988) as a procedure to intercompare the climate sensitivities produced by distinct global climate models. The idea is to specify the sea-surface temperature, run the model until a steady-state is achieved, and record the flux imbalance at the top of the atmosphere. Afterwards, a different sea-surface temperature is specified, the model is run out to steady-state once again, and a new flux imbalance is obtained. The gain and the feedback factors are then calculated. All of this is done without changing the top of atmosphere solar radiation fluxes or the carbon dioxide concentration. The sensitivity of a "global" atmosphere is essentially the ratio between the surface temperature perturbation and the top of the atmosphere infrared heat flux changes. The tropical region, however, is open not only to TOA fluxes but also to meridional heat fluxes. A suggestion on how to estimate the tropical sensitivity was advanced in Lindzen (1997):

$$\text{Tropical sensitivity} = \frac{\Delta T_{tropics}}{\Delta F_{meridional} + \Delta F_{TOA}} \tag{2.11}$$

where $\Delta T_{tropics}$ is the imposed average sea-surface temperature perturbation, $\Delta F_{meridional}$ and ΔF_{TOA} are, respectively, the meridional heat flux changes and the top of the atmosphere radiative heat flux changes. In this study, there are no meridional fluxes as stated earlier, and I analyze only changes in TOA heat fluxes to temperature perturbations. As a result, the tropical *model* sensitivity is given by:

$$\text{Tropical model sensitivity} = \frac{\Delta T_{tropics}}{\Delta F_{TOA}} \tag{2.12}$$

It is important to understand the limitation implied in (2.12). As described in chapter 1, the change of the meridional heat fluxes is an important variable in calculating the tropical climate sensitivity. Hence, one may worry if the climate model equilibrium has any resemblance to what is observed. To achieve a steady-state without allowing meridionally adjusted heat fluxes would call for an enhanced artificial thermal radiation out of the tropics to balance the incoming insolation. If current values of solar input for low latitudes are used, a quick calculation gives a sea-surface temperature of 320 K! Let's not despair at this point, and remember once again that the approach is the so-called inverse climate simulation. Consequently, a realistic solar constant is used, as well as a sea-surface temperature distribution compatible with what is observed. The difference is the output of longwave radiation, something that is partially dependent on the SST specified. The tropical climate equilibrium, in turn, has a mean flux imbalance at the top of the atmosphere. Obviously, the Hadley cell intensity, as simulated by the model, is not comparable to the observed Hadley motion. But, since I am interested in computing the *sensitivity* of the system, the actual strength of the meridional circulation is not the relevant parameter: the *change* of it imposed by the SST perturbation is. The important thing to realize here is that the changes of the meridional circulation, along with the changes of the hydrological cycle and of the thermal structure will impose a *lower* bound for the climate sensitivity that would be obtained for the open tropics in a warmer *equilibrium* response. It is a lower bound because the equilibrium meridional temperature gradient is generally understood to be smaller in a warmer climate, implying less meridional heat fluxes out of equatorial regions. That is, $\Delta F_{meridional}$ would be negative if accounted for.

In order to estimate the so-called feedback factors, the following expression is used:

$$\sum_i f_i = 1 - \frac{1}{Gain} \tag{2.13}$$

where gain is the ratio of the system response, including feedbacks, to the unamplified response, when feedbacks are turned off [equation (2.23)]. The usefulness of using a numerical model to perform these experiments lies on the ability of turning switches on and off for different feedbacks. Therefore, one can obtain an estimate for each individual feedback factor by calculating individual gains. One must be careful in analyzing such feedback factors, since their summation expresses nonlinearly in (2.13). Adding a small f_i to the expression may cause the gain to change significantly, thus giving a misleading impression that such factor is very dominant. That's why it is important to analyze these factors individually in attempting to describe the causes for the climate sensitivity. In the inverse method, such analysis is accomplished by calculating the individual gains from the model simulation, and then applying (2.13) to obtain the individual f_i's. In the axisymmetric model, three of such factors are included: lapse-rate, water vapor and cloud cover (actually four, since the water vapor feedback is split into feedbacks due to distribution and amount).

The lapse-rate feedback factor can be computed when a convective adjustment employing the moist-adiabatic lapse-rate is used as the critical value for adjustment. If a constant critical lapse-rate is applied instead, then such effect is excluded. Likewise, the feedback factor due to water vapor can be estimated when the lapse-rate and the cloud cover switches are turned off. Moreover, the ability of computing the cloud cover feedback factor comes from the use of a cumulus representation. In closing, an estimate of the sum of all feedback factors appearing in the denominator of (2.13) is calculated when all the switches are on during a numerical experiment.

Usually, the gain is calculated through the more traditional computation of the surface temperature for a given external perturbation (doubled CO_2 or change in solar input). In the inverse method, only the tropical sensitivity can be directly calculated, but not the gain and the feedback factors. Thanks to an interrelationship procedure developed for this study, it is possible to calculate the gain and the feedback factors from the tropical model sensitivity.

Let the net downward flux (tropically averaged) at the top of the atmosphere be:

$$Q - F = F_{TOA} \tag{2.14}$$

Q is the net downward shortwave flux and F is the net upward longwave flux. In equilibrium, F_{TOA} is a constant different than zero for the tropical domain. In the Hadley model, F dependency on surface temperature T_s, water vapor concentration h, lapse-rate Γ and cloud cover a will be accounted for. In order to assess changes in T_s due to perturbations in the carbon dioxide concentration c, one begins with:

$$dF = dQ \tag{2.15}$$

or

$$\frac{\partial F}{\partial c}dc + \frac{dF}{dT_s}dT_s = \frac{dQ}{dT_s}dT_s \tag{2.16}$$

or

$$dT_s = \lambda_{TM} \cdot \frac{\partial F}{\partial c}dc \tag{2.17}$$

where

$$\lambda_{TM} = [d(Q - F)/dT_s]^{-1} = (dF_{TOA}/dT_s)^{-1} \tag{2.18}$$

λ_{TM} is called the *tropical model sensitivity*. It can easily be related to the dimensionless *gain*. Let

$$\frac{dF_{TOA}}{dT_s} = \frac{\partial F_{TOA}}{\partial T_s} + \frac{\partial F_{TOA}}{\partial h}\frac{\partial h}{\partial T_s} + \frac{\partial F_{TOA}}{\partial \Gamma}\frac{\partial \Gamma}{\partial T_s} + \frac{\partial F_{TOA}}{\partial a}\frac{\partial a}{\partial T_s} \tag{2.19}$$

Dividing (2.19) by $\partial F_{TOA}/\partial T_s$:

$$\frac{dF_{TOA}/dT_s}{\partial F_{TOA}/\partial T_s} = 1 + \frac{\partial F_{TOA}/\partial h \cdot \partial h/\partial T_s}{\partial F_{TOA}/\partial T_s} + \frac{\partial F_{TOA}/\partial \Gamma \cdot \partial \Gamma/\partial T_s}{\partial F_{TOA}/\partial T_s} + \frac{\partial F_{TOA}/\partial a \cdot \partial a/\partial T_s}{\partial F_{TOA}/\partial T_s} \tag{2.20}$$

or, inverting and writing it more compactly

$$\frac{\partial F_{TOA}}{\partial T_s}\left(\frac{dF_{TOA}}{dT_s}\right)^{-1} = \frac{1}{1 - \sum_i f_i} = \text{Gain} \tag{2.21}$$

where

$$f_i = -\frac{\partial F_{TOA}/\partial \chi \cdot \partial \chi/\partial T_s}{\partial F_{TOA}/\partial T_s} \tag{2.22}$$

χ may be one of h, Γ, or a. They stand for the water vapor, the lapse-rate and the cloud cover feedback factors. Using (2.18) and (2.21):

$$\mathrm{Gain} = \frac{\partial F_{TOA}}{\partial T_s} \cdot \lambda_{TM} \tag{2.23}$$

The term $\partial F_{TOA}/\partial T_s$ is calculated by disabling the feedbacks due to water vapor, lapse-rate, and cloud cover in a model run.

Chapter 3

Control Climate

3.1 Digression

The idea of presenting the current climate, as obtained by the Hadley circulation model, is somewhat misleading. The issue in question is the fact that, in attempting to compare model results with pertinent observations, one is led to miss the perception that the physics accounted in models is nothing more than a manifestation of mathematical principles (as a matter of fact, the model physics is always less than the "model math" since discretizations and parameterizations are inevitably needed in constructing a climate model). Let's digress here to comment on the idea put forward in Goody et al. (1998). Their proposal of deploying observing systems that are low-cost, global in coverage, and with accuracy of decadal global warming projections is nothing less than interesting and inspirational. But the premise on which it is based — that the scientific merit of climate predictions can only be established with direct comparisons to observations — underlies an approach widely used in meteorology. In particular, some of the issues on using higher-order statistics for testing climate models are discussed further below.

To begin with, it is important to recognize that a physical law (e.g., the first law of thermodynamics) has no predictive value until it can be represented in mathematical jargon. Climate models are built based on such representations. The climate system itself does not follow mathematical relationships in establishing inter-dependencies among its environmental quantities. Thus, to directly compare a set of observational relations (e.g., covariances), no matter how absolute, global and precise they might be, with those that can be calculated from models does not seem at first to be a relevant approach in testing them. By the way of contrast, a relevant test is the establishment of *observational bounds* limiting the range in which models' results must lie. Sophisticated and low-cost observations can more effectively be used in narrowing the above-mentioned range.

It is worth discussing Goody et al. (1998)'s assertion that the sensitivity of the atmosphere to forcing by greenhouse gases can be established in a seasonal dataset. Such sensitivity, although not clearly mentioned there, is likely referring to the dependency on water vapor and clouds, the two major greenhouse substances in the terrestrial atmosphere. As noted in Lindzen (1997), the kind of sensitivity discussed in Goody et al. (1998) is associated with climate changes resulting from a rearrangement of regional climatic patterns (e.g., ENSO), but it is not necessarily relevant to the quantification of climate sensitivities associated with the thermal contrast between equatorial and polar regions. The later is thought to be the relevant one for decadal (and beyond) climate projections. Moreover, under a model approach, the response of the climate system to changes in water vapor and clouds is better established as feedbacks imposed on the system due to an external forcing perturbation (e.g., change in solar flux reaching the planet, increase in atmospheric CO_2, surface temperature perturbation, etc.). Again, the issue of time-scale hinders the problems discussed here and there, but it is important to clearly suggest that nonlinear interactions in seasonal data sets, or, for such purpose, in seasonal climate simulations, will not necessarily establish a credible test for a decadal model projection.

Moreover, it is relevant to note that the representation of water vapor-cloud interactions in a climate model inevitably requires the use of so-named tuning parameters. One may — based on their suggestion that a comparison of second-order moments between a GCM and the observed atmosphere is an objective test of model believability — attempt to optimize the set of tuning parameters to compare with the observed statistics. It might provide a successful test within one particular set of statistics, but it will not imply a credible model, since a particular optimization of tuning parameters constrains a model's response to an external forcing in general. This particular constraint will hardly be an invariant in comparing a distinct set of statistics than the one attempted in the first place. It is based on such contentions that the point of establishing bounds on the parameter space in which a model prediction should lie is perhaps a more relevant one to approach with more precise and global observations. The suggestion of directly comparing observations with a GCM output set will likely serve to maintain the uncertainty about the scientific merit of climate predictions.

A more specific caveat that should be kept in mind is the distinctly different nature of the data obtained from the Hadley model and the observations to be contrasted with. It is important to note that the model results are obtained based on the idealization of a zonally symmetric atmosphere that is also symmetric about the equator. Such approach implies a rectification of the "observed" thermal circulation of the tropics. As a consequence, one is looking for orders of magnitude in the comparisons, not absolute values. The model results should be interpreted as the background state upon which the actual cyclic nature of atmospheric behavior is superimposed. This cyclic nature is always accounted for in observed quantities. It is not accounted for in the model plots. Nevertheless, such comparison is a common practice in observational sciences. Thus, a *descriptive* attempt to compare a steady-state solution with some published pertinent data is presented here.

3.2 A Steady-State Solution

In this section, a simulation that does not include any deep cumulus scheme is presented for purposes of showing the Hadley model behavior. The only representation of sub-grid convection included is the lapse-rate adjustment.

Figures 3.1 and 3.2 show the time evolution of maximum winds and of selected radiative and convective fluxes. The steady-state values from figure 3.1 can be roughly compared to figures 7.15 and 7.17 of Peixoto and Oort (1992). One sees a reasonable agreement, particularly if the results are also contrasted to previous symmetric models in published literature [Schneider (1977), Held and Hou (1980)].

Figure 3.3 shows the horizontally averaged vertical profiles of temperature and static energies. Again, the results are essentially comparable to observed profiles in the tropics (an example of an observed temperature profile is the top panel of figure 7.5 from Peixoto and Oort (1992)). In particular,

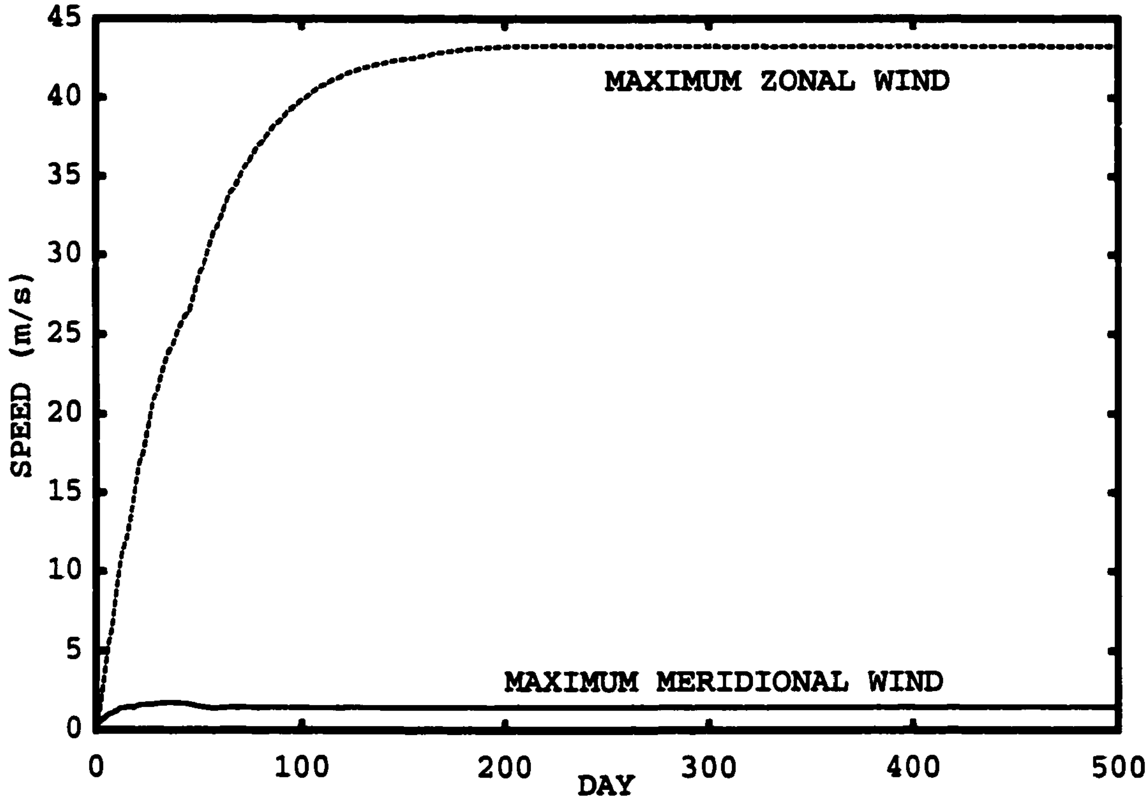

Figure 3.1: Time evolution of maximum winds. This run was performed with a moist-adiabatic lapse-rate adjustment only.

the tropopause temperature inversion has the minimum value close to what is observed.

Figures 3.4 and 3.5 show, respectively, the vertical profiles of horizontally averaged fluxes and heating/cooling rates. Note that the net flux imbalance is roughly constant throughout the depth of the model atmosphere, and that the net rate is zero. These results serve as checks that steady-state conditions have been achieved, as well as that the radiation code has been implemented correctly.

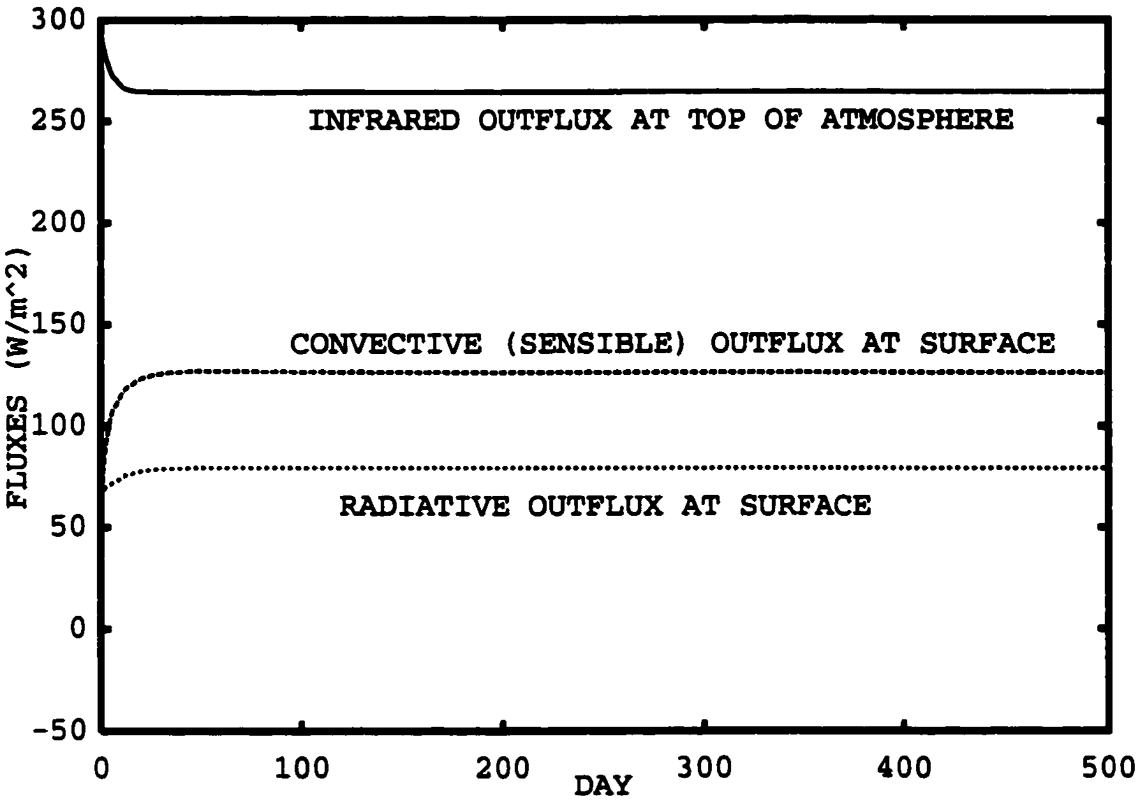

Figure 3.2: Time evolution of fluxes out of the top of the atmosphere and out of the surface for the grid point located at 1.4° N (same run as the previous figure).

One latitudinal distribution of the sea-surface and of the first grid point temperatures is given in figure 3.6. The meridional gradient and the mean SST are determined as input parameters for the model run trough the relation:

$$T_s(\varphi) = [T]_s + \Delta \cdot \cos(6\varphi) \tag{3.1}$$

where φ is the latitude in radians, $[T]_s$ is the *horizontally averaged* tropical sea-surface temperature, and Δ is a factor that determines the meridional gradient. I use $[T]_s = 297\,\mathrm{K}$, and $\Delta = 3\,\mathrm{K}$ to approximate the observed zonally

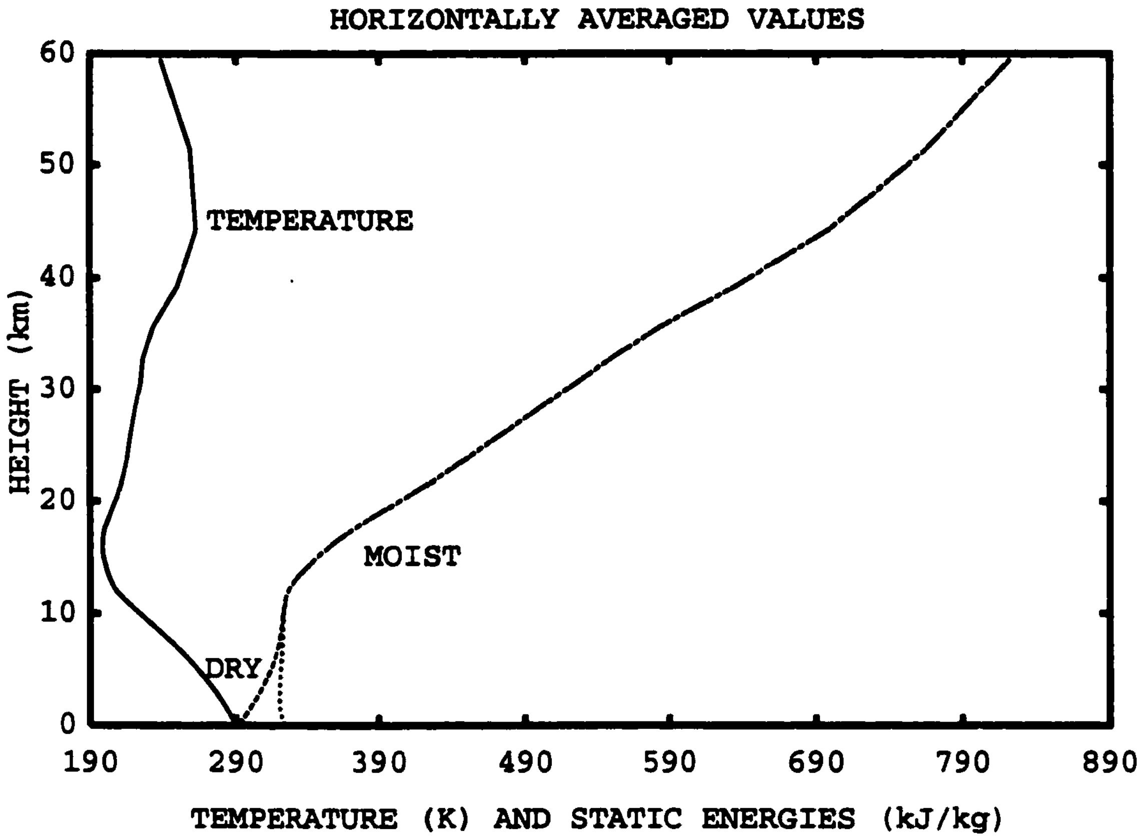

Figure 3.3: Steady-state profiles of temperature and static energies (same run as previous two figures).

and annually averaged sea-surface temperature distribution from the equator to 30°.

In figure 3.7, the latitudinal distribution of short and longwave radiative fluxes at the top of the atmosphere is presented. The solar fluxes are ascertained by disabling the annual and diurnal cycles in the radiation scheme. The longwave infrared fluxes show that, due to the water vapor opacity, less radiation is coming out of the model domain in the ascending branch region of the Hadley cell. Conversely, more longwave radiation comes out of the

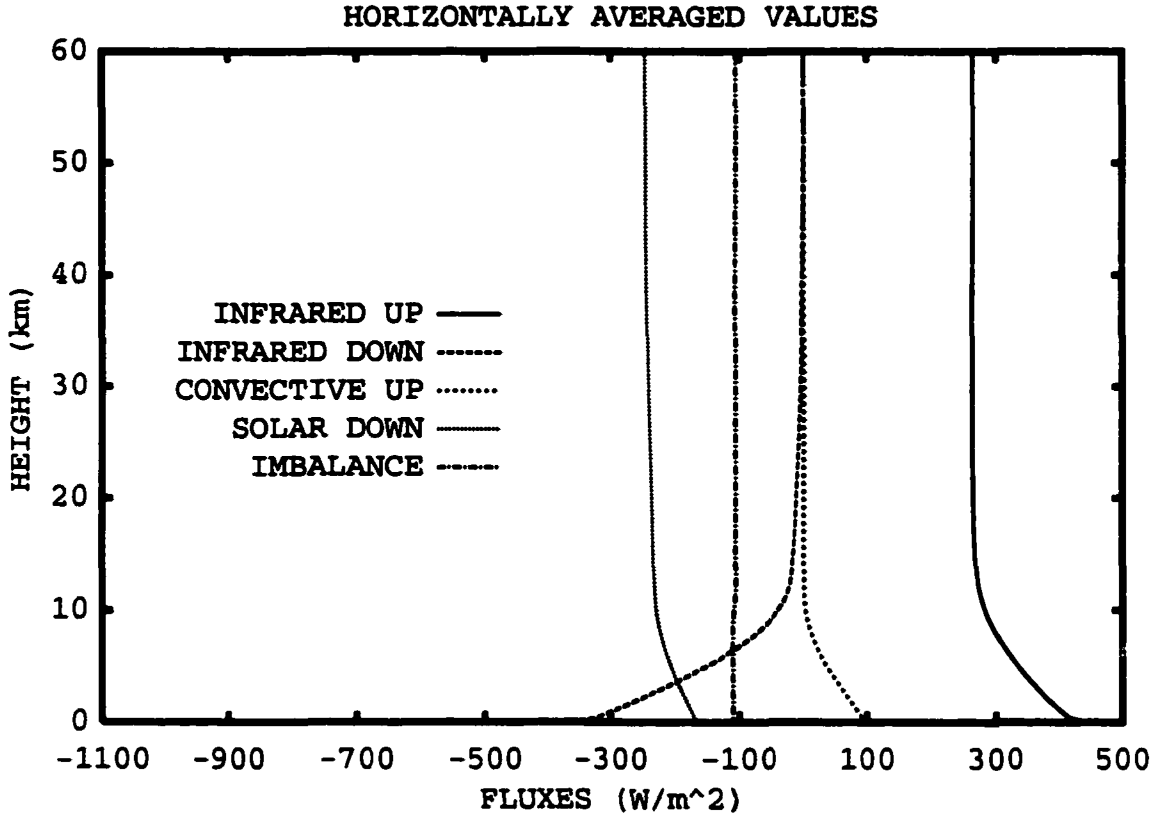

Figure 3.4: Steady-state profiles of radiative and convective fluxes.

model domain in the descending branch of the cell due to the drying effect promoted by such sinking motion.

Figure 3.8 shows contour plots depicting temperature, moisture, zonal wind and Hadley cell structures. Of particular notice is the smoothing of the meridional temperature gradient as one moves upward in panel a. Moreover, the upper-troposphere is subject to drying due to the descending branch of the meridional circulation in panel b. Still in the same panel, the troposphere is essentially saturated in the region of flat contours close to the equator. In panel c, a region of surface easterlies along with an upper-tropospheric

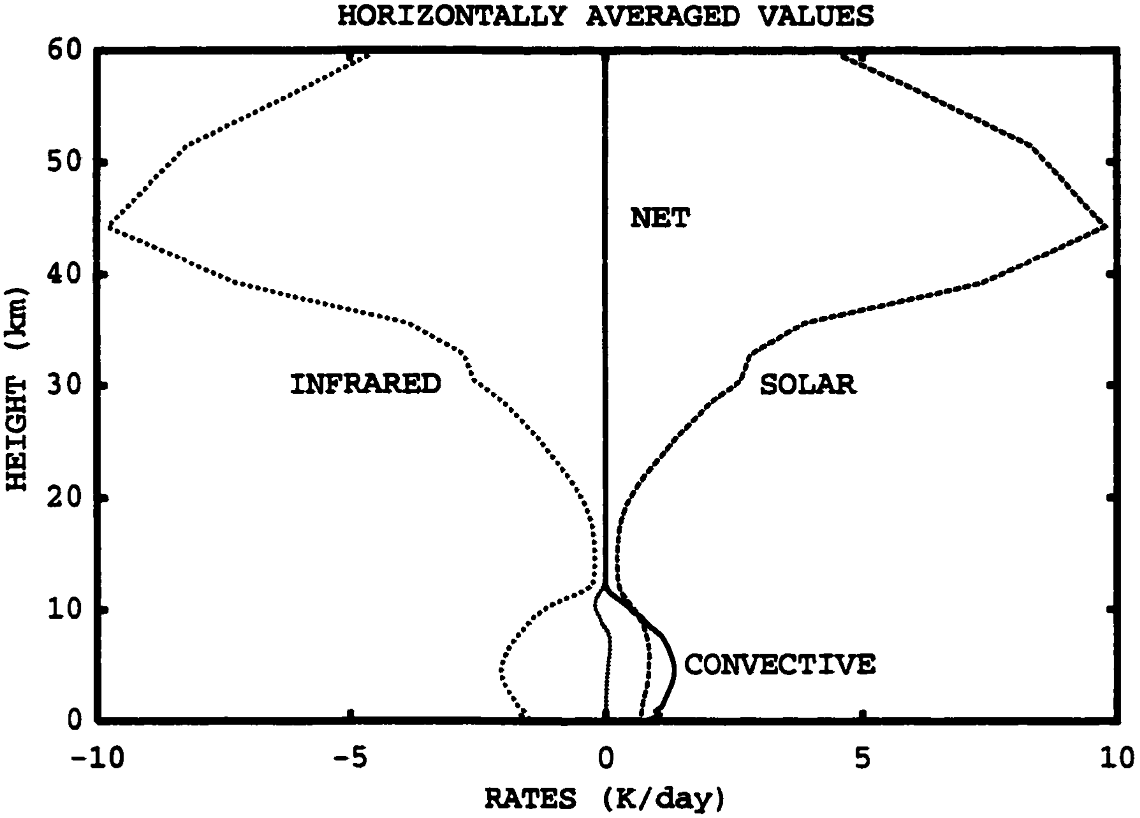

Figure 3.5: Steady-state profiles of heating and cooling rates.

westerly jet arise. Finally, panel d shows the steady structure of the Hadley cell for this simulation.

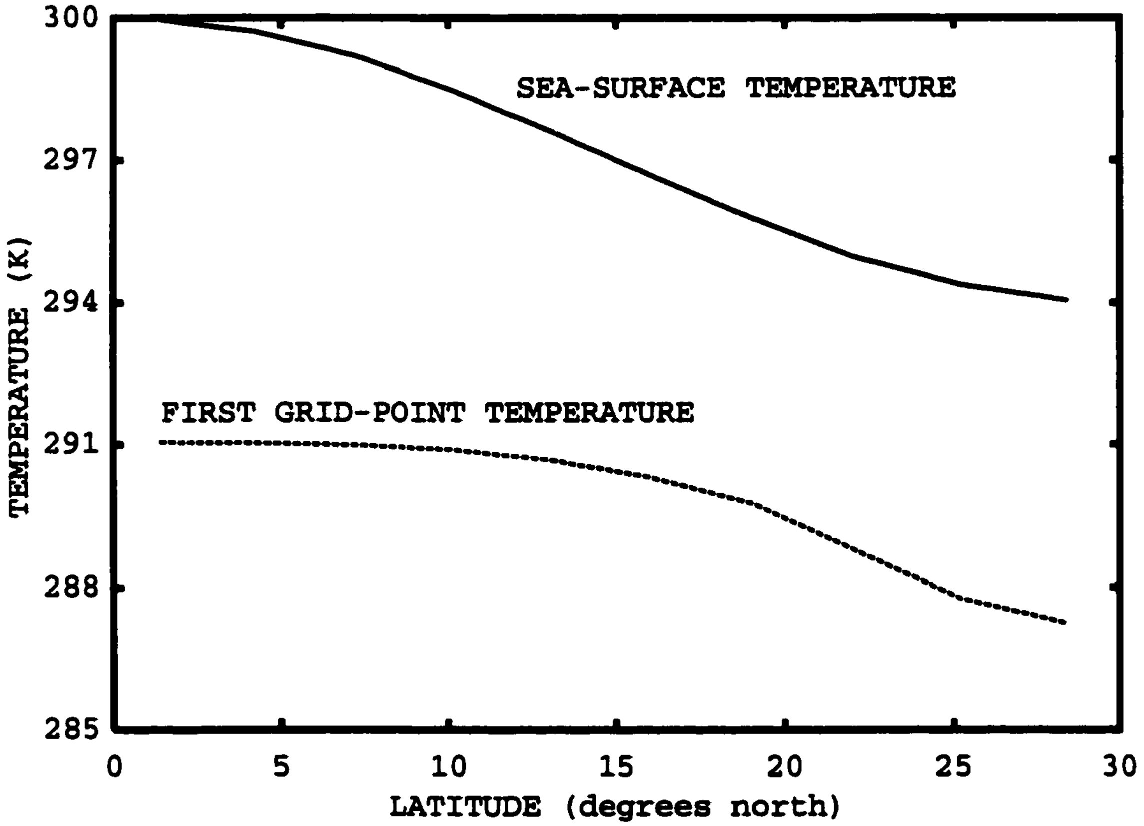

Figure 3.6: Sea-surface and first grid-point temperature distribution in the model domain.

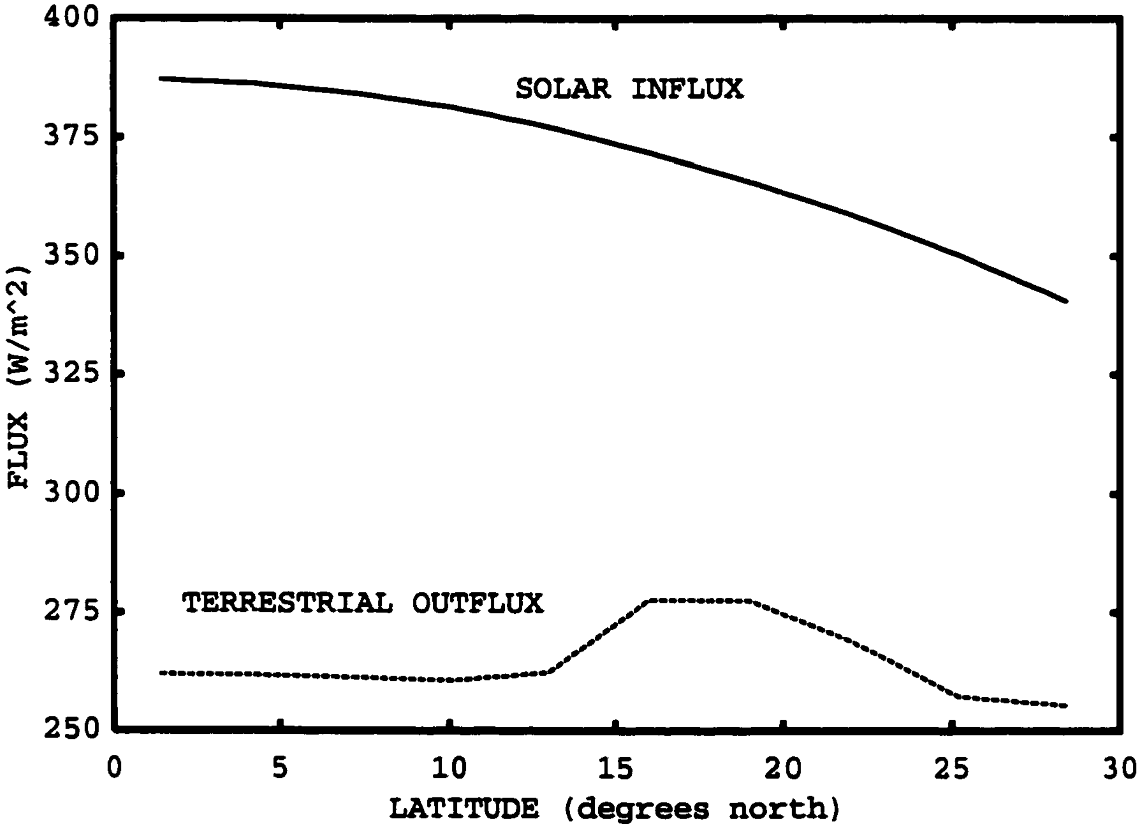

Figure 3.7: Top of atmosphere latitudinal distribution of short and longwave fluxes.

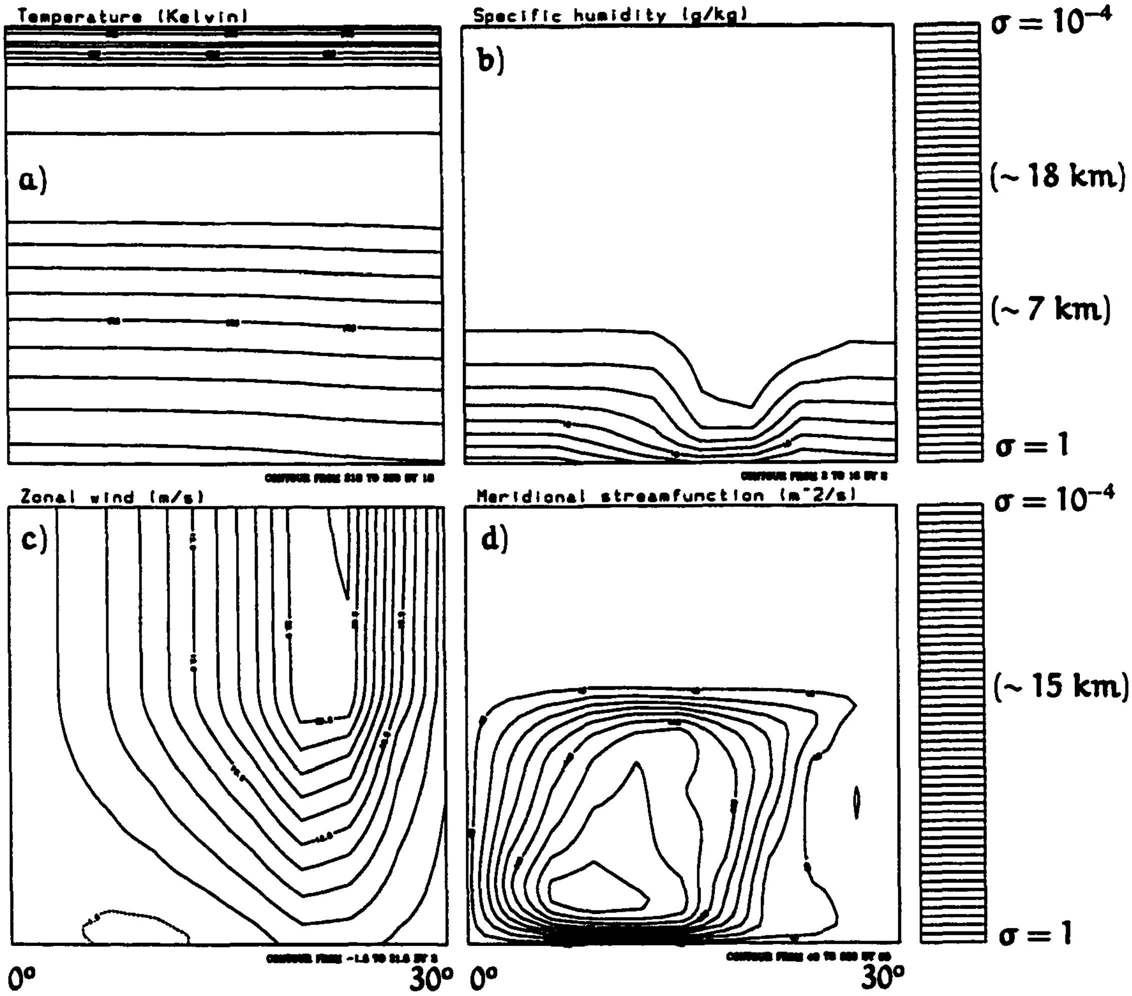

Figure 3.8: Computed two-dimensional fields in the model domain. a) Temperature in Kelvin; b) Specific humidity in g of vapor/kg of moist air; c) Zonal wind in m/s; d) Meridional stream-function in m^2/s. The contour intervals, as well as the maximum and minimum contours are indicated for each plot. Negative contours are dashed. The rules on the far right are the vertical σ - pressure model levels (the grid adopted employs a third-order *stretching* polynomial). The approximate height of certain levels are indicated in parenthesis.

Chapter 4

Deep Cumulus Models

Two options for the representation of tropical deep cumulus convection are used in the Hadley model: a mass-flux deep cumulus parameterization that is currently used in the NCAR/CCM3 [Zhang and McFarlane (1995)], and a new deep cumulus representation developed for this study [Fleischfresser (1999a)]. These parameterizations are described next.

4.1 The Zhang/McFarlane Deep Cumulus Scheme

This mass flux scheme (hereafter Z&M/NCAR) is a member of the A&S - type family of cumulus parameterizations. As all schemes in this category, it attempts to simplify the original complexities of the Arakawa and Schubert (1974) formulation. First, Z&M/NCAR abandons the idea of a "spectral" representation of the cumulus ensemble in favor of a "bulk" cumulus model, an approach identical to the one used in Tiedtke (1989) (hereafter, T89). It also includes downdraft formulations, similarly to T89. A third distinction is the assumption that cumulus convection acts to remove CAPE at an exponential rate with a specified adjustment time-scale. Naturally, the parameterization only works when CAPE is present. Following the classification put forward by Gregory (1997), this is an adjustment-type closure.

What apparently remained unchanged from the original A&S model is how precipitation quantification is handled by the parameterization. It is assumed that all condensation takes place in the updraft ensemble. Moreover, precipitation production is taken to be proportional to the vertical flux of cloud water in the updraft. Similar ideas for precipitation calculations are employed in T89. These concepts can be traced back to the classic paper of Yanai (1973), which was strongly intertwined with the ideas developed in Arakawa and Schubert (1974).

Concerning adjustable parameters in Z&M/NCAR, there are at least two important ones. The first is the time-scale for adjustment of the cumulus ensemble with the large-scale forcing (the consumption of CAPE). It appears in the determination of the cloud base updraft mass flux, i.e., the closure assumption. Another important parameter in the scheme is a coefficient determining the strength of the downdraft ensemble. Zhang and McFarlane (1995) specify such coefficient so as to ensure that the strength of the downdraft ensemble is constrained both by the availability of precipitation and by the requirement that the net mass flux at cloud base be upward. This coefficient depends, in turn, on another parameter specifying an upper-bound for the fraction of precipitation that is evaporated in the downdraft.

In what follows, a summary of the Z&M/NCAR formulation is presented. The presentation closely follows the description given in Kiehl et al. (1996). The large-scale budget equations distinguish between a cloud and a sub-cloud layer where temperature and moisture responses to convection in the cloud layer are written in terms of bulk convective fluxes:

$$c_p\left(\frac{\partial T}{\partial t}\right)_{DEEP} = -\frac{1}{\rho}\cdot\frac{\partial}{\partial z}(M_u S_u + M_d S_d - M_c S) + L\cdot(C - E) \quad (4.1)$$

$$\left(\frac{\partial q}{\partial t}\right)_{DEEP} = -\frac{1}{\rho}\cdot\frac{\partial}{\partial z}(M_u q_u + M_d q_d - M_c q) + E - C \quad (4.2)$$

and the sub-cloud layer response is written as

$$c_p\left(\rho\cdot\frac{\partial T}{\partial t}\right)_m = \frac{1}{\Delta z_m}\cdot\{M_b\cdot[S(z_m) - S_u(z_m)] + M_d\cdot[S(z_m) - S_d(z_m)]\} \quad (4.3)$$

$$\left(\rho\cdot\frac{\partial q}{\partial t}\right)_m = \frac{1}{\Delta z_m}\cdot\{M_b\cdot[q(z_m) - q_u(z_m)] + M_d\cdot[q(z_m) - q_d(z_m)]\} \quad (4.4)$$

where the net vertical mass flux in the convective region, M_c, is comprised of upward, M_u, and downward, M_d, components; C and E are the large-scale condensation and evaporation rates; S, S_u, S_d, q, q_u and q_d are the corresponding values of the dry-static energy and of the specific humidity; Δz_m is the depth of the mean sub-cloud layer (the subscript m denotes sub-cloud layer properties); z_m is the height of the sub-cloud layer; and M_b is the cloud base mass flux.

The cloud model is composed of two components, the updraft ensemble and the downdraft ensemble. The updraft ensemble is represented as a collection of entraining plumes, each with a characteristic fractional entrainment rate. Mass carried upward by the plumes is detrained into the environment in a thin layer at the top of the plume where the detrained air is assumed to have the same thermal properties as in the environment. The top of the shallowest of the convective plumes is assumed to be no lower than the mid-tropospheric minimum in saturated moist-static energy, h^*, ensuring that the cloud top detrainment is confined to the conditionally stable portion of the atmospheric column. Each plume is assumed to have the same value for the cloud base mass flux, and the vertical distribution of the cloud updraft mass flux is given by

$$M_u = M_b \cdot \int_0^{\lambda_D} \frac{1}{\lambda_0} \cdot e^{\lambda(z-z_m)} \cdot d\lambda \tag{4.5}$$

λ_0 is the maximum detrainment rate, and λ_D is the entrainment rate for the updraft that detrains at height z which is iteratively determined by requiring that

$$h_b - h^* = \lambda_D \cdot \int_{z_m}^{z} [h_b - h(z')] \cdot e^{\lambda_D \cdot (z'-z)} \cdot dz' \tag{4.6}$$

h_b is the environmental moist-static energy at the detrainment level. The budget equations for dry-static energy, specific humidity, and cloud liquid water, l, are written as

$$\frac{\partial}{\partial z}(M_u S_u) = (E_u - D_u) \cdot S + LC_u \tag{4.7}$$

$$\frac{\partial}{\partial z}(M_u q_u) = E_u q - D_u q^* - C_u \tag{4.8}$$

$$\frac{\partial}{\partial z}(M_u l) = -D_u l + C_u - R_r \tag{4.9}$$

where the conversion from cloud water to rain is given by

$$R_r = c_0 \cdot M_u \cdot l \tag{4.10}$$

and $c_0 = 2 \cdot 10^{-3} m^{-1}$.

Downdrafts are assumed to exist whenever there is precipitation production in the updraft ensemble, where the downdrafts start at or below the bottom of the updraft detrainment layer. Detrainment from the downdrafts is confined to the sub-cloud layer, where all downdrafts have the same mass flux at the top of the downdraft region.

Accordingly, the ensemble downdraft mass flux takes a similar form to (4.5) but includes a "proportionality factor" to ensure that the downdraft strength is physically consistent with precipitation availability. This coefficient takes the form

$$\alpha = \mu \cdot (\frac{P}{P + E_d}) \tag{4.11}$$

where P is the total precipitation in the convective layer, and E_d is the rain evaporation required to maintain the downdraft in a saturated state. This formalism ensures that the downdraft mass flux vanishes in the absence of precipitation, and that evaporation cannot exceed some fraction μ, of the precipitation, where $\mu = 0.2$.

The parameterization is closed, i. e., the cloud base mass fluxes are determined as a function of the rate at which the cumulus consume CAPE. Since the large-scale temperature and moisture changes in both the cloud and subcloud layer are linearly proportional to the cloud base updraft mass flux, the CAPE change due to convective activity can be written as

$$(\frac{\partial A}{\partial t})_{DEEP} = -M_b \cdot F \tag{4.12}$$

where F is the CAPE consumption rate per unit cloud base mass flux. The closure condition is that CAPE is consumed at an exponential rate by cumulus convection with characteristic adjustment time-scale τ;

$$M_b = \frac{A}{\tau \cdot F} \tag{4.13}$$

A more complete discussion of the formulation can be found in Zhang and McFarlane (1995).

4.2 New Model for Tropical Deep Cumulus

Three important features of the proposed deep cumulus formulation include the ability to calculate precipitation efficiencies, a new postulation relating cumulus buoyancy to solar radiation, and the implicit account of latent heat release that manifest itself by scaling cumulus drafts to observed magnitudes. Some of its outstanding limitations include the following:

- the scheme considers the cumulus effects only in the energy and in the moisture budgets but not in the momentum budget and;
- the representation is *not* suitable for a time evolution approach where the cyclic level of model complexity would have to be included[1].

[1]This is why one can postulate that solar radiation ultimately maintains cumulus buoyancy.

In the context of the model being studied, the relevant state is the zonally and annually averaged tropical thermally direct circulation (Hadley cell). Therefore, the scheme is aiming to represent *first order* effects of deep cumulus convection associated with the zonally and annually averaged ascending motion of this cell.

Conservation of energy and water vapor are written as:

$$\frac{\partial \overline{s}}{\partial t} = -\frac{1}{a_e c} \cdot \frac{\partial}{\partial \varphi}(\overline{v}\,\overline{s}\,c) - \frac{\partial}{\partial \sigma}(\overline{\omega}\,\overline{s}) + Q - \frac{\partial}{\partial \sigma}(\overline{\omega' s'})|_{DEEP} \tag{4.14}$$

$$\frac{\partial \overline{q}}{\partial t} = -\frac{1}{a_e c} \cdot \frac{\partial}{\partial \varphi}(\overline{v}\,\overline{q}\,c) - \frac{\partial}{\partial \sigma}(\overline{\omega}\,\overline{q}) + S - \frac{\partial}{\partial \sigma}(\overline{\omega' q'})|_{DEEP} - C_{grid} \tag{4.15}$$

$\overline{s}$ and $\overline{q}$ are the dry-static energy and the specific humidity respectively. Q encompasses the shortwave and longwave radiation terms (Q_{sw} and Q_{lw}, respectively), as well as a convective heating rate representing the effects of all types of sub-grid convection other than deep cumulus.

$\partial(\overline{\omega' s'})|_{DEEP}/\partial\sigma$ is the cumulus heating/cooling term that one wishes to parameterize. In (4.15), S includes the source of humidity to the Hadley domain thru a bulk aerodynamic surface evaporation, and a Fickian-type eddy diffusion also meant to account for the effects of other sub-grid convection in the moisture budget. $\partial(\overline{\omega' q'})|_{DEEP}/\partial\sigma$ is the deep cumulus moistening/drying term that will be parameterized, and C_{grid} accounts for the grid point condensation. Note that the heating due to this condensation is neglected. The main reason for this is that grid point saturation is viewed here mainly as an artifact to maintain "physically" reasonable values for specific humidity. Furthermore, it accounts for the precipitation that, ideally, should have been discounted in the parameterized term for deep cumulus. As described ahead, latent heat is being *implicitly* accounted in the deep cumulus scheme with the use of the coefficient C_{emp} in (4.28). The current inability to properly satisfy the water vapor budget without violating the continuum requirement is what prompts one to still include a C_{grid} term in (4.15). If the ultimate representation for precipitating clouds was available, this term would not be needed. Moreover, one must not forget that, in the Hadley model, each grid point is representing a 3° latitude band *over the whole tropics*. For example, the first grid point is centered at about 1.5°N, representing the latitude belt from the Equator to 3°N. This region covers an area of approximately 13 million square kilometers. Saturation at only this grid point would imply precipitation over the aforementioned area, which is quite out of proportions. Therefore, to include such heating is equivalent to state that grid point saturation is comparable to observed precipitation. That it is not should already be clear from the context of the Hadley cell under investigation here.

Figure 4.1 presents a 2-D schematic of the processes responsible for building the deep cumulus representation. Also shown is a plane view of a grid box with the cloudy area of the deep cumulus. Inside the cloud, the temperature (T_c) and the specific humidity (q_c) take the values of the moist-adiabatic lapse-rate and of the correspondent saturation. A three-dimensional grid box column showing remaining aspects of the deep cumulus representation is shown in figure 4.2. V_c and V_d represent the bulk in-cloud draft and the compensating subsidence in the grid box, respectively.

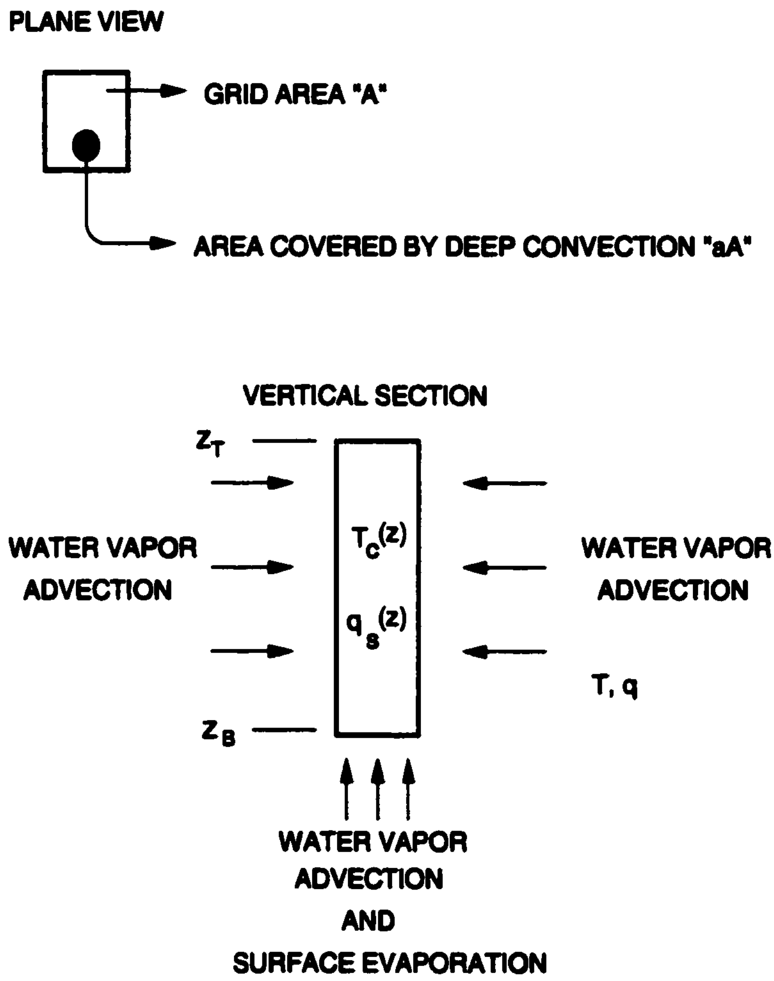

Figure 4.1: Schematic illustration showing the 2-D geometry of the deep cumulus scheme. In the plane view, a grid box with generic area A of a numerical model is shown. Lower-case a has the same meaning as in the equations. In the vertical section, a cross-section of the *cloud* is shown.

The top-hat method [Bjerknes (1938); Kuo (1974); Anthes (1977)] is used here to derive expressions for the sub-grid terms. It is defined that,

$$X \equiv \overline{X} + X' \tag{4.16}$$

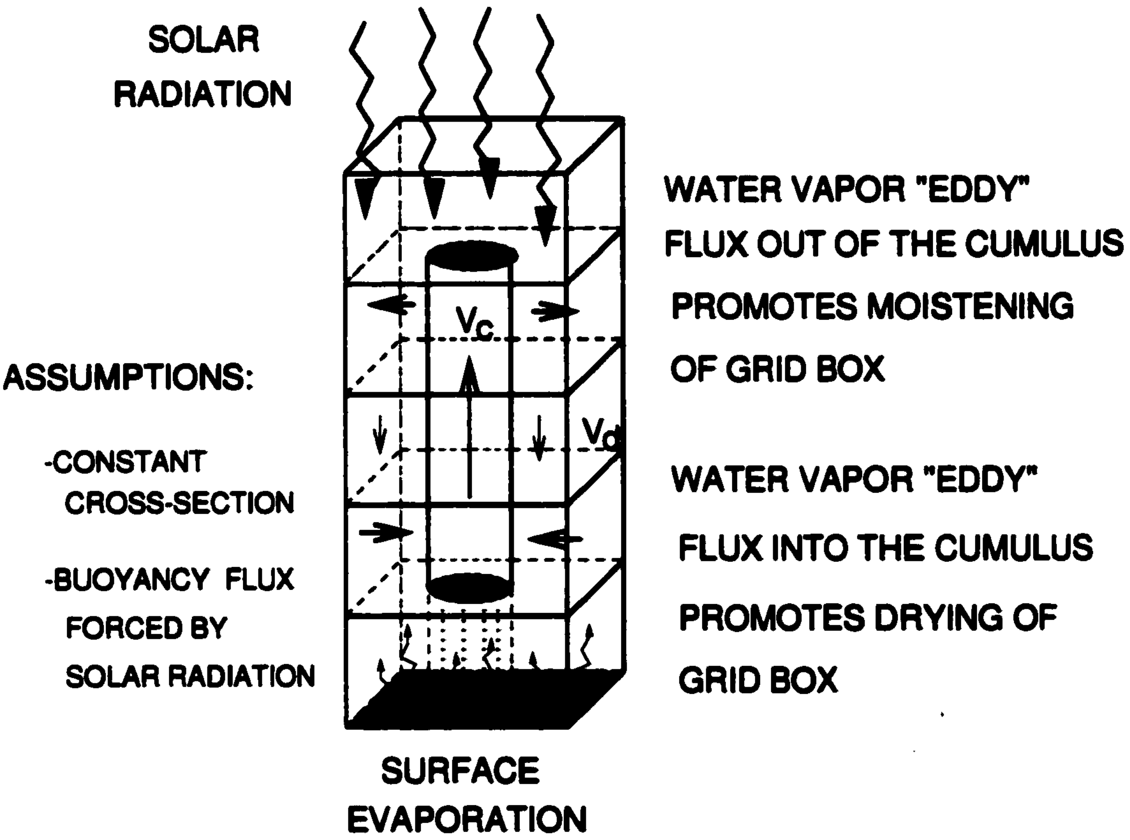

Figure 4.2: Three-dimensional schematic of the deep cumulus representation showing relevant physical processes accounted for in the scheme. The water vapor eddy fluxes are indicated to illustrate how the drying and moistening would occur if the cloud "boundaries" were represented.

$$X_c \equiv \overline{X} + X'_c \tag{4.17}$$

$$X_d \equiv \overline{X} + X'_d \tag{4.18}$$

$\overline{X}$ is the average value of X over the entire grid area A depicted in figure 4.1. Thus, following Anthes (1977):

$$\overline{X} \equiv \int_A X \cdot dA' = (1-a)\overline{X}_d^d + a\overline{X}_c^c \tag{4.19}$$

$\overline{X}_c^c$ and $\overline{X}_d^d$ are given by:

$$\overline{X}_c^c \equiv \int_{aA} X_c \cdot dA' \tag{4.20}$$

$$\overline{X}_d^d \equiv \int_{(1-a)A} X_d \cdot dA' \tag{4.21}$$

From (4.19) one obtains:

$$\overline{\omega' X'} = (1-a)\overline{(\omega_d - \overline{\omega})(X_d - \overline{X})}^d + a\overline{(\omega_c - \overline{\omega})(X_c - \overline{X})}^c \tag{4.22}$$

Making the approximations that:

$$\overline{X_c \omega_c}^c = \overline{X}_c^c \overline{\omega}_c^c \tag{4.23}$$

$$\overline{X_d \omega_d}^d = \overline{X}_d^d \overline{\omega}_d^d \tag{4.24}$$

And then substituting for $\overline{\omega}_d^d$ and $\overline{X}_d^d$ from (4.19) into (4.22), one finds:

$$\overline{\omega' X'} = \frac{a}{1-a}(\overline{\omega}_c^c - \overline{\omega})(\overline{X}_c^c - \overline{X}) \tag{4.25}$$

The determination of the cloudy area a follows Kuo (1974). The underlying hypothesis is that the source of moisture to create the deep cumulus in this fractional area is supplied by its surroundings in a certain time-scale τ (see fig. 4.1). Thus,

$$a = \tau \cdot \frac{\int_0^1 (\partial \overline{q}/\partial t)_{\mathrm{GRID}} \cdot d\sigma}{M_c} \tag{4.26}$$

M_c, the amount of moisture needed to create the deep cumulus ensemble, is given by:

$$M_c = \frac{1}{L_v} \cdot \int_{\sigma_{TOP}}^{\sigma_{BOTTOM}} (\overline{h_c^c} - \overline{h}) \cdot d\sigma \tag{4.27}$$

L_v is the latent heat of evaporation, and $\overline{h_c^c}$ and $\overline{h}$ are the moist-static energies of the cloud and of the grid point respectively. σ_{TOP} and σ_{BOTTOM} are the sigma-pressures of the top and of the bottom of the deep cumulus. One purpose of the fractional area a in the Hadley model is to serve as input for the cloudy-sky calculations of the NCAR radiation scheme. Even though our determination of cloud cover may seem rudimentary, it is noted that the radiation calculations based on it employ many *ad-hoc* assumptions, such that a complex formulation for a is not needed [Briegleb (1992)].

Experimental studies of fully turbulent dry convection between horizontal plates have indicated that, away from boundary layers and lateral walls, the balances of turbulent kinetic energy and entropy perturbation establish two controlling quantities when the convective regime is not affected by molecular diffusivity: the separation between plates and the buoyancy flux [Townsend (1998)]. Tropical deep cumulus convection should, to a first approximation, be similar to turbulent dry convection modified to account for buoyancy increase due to latent heat release. Thus, a scale for the cloud bulk draft may be written as:

$$\overline{\omega_c^c} - \overline{\omega} = C_{emp} \cdot (\frac{\Delta p}{\rho g})^{-2/3} \cdot (\overline{\omega_c' s_c'}^c)^{1/3} \tag{4.28}$$

C_{emp} is an empirical constant (non-dimensional) that is used to account for latent heat effects on buoyancy. Δp is the pressure difference between the surface and the tropopause, ρ is the air density and g is the acceleration of gravity.

The hypothesis that cumulus buoyancy is ultimately maintained by solar radiation translates into:

$$-\frac{\partial}{\partial\sigma}(\overline{\omega_c' s_c'}^{c}) = a Q_{sw} \tag{4.29}$$

Thus,

$$-\frac{\partial}{\partial\sigma}(\overline{\omega' s'})|_{DEEP} = \frac{a}{1-a} \cdot a Q_{sw} = \frac{a^2}{1-a} \cdot Q_{sw} \tag{4.30}$$

It should be noted that evidence of enhanced absorption of solar radiation in cloudy atmospheres is being accumulated in observational studies [e.g., Cess et al. (1999), Ramanathan et al. (1995)]. While the physics of this "anomalous" absorption is still unknown, it does not seem amiss to postulate causality between solar heating and cumulus buoyancy. The relation given by (4.30) is an attempt towards the reconciliation between theory and observations.

There is a technical problem with the implementation of (4.30) in the model. Strictly speaking, its use violates energy conservation since the cloud boundary fluxes are not used to calculate the heating/cooling just below and just above the cloud bottom and top. As explained later, if the theoretical framework to account for precipitating clouds as heat sources to the environment was in hand, this would not be problematic anymore. In truth, such deficiency has no important consequences in this study since the order of magnitude of the neglected term is much smaller than the remaining ones of the heat budget. The reason for this smallness is that the fractional area coverage a is on the order of 1% for the Hadley model. A simple scale analysis shows that the violation of energy conservation is less than 10^{-4} K/day.

A question that might arise related to the proposed postulation is due to claims that tropical precipitation over the oceans occurs primarily at night. Thus, how can one account for nocturnal deep cumulus convection in the framework being described? This question cannot be addressed by the proposed model. The aim in developing this scheme is to represent deep cumulus clouds for a climate (radiative-convective) equilibrium analysis. The Hadley model does not account for diurnal and annual cycles. Only the latitudinal distribution of top of atmosphere solar radiation is considered. The *life cycle* of deep precipitating systems cannot be accounted for in this context.

The remaining problem is the formulation of the precipitation efficiency equation. One begins by re-writing the moisture conservation law as:

$$\frac{\partial \overline{q}}{\partial t} = \frac{\partial \overline{q}}{\partial t}_{\mathrm{GRID}} + \frac{\partial \overline{q}}{\partial t}_{\mathrm{DEEP}} - C_{grid} \tag{4.31}$$

where, by analogy with (4.15):

$$\frac{\partial \overline{q}}{\partial t}_{\mathrm{GRID}} = -\frac{1}{a_e c} \cdot \frac{\partial}{\partial \varphi}(\overline{v}\,\overline{q}\,c) - \frac{\partial}{\partial \sigma}(\overline{\omega}\,\overline{q}) + S \tag{4.32}$$

and

$$\frac{\partial \overline{q}}{\partial t}_{\mathrm{DEEP}} = -\frac{\partial}{\partial \sigma}(\overline{\omega' q'})_{\mathrm{DEEP}} \tag{4.33}$$

The difficulty here lies in obtaining the precipitation efficiencies while satisfying the requirement of complete miscibility between water vapor and air in the specific humidity equation. A rational way to do so is to relate the precipitation efficiencies to the column integrated water vapor changes with:

$$\int_0^1 \frac{\partial \overline{q}}{\partial t} \cdot d\sigma = (1 - \mathrm{PE}) \cdot \int_0^1 \frac{\partial \overline{q}}{\partial t}_{\mathrm{GRID}} \cdot d\sigma \tag{4.34}$$

From (4.34) one can show that:

$$\mathrm{PE} = -\frac{\int_0^1 [(\partial \overline{q}/\partial t)_{\mathrm{DEEP}} - C_{grid}] \cdot d\sigma}{\int_0^1 (\partial \overline{q}/\partial t)_{\mathrm{GRID}} \cdot d\sigma} \tag{4.35}$$

Expanding (4.35):

$$\mathrm{PE} = -\frac{\int_0^1 [-\frac{\partial}{\partial \sigma}(\overline{\omega' q'})_{\mathrm{DEEP}} - C_{grid}] \cdot d\sigma}{\int_0^1 (\partial \overline{q}/\partial t)_{\mathrm{GRID}} \cdot d\sigma} = \frac{P}{\int_0^1 (\partial \overline{q}/\partial t)_{\mathrm{GRID}} \cdot d\sigma} \tag{4.36}$$

With $P = P_{\mathrm{DEEP}} + P_{\mathrm{GRID}}$, $P_{\mathrm{DEEP}} = \overline{\omega' q'}|_{\mathrm{DEEP}_{(\sigma=1)}}$, and $P_{\mathrm{GRID}} = \int_0^1 C_{grid} \cdot d\sigma$. Note that PE is calculated instead of specified. This is a crucial distinction between this method and previous ones. In other schemes, PE, or its equivalent, has been specified in many different ways with the aim of obtaining vertical profiles that are comparable to observations of tropical cumulus clouds. In analogy with (4.25), and given the schematic shown in figure 4.2, P_{DEEP} is written as:

$$P_{\mathrm{DEEP}} = \frac{a}{1-a} \cdot (\overline{\omega}_p^c - \overline{\omega}) \cdot (\overline{q}_p^c - \overline{q}_{\mathrm{SAT}}) \tag{4.37}$$

Where $\overline{\omega}_p^c$ and $\overline{q}_p^c$ are, respectively, the speed of ground-reaching precipitation and its specific humidity. Ideally, the calculation of these quantities must be based on micro-physical considerations. In this dissertation, $\overline{\omega}_p^c$ and

$\overline{q}_p^c$ are provisionally related to the bulk drafts and the water vapor specific humidity as follows:

$$\overline{\omega}_p^c - \overline{\omega} = -(\overline{\omega}_c^c - \overline{\omega})_{\text{at cumulus bottom}} \tag{4.38}$$

and

$$\overline{q}_p^c = \alpha \cdot (\overline{q})_{\text{at cumulus bottom}} \tag{4.39}$$

where α is a dimensionless coefficient. The ground-reaching precipitation calculated by (4.37) must not be taken from the water vapor budget at the lowest grid point. Here, the parameterized water vapor fluxes $\overline{\omega' q'}|_{\text{DEEP}}$ are re-calculated to partially account for P_{DEEP} as follows:

$$\overline{\omega' q'}|_{\text{DEEP}} = \frac{a}{1-a} \cdot (\overline{\omega}_c^c - \overline{\omega}) \cdot (\overline{q}_c^c - \overline{q}) - \frac{P_{\text{DEEP}}}{n} \tag{4.40}$$

where n is the number of grid box interfaces under conditional unstable stratification. Figure 4.3 illustrates the calculation of (4.40). In practice, such re-calculation only affects the flux divergences just below and just above the cumulus bottom and top, respectively. Moreover, the change in these flux divergences is not equivalent to the change that the removal of P_{DEEP} at the lower boundary would imply. This is one reason why grid point precipitation must still be included to satisfy the water vapor balance. As discussed earlier, the proper handling of P_{DEEP} would make the use of grid-scale saturation unnecessary to account for deep cumulus precipitation. It is not a trivial matter to accomplish such task. The problem is not one of simply removing the

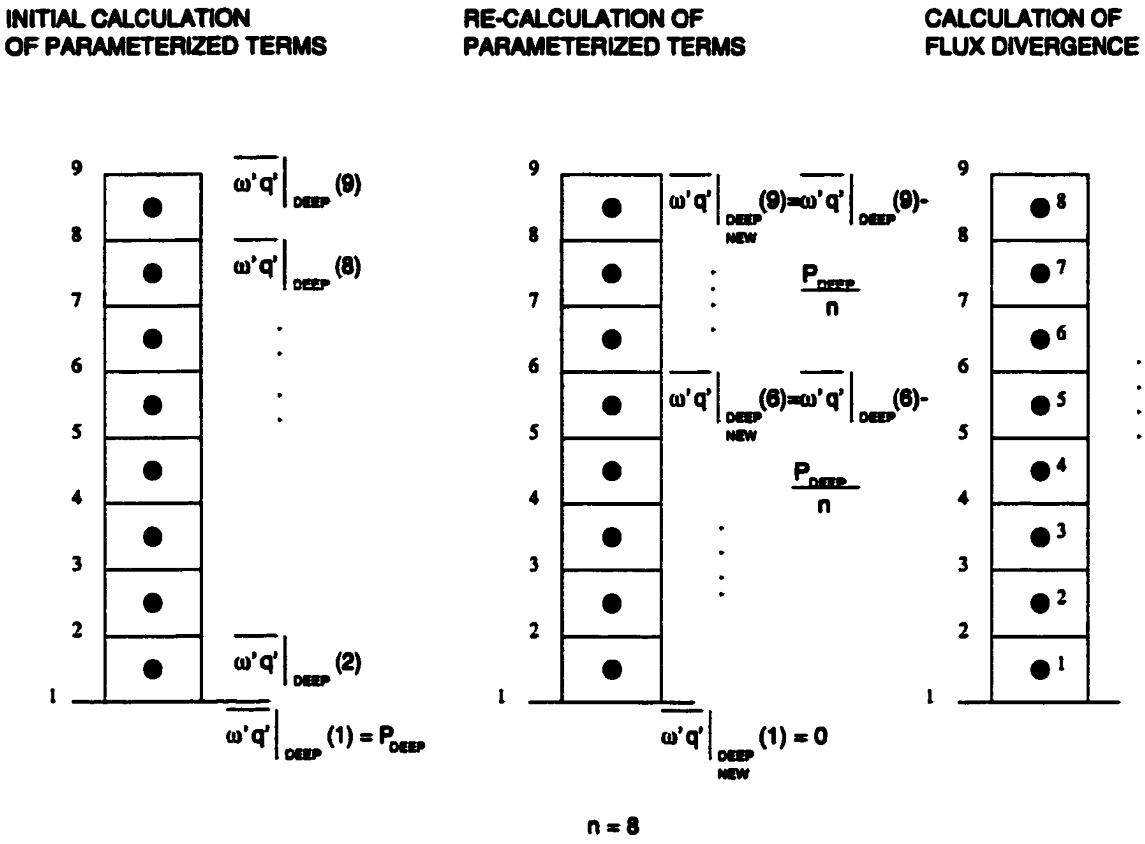

Figure 4.3: Calculation of the eddy water vapor fluxes due to the precipitating cumulus parameterization. Note that the ground-reaching precipitation is evenly discounted from the eddy fluxes in the conditionally unstable layer. In this example, this layer goes from grid point 2 to grid point 9.

ground-reaching precipitation from the overlying "cloud", but of removing it in a proper way, which would likely be model dependent.

Figures 4.4 and 4.5 highlight the crucial conceptual differences between the approach developed here and parameterizations in the A&S-type and Kuo-type categories. Note in figure 4.5 that the cumulus condensation rate term C occurs out of the model boundaries, as well as the ground-reaching precipitation flux P. The effects of precipitating clouds on their environment happens through modification of the eddy flux divergence terms over the "extended" lower boundary. Furthermore, the traditional surface fluxes associated with latent heat indicated in figure 4.4 are not needed anymore, since such fluxes do not materialize inside the model domain as indicated in figure 4.5. The main problem becomes the proper handling of the drying that must be accounted throughout the extended lower boundary, as discussed before.

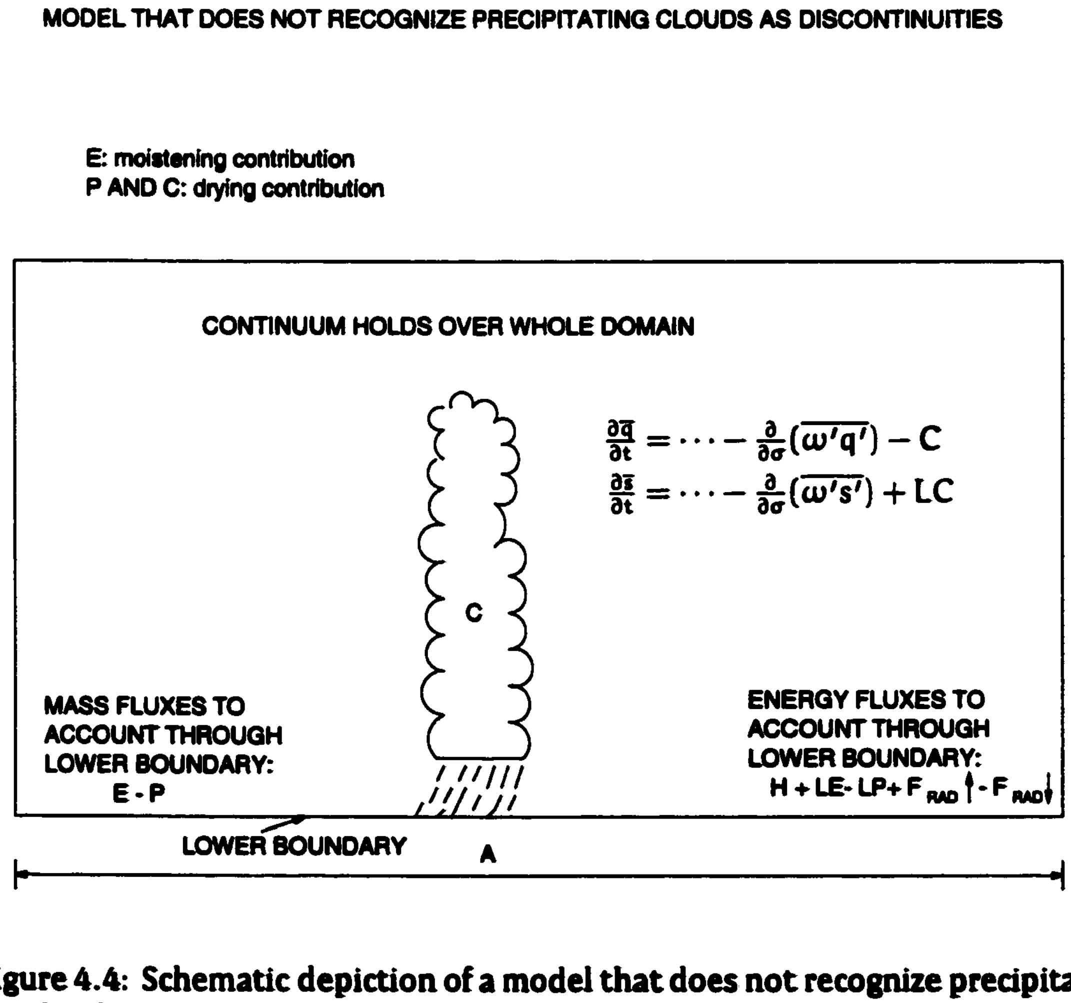

Figure 4.4: Schematic depiction of a model that does not recognize precipitating clouds as discontinuities. E: evaporation from surface; P: precipitation at surface; C: cumulus condensation rate; H: sensible heat fluxes from surface; L: latent heat of vaporization/condensation; F_{RAD}: radiative fluxes from and to surface; A: area.

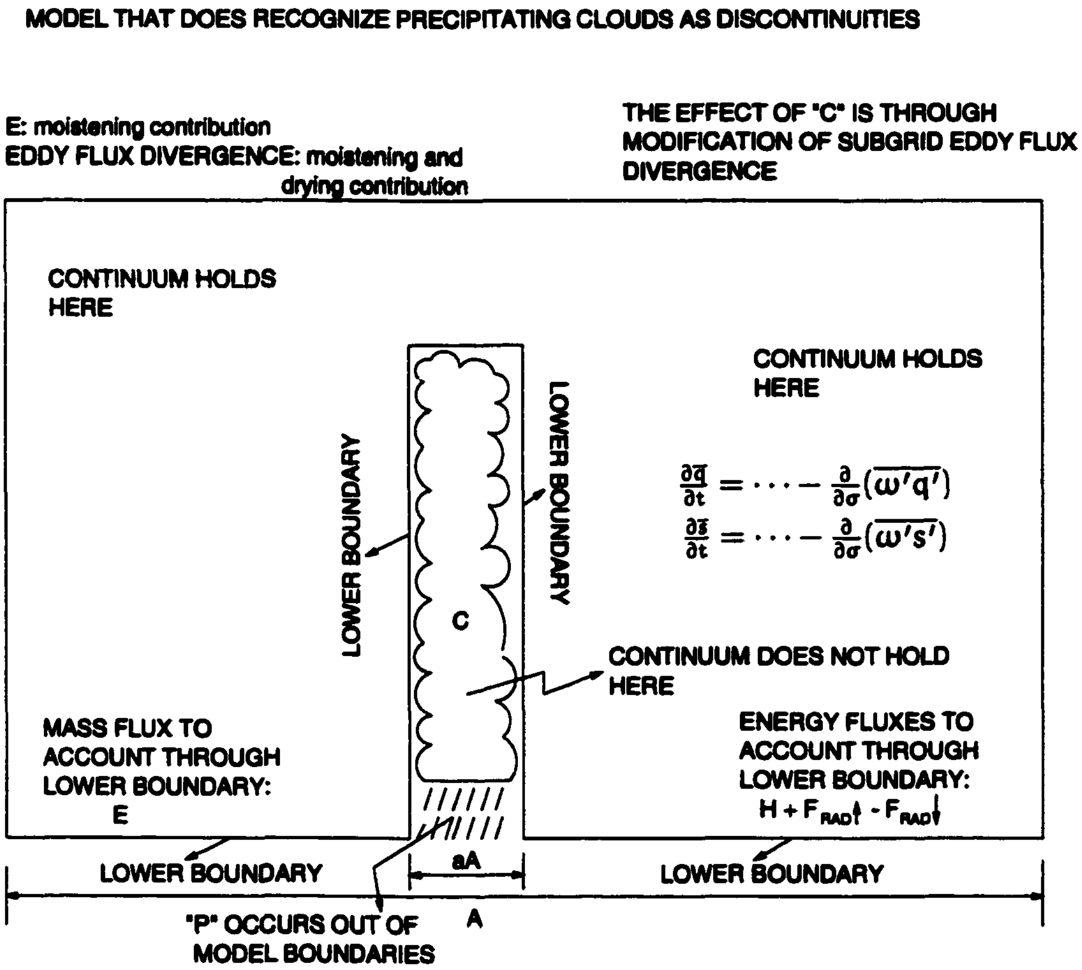

Figure 4.5: Schematic depiction of a model that does recognize precipitating clouds as discontinuities. a: fractional cloud coverage. Other terms have same meaning as in previous figure.

A control simulation that uses an equilibrium mean SST of 297 K has been performed to ascertain the model characteristics. The time evolution of surface evaporation and precipitation rates is shown in figure 4.6, while the latitudinal distribution of these quantities is presented in figure 4.7. Even though significant rain occurs up to 10°N, deep cumulus is present until 13°N. Sellers (1965) presents a zonally and annually averaged climatology of precipitation efficiencies for 10° latitude bands[2]. From 0° to 10° N, a value of 12.9 % is given there. I used an equivalent calculation to obtain precipitation efficiencies due to the cumulus parameterization. The results are shown in table 4.1 along with the PE values given by (4.36).

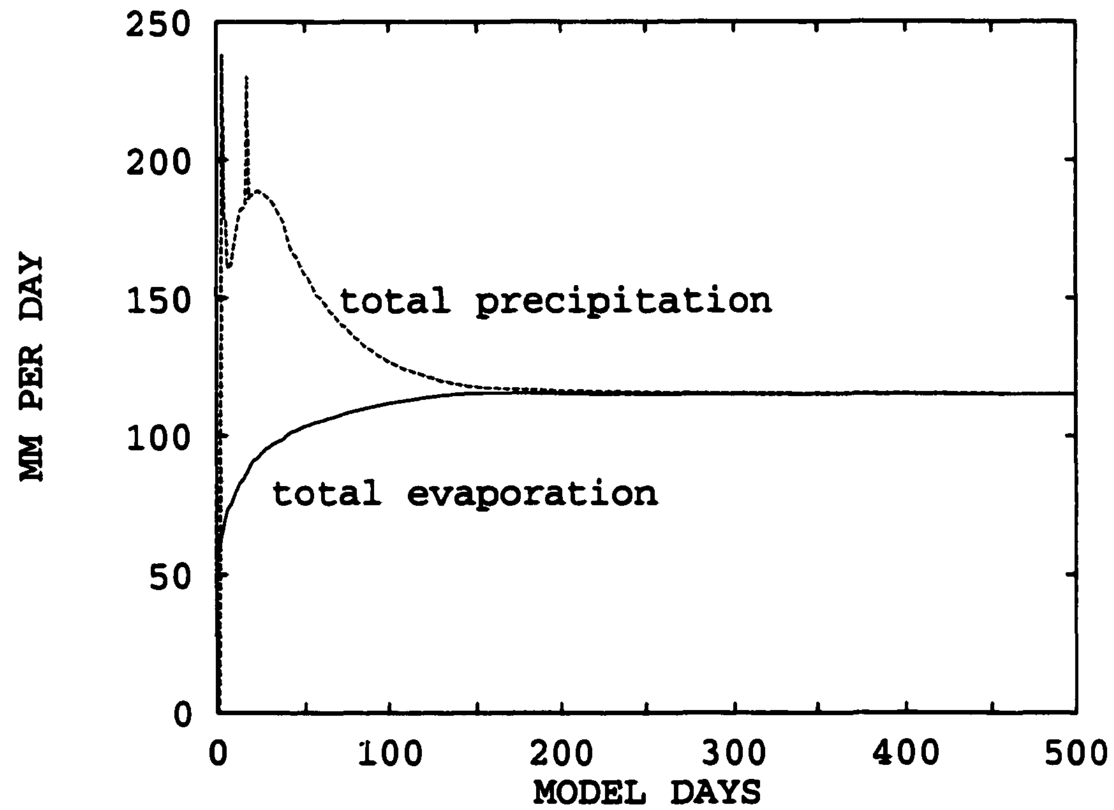

Figure 4.6: Time evolution of surface evaporation and ground-reaching precipitation rates for $\tau = 1700$ sec and $C_{emp} = 4$.

[2]His definition used the ratio between precipitation and total precipitable water.

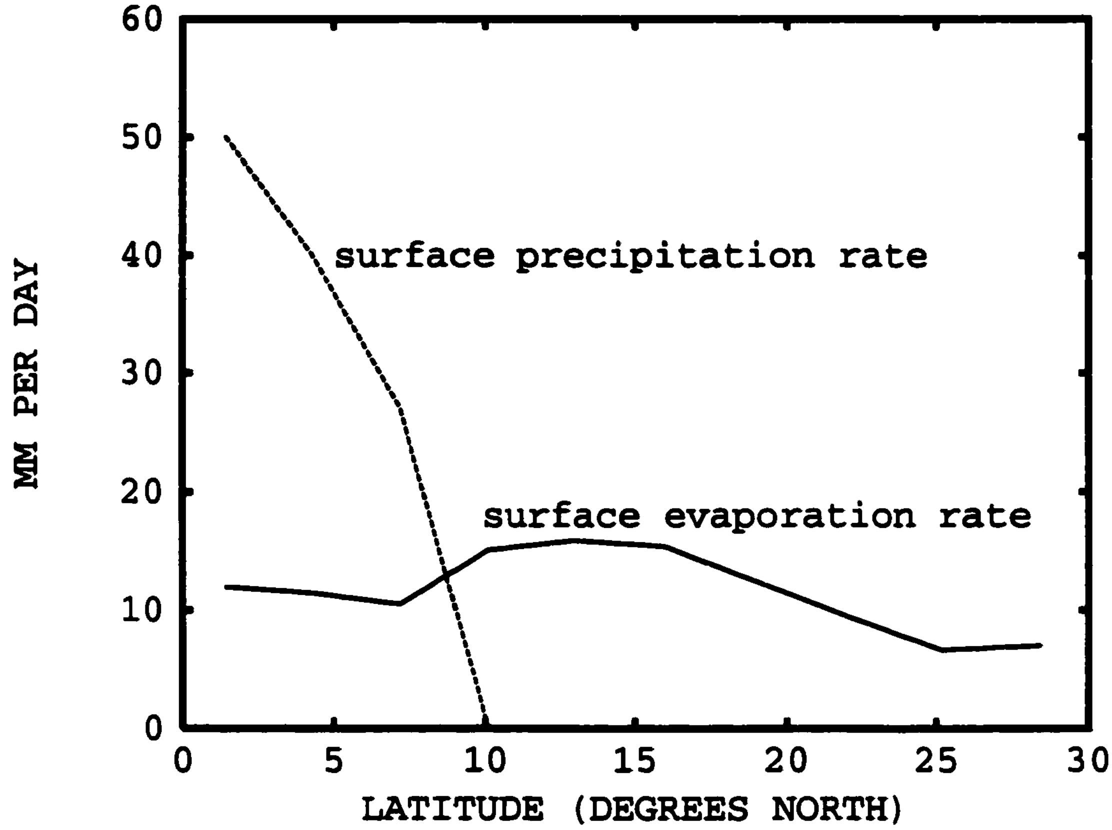

Figure 4.7: Latitudinal distribution of evaporation and precipitation rates at the surface.

Latitude	*PE (Sellers)(%)*	*PE (4.36)*
1.4° N	16.1	3.8
4.3° N	12.9	3.1
7.2° N	8.8	2.6

Table 4.1: Precipitation efficiencies calculated from the model simulation.

A problem with *any* parameterization of precipitating cumulus is that one is not able to strictly account for internal sources and sinks without violating the divergence theorem. Figure 4.2 allows for a different interpretation of this situation. What this figure attempts to illustrate is that the deep cumulus representation should not be viewed as part of the model domain. It is as if a hollow is punched from the lower boundary up to the level of neutral buoyancy whenever the closure is satisfied (that is, whenever the deep conditionally unstable layer is present). With this interpretation in mind, the cumulus boundary is an extension of the lower boundary, and the eddy fluxes figuratively indicated become "boundary" fluxes. Note that the problem of internal source/sink looses significance in this context. In developing the present parameterization, the attempt was made to alleviate this problem in the mathematical formulation. But to fully realize the idea of a moving lower boundary requires developments in the theory of fluid mechanics that are believed to be currently unavailable.

Chapter 5

Results

The approach taken in this chapter is to build the overall picture piece by piece. Latitudinal distributions close to the surface and at the top of the atmosphere are analyzed first. Then, vertical profiles throughout the symmetric tropical atmosphere are investigated. Finally, the results are summarized and framed in the context of the equilibrium climates obtained.

5.1 Latitudinal Distributions

Figures 5.1 and 5.2 show the latitudinal distributions of temperature differences at the sea surface and on the first grid point above the surface for the new and the ZM schemes, respectively. With regard to figure 5.1, two effects are distinguished: one associated with the Hadley cell and a more subtle one due to the lapse-rate feedback. The ascending and subsiding branches of the circulation produce modified responses. Essentially, the thermal damping[1] is, regardless of feedback, higher under the ascending branch region from the

[1]Here, *thermal damping* refers to the reduced air-sea temperature difference, when compared with the +2 K SST difference.

equator to about 13°N. This is understandable since the rising motion transports the heat away from low levels, making above-surface convective heating less efficient. By contrast, subsiding air in the sub-tropics is cooler than the surroundings at the level of the first grid point. As a result, above-surface heating is more efficient.

The effect of the lapse-rate feedback is to damp more the SST perturbation in the air above the surface than what it is otherwise. This can be seen by noting that curves B, E and F — all of them including the feedback due to lapse-rate change — are more effectively "packed" together. Curve D, which includes the feedback due to water vapor amount only, has less thermal damping than curves B, E and F. The response without feedbacks (curve C) establishes an upper-bound for the other distributions.

Figure 5.2 depicts a whole different scenario. In short, the results are much more sensitive to the deep cumulus scheme itself, while the previous analyses showed that they are predominantly modulated by the Hadley motion. In particular, the water vapor amount feedback has a strong effect on the equilibrium temperature difference of the first grid-point, amplifying the imposed surface warming (curves B, D and E). When the amplifying effect of the water vapor feedback is disabled, there is cooling of the air above the surface under the ascending branch of the Hadley cell, as evidenced by negative air-sea temperature differences (curves C and F). The lapse-rate feedback (curve F) tends to smooth such pattern as contrasted to the result with no feedbacks (curve C). Interestingly, the pattern of warmer air under the descending branch than under the ascending one is noticeable only with no feedbacks (curve C), or when they are operating individually (curves D and F). When a combination of them is used (curves B and E), the first grid point

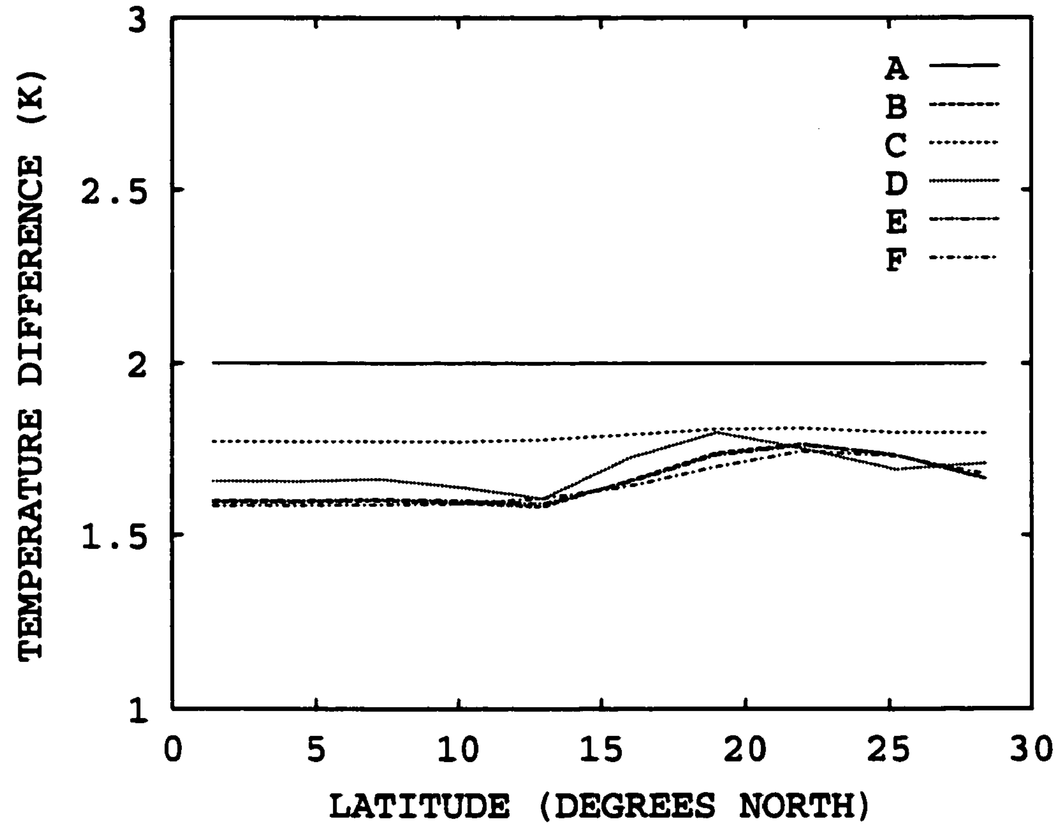

Figure 5.1: Latitudinal distribution of SST difference and temperature difference of the first grid point in the Hadley model using novel cumulus model. A: SST difference; B: temperature difference with all feedbacks; C: temperature difference without feedbacks; D: temperature difference with water vapor amount feedback only; E: temperature difference with water vapor and lapse-rate feedbacks; F: temperature difference with lapse-rate feedback only.

temperature difference is more sensitive under the ascending branch. These results hint on the comparative role of the ZM scheme and the mean thermal circulation in affecting the air-sea temperature differences.

The schematic shown in figure 5.3 illustrates the compensative effect of the lapse-rate feedback when the inverse experiments are performed with the new cumulus model, and the additive effect of the water vapor feedback when the experiments are done with the ZM scheme. These results are better appreciated upon looking at tables 5.1 and 5.2 simultaneously.

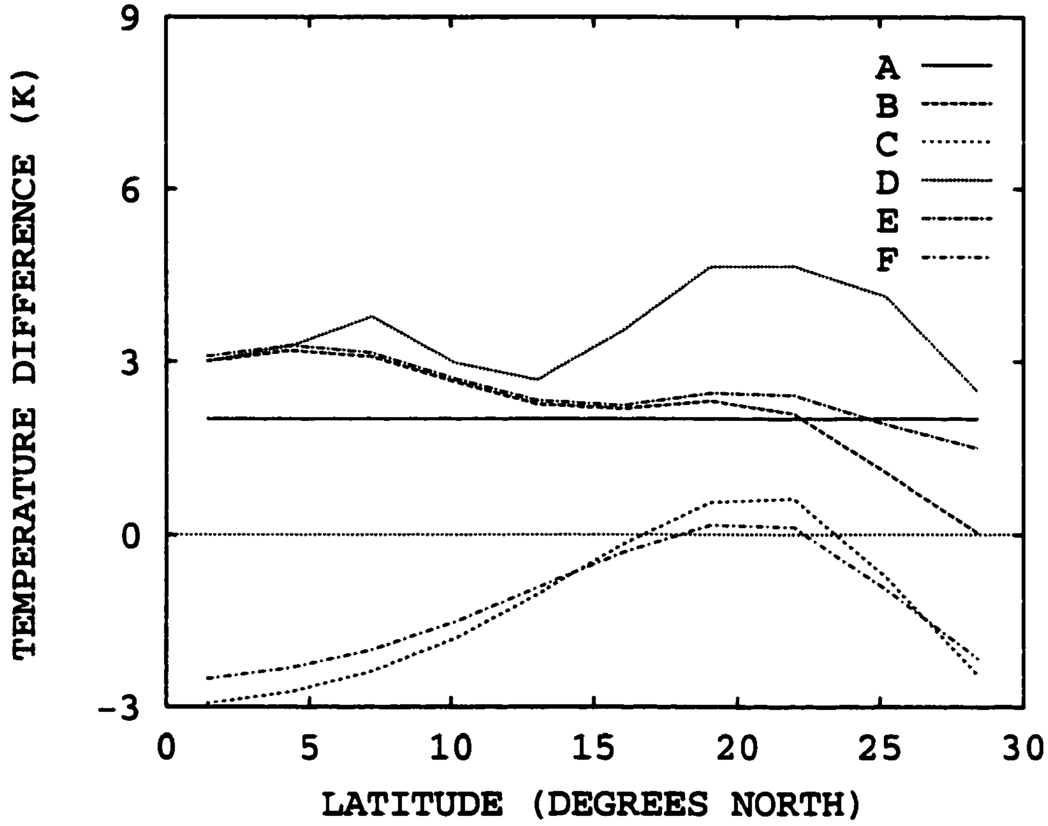

Figure 5.2: Latitudinal distribution of SST difference and temperature difference of the first grid point in the Hadley model using ZM cumulus model. A: SST difference; B: temperature difference with all feedbacks; C: temperature difference without feedbacks; D: temperature difference with water vapor amount feedback only; E: temperature difference with water vapor and lapse-rate feedbacks; F: temperature difference with lapse-rate feedback only.

Distributions of top of the atmosphere radiative flux differences are presented in figures 5.4, 5.5, and 5.6. Using the new cumulus model and including all feedbacks, figure 5.4 shows the strongly nonlinear sensitivity of the longwave fluxes over the subsiding branch of the Hadley cell. This sensitivity is due to the drying promoted by an acceleration of the thermal circulation,

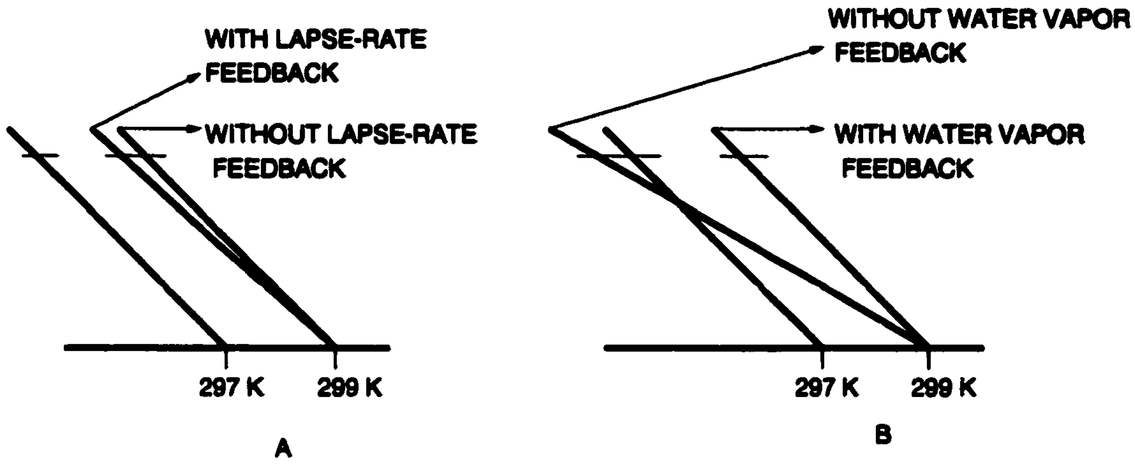

Figure 5.3: Schematic showing the role of: A) lapse-rate feedback with new cumulus model and; B) water vapor feedback with ZM cumulus model (as pertaining to first model grid point.)

which in turn reduces the infrared opacity in the region of subsidence. A similar behavior has been found in inverse experiments without including a parameterization for deep clouds [Fleischfresser (1999b)]. As a consequence, it is concluded that the Hadley cell has a crucial role in establishing this pattern. Specifically, the nonlinear behavior of the infrared flux difference is a consequence of the formulation in the NCAR column radiation model [equation (2.6)]. Thus, one appreciates the importance of using a detailed radiation parameterization in studying climate stability. Newtonian cooling formulations, specified cooling rates, and gray radiation codes would not show this feature.

The above-mentioned behavior is due to the water vapor feedback, which allows for changes of the moisture amount and distribution when the surface temperature is perturbed. When no feedbacks are allowed, as in figure 5.5,

Table 5.1: Zonally-averaged temperature differences of the first grid point using new cumulus model ($[T]_{(1)}(297\,K) = 289.919\,K$). Symbols used are: $f_{h,T}$ - water vapor amount feedback factor due to surface temperature change; $f_{h,\Gamma}$ - water vapor distribution feedback factor due to lapse-rate change; f_{Γ} - lapse-rate feedback factor; f_{α} - cloud cover feedback factor.

FEEDBACKS	$[T]_{(1)}(299\,K)$ [K]	$\Delta[T]_{(1)}$ [K]
-	291.707	1.788
$f_{h,T}$	291.610	1.691
f_{Γ}	291.567	1.648
$f_{h,T}$, $f_{h,\Gamma}$, f_{Γ}	291.575	1.656
$f_{h,T}$, $f_{h,\Gamma}$, f_{Γ}, f_{α}	291.574	1.655

the nonlinear sensitivity is suppressed. The reason is simple: without feedbacks, even with an acceleration of the thermal circulation, the moisture distribution is kept constant at the equilibrium climate state with mean SST of 297 K. The suppression of this feedback allows for the appearance of a more subtle role for the Hadley circulation. The cell acceleration imparts more cooling to space in the ascending branch than in the subsiding flow, as evidenced by higher TOA infrared flux differences until 15° N. This result somewhat reflects the SST latitudinal distribution. Higher SST results in enhanced convective heat flux to the atmosphere. The circulation's rising motion transports this heat to higher levels where it is more effectively radiated to space, explaining the larger infrared flux difference over the ascending motion region. With no changes in the water vapor amount and distribution, the radiative opacity is not significantly altered.

Figure 5.6 shows results for the ZM scheme with all feedbacks. What one notes more prominently is the significant increase of infrared opacity over the

Table 5.2: Zonally-averaged temperature differences of the first grid point using ZM cumulus model ($[T]_{(1)}(297\,K) = 292.523\,K$). Symbols have the same meaning as in table 5.1.

FEEDBACKS	$[T]_{(1)}(299\,K)$ [K]	$\Delta[T]_{(1)}$ [K]
-	291.232	-1.291
$f_{h,T}$	296.044	3.521
f_{Γ}	291.295	-1.228
$f_{h,T}$, $f_{h,\Gamma}$, f_{Γ}	295.003	2.480
$f_{h,T}$, $f_{h,\Gamma}$, f_{Γ}, f_{α}	294.670	2.147

region of ascending motion, accompanied by some decrease over the descending air in the sub-tropics. The later is a consequence of an intensification of the mean circulation, as discussed before. The enhanced opacity at low latitudes is a result of the significant local moistening that occurs when the ZM scheme is used. This behavior will be fully discussed in section 5.3.

5.2 Symmetric Vertical Distributions

Profiles of zonally-averaged relative humidities are shown in figure 5.7. Two important contrasts are noteworthy: first, the ZM scheme is much more effective in drying middle and low tropospheric levels, when compared to the new cumulus representation. The difference is a result of the explicit formulation of the downdraft ensemble in the ZM model, which has a strong drying effect. Conversely, the new cumulus scheme accounts for downdrafts only in an implicit way, resulting in a much moister troposphere. Second, the ZM scheme causes a *moister* equilibrium climate when the SST is increased by 2

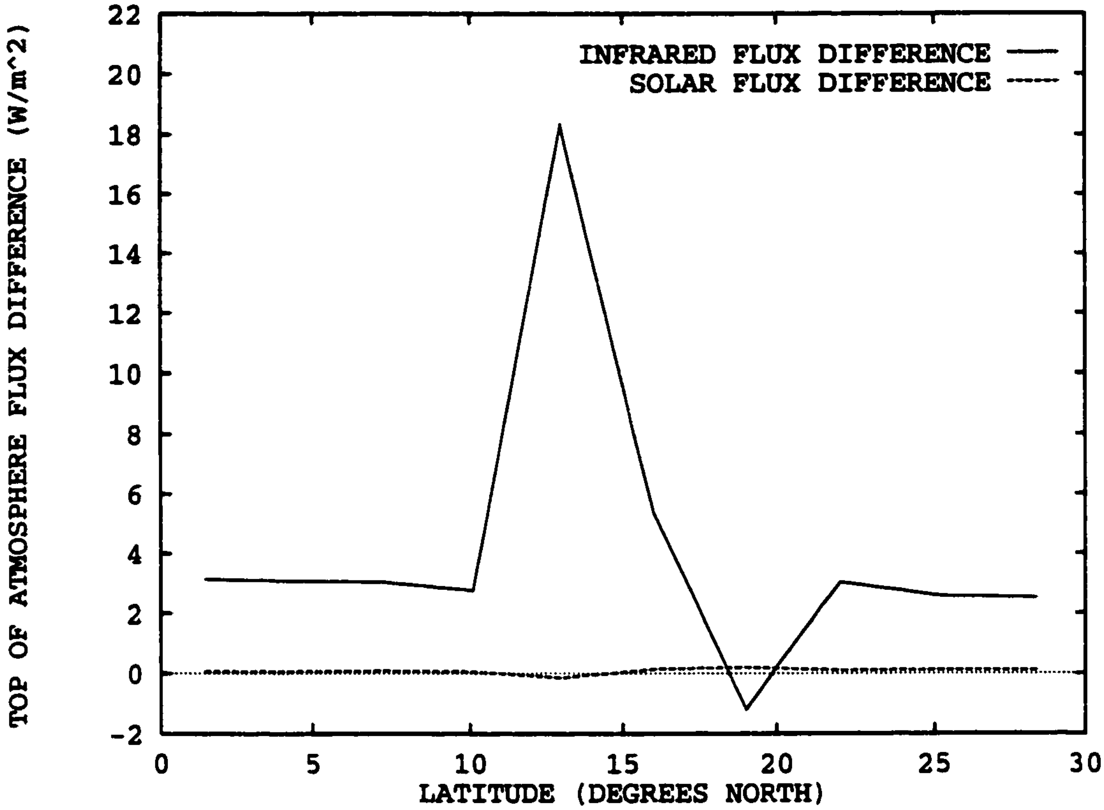

Figure 5.4: Top of atmosphere radiative flux differences including all feedbacks with the new cumulus model.

K. Notwithstanding, the new cumulus model causes a *drier* equilibrium climate. To fully understand these results,one must appreciate the synergism of the deep cumulus convection with the Hadley motion. A more complete discussion will be presented in the next section.

Figures 5.8 and 5.9 show the effect of the two most dominant feedbacks on relative humidity for both schemes. The convective schemes are generally effecting relative humidity changes in opposite directions. Figure 5.8 shows that the new cumulus model dries the lower troposphere (except for the boundary-layer) while moistening of upper-levels is predominant. The simulation with the ZM model behaves almost exactly in a reverse manner.

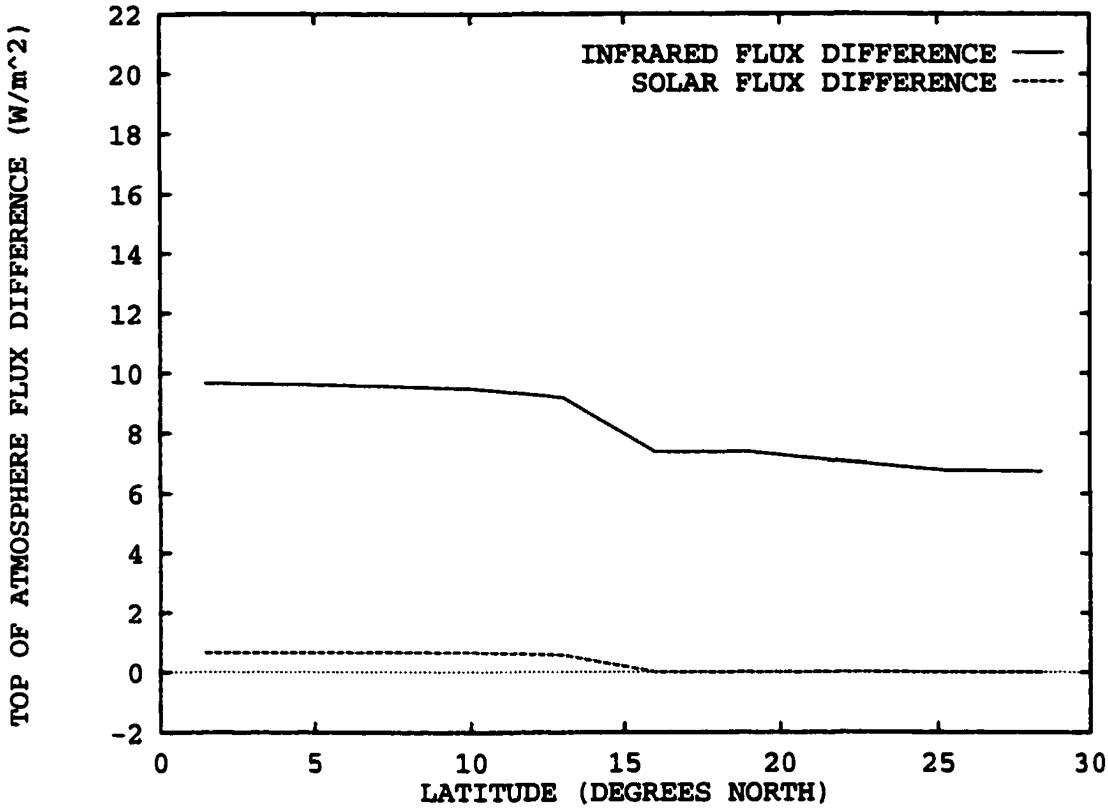

Figure 5.5: Top of atmosphere radiative flux differences *not* including feedbacks with the new cumulus model.

Moreover, its relative humidity changes are much more sensitive to the +2 K SST perturbation experiments. The lapse-rate feedback is more effective when the new cumulus model is used, since it dries the model atmosphere more significantly than what it moists with the ZM scheme (figure 5.9). This drying effect becomes more important at upper-levels, a result that is consistent with a reduced slope for the moist-adiabat in a warmer climate.

The behavior of the cloud cover feedback can be appreciated in figures 5.10 and 5.11. Again, the cumulus models have opposite effects. While the low and mid-levels are effected by drying when cloud cover is allowed to change with the new cumulus model, the ZM scheme promotes moistening at these

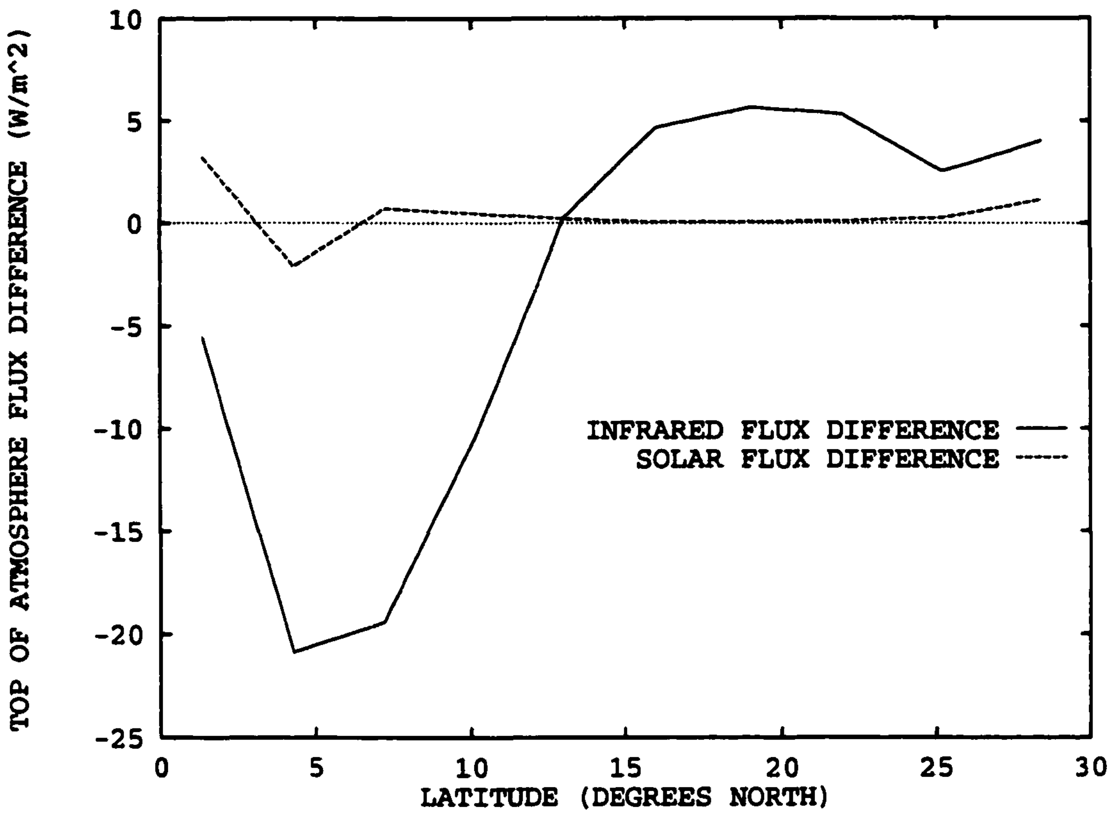

Figure 5.6: Top of atmosphere radiative flux differences including all feedbacks with the ZM cumulus model.

levels. These results are related to a reduction (increase) of the area coverage of clouds when the new (ZM) cumulus scheme is employed. Also, the cloud tops, in an average sense, are higher (lower) with the new (ZM) scheme in the warmer climate.

In figures 5.12, 5.13 and 5.14, the zonally-averaged vertical profiles of temperature difference using both schemes are presented. In connection with the new cumulus scheme, figure 5.12 shows that a + 2 K SST perturbation results in about + 3 K change in the upper-troposphere. The warming throughout the troposphere is mainly due to water vapor and lapse-rate feedbacks, the later being responsible for shifting it to upper-levels (figures 5.13

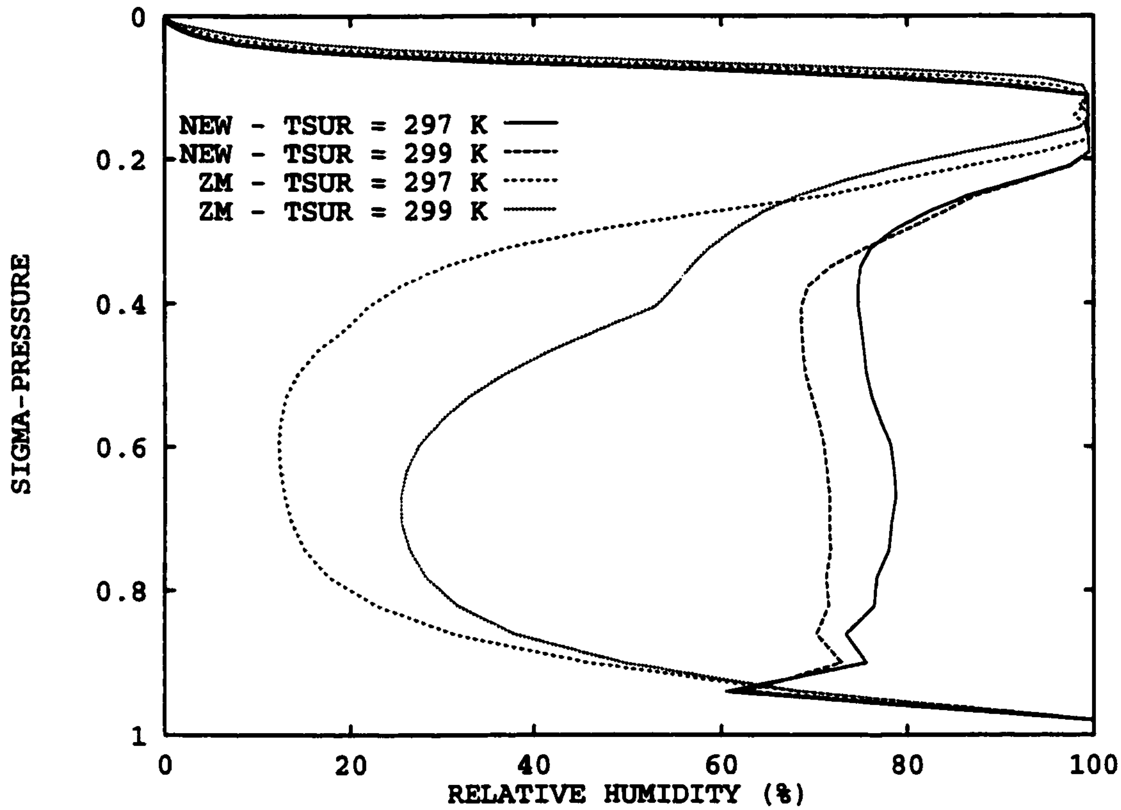

Figure 5.7: Profiles of zonally-averaged relative humidity.

and 5.14). Also noticeable from these figures, stratospheric cooling is a result of the water vapor feedback, regardless of the deep cumulus model used.

The thermal structure is much more sensitive when the ZM scheme is used. Figure 5.12 shows that an almost 8 K warming in the upper-troposphere is accomplished. In contrast with the results using the new cumulus model, the upper-tropospheric warming seems to be mainly due to the water vapor distribution feedback ($f_{h,\Gamma}$). The lapse-rate feedback alone is actually counteracting the warming in the upper-troposphere (figure 5.14). But since $f_{h,\Gamma}$ cannot be assessed in isolation, the exact cause of the upper-tropospheric

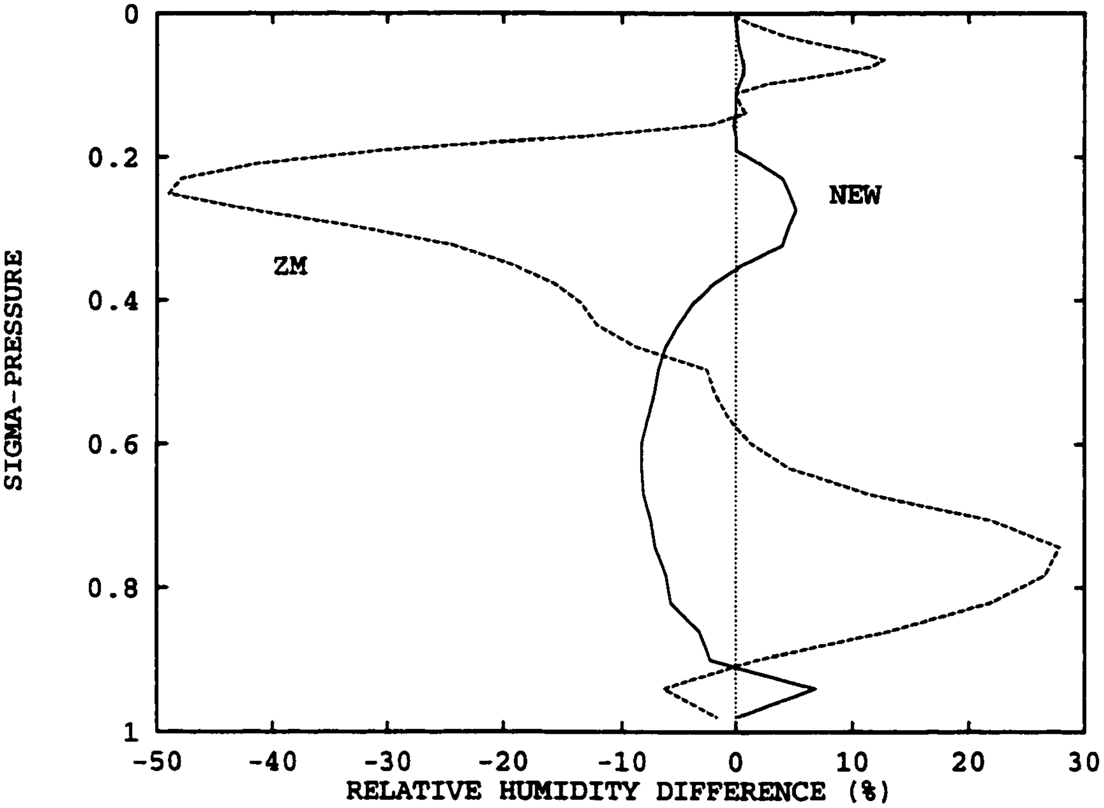

Figure 5.8: Profiles of zonally-averaged relative humidity differences between runs with surface temperatures of 299 K and 297 K. Results include water vapor amount feedback only ($f_{h,T}$).

warming is a bit more uncertain due to the inherent nonlinearity of the interaction between lapse-rate and water vapor changes.

In closing, figures 5.15 and 5.16 show profiles of zonally-averaged infrared cooling rates for SST = 297 K and 299 K with the new and the ZM schemes, respectively. In general, the infrared cooling rate sensitivity is more pronounced when the ZM scheme is used. The two figures show more infrared cooling at upper-levels. At lower levels, figure 5.15 shows more cooling until about $\sigma = 0.7$, and less cooling in between $\sigma = 0.7$ and $\sigma \simeq 0.55$. Figure 5.16 shows less cooling up to $\sigma = 0.6$. These differences are a consequence of the

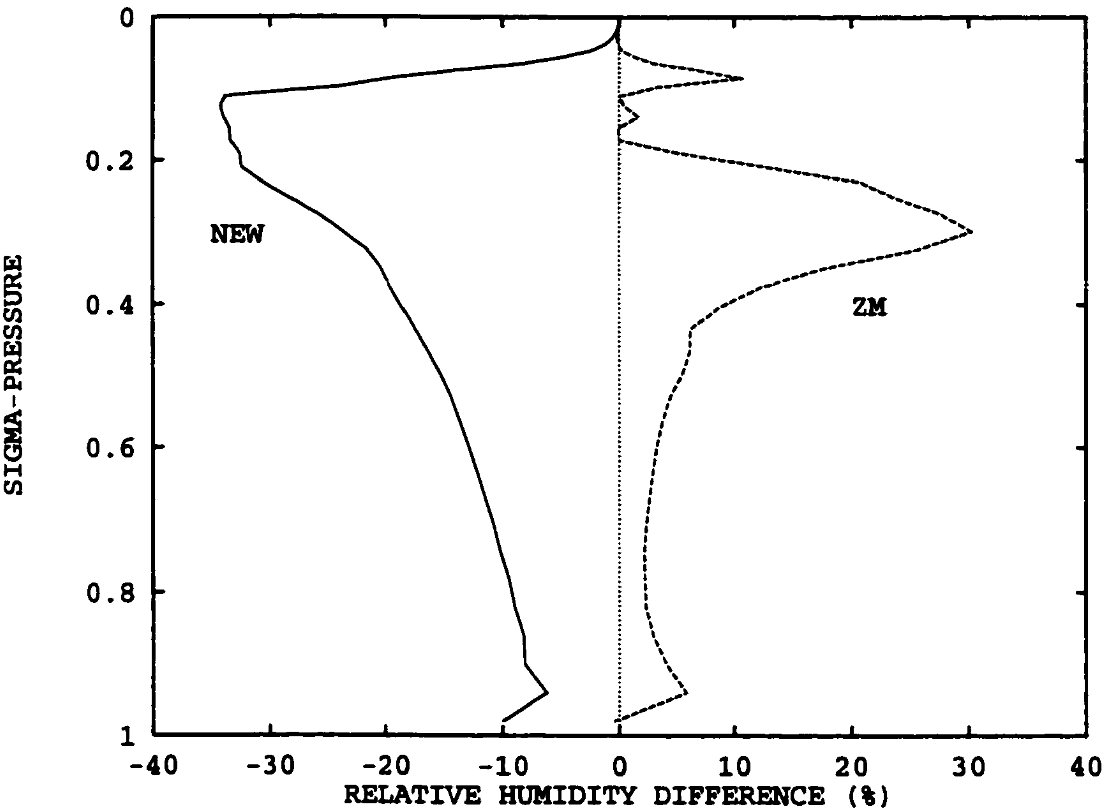

Figure 5.9: Profiles of zonally-averaged relative humidity differences between runs with surface temperatures of 299 K and 297 K. Results include lapse-rate feedback only (f_r).

distinct ways in which moisture is redistributed due to the synergism of the deep cumulus convection and the Hadley cell.

5.3 Discussion

A summary of the results from the previous sections is now attempted, and their significance in terms of the equilibrium analyses is presented.

Figures 5.17 to 5.20 show contour plots of the specific humidity and temperature difference fields respectively using the two deep cumulus schemes.

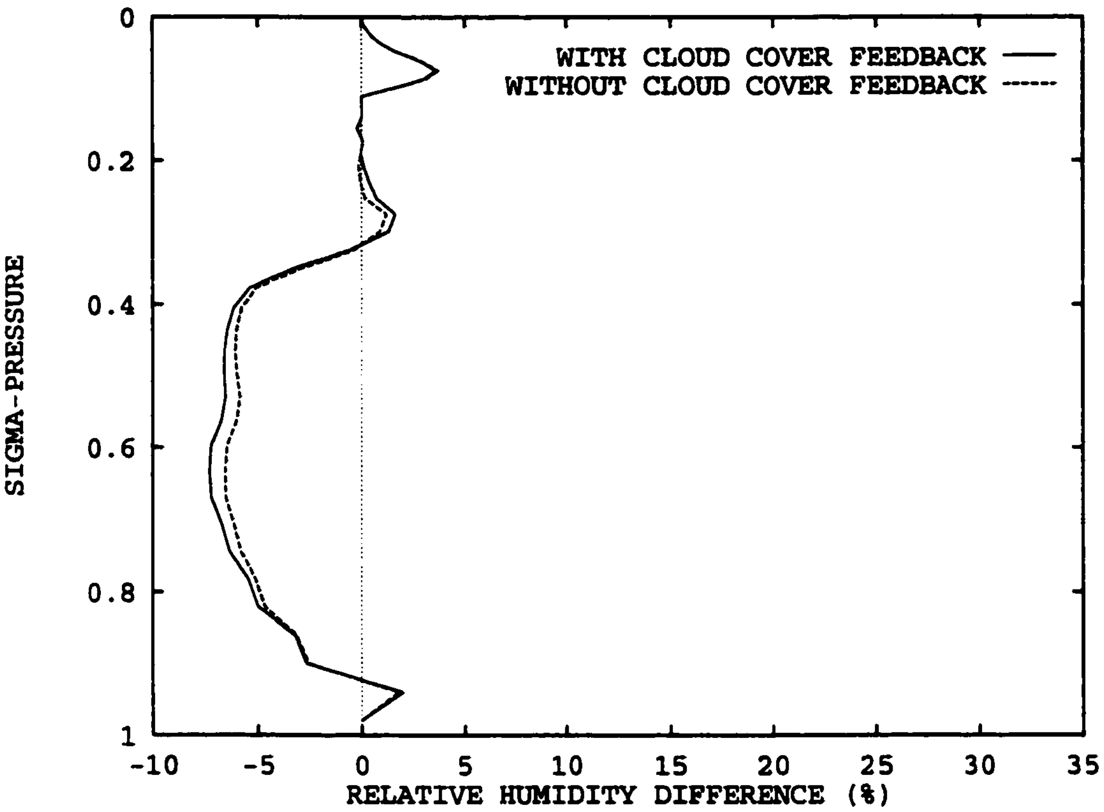

Figure 5.10: Profiles of zonally-averaged relative humidity differences between runs with surface temperatures of 299 K and 297 K using the new deep cumulus scheme.

Regarding figure 5.17, the results show a much more delicate balance between cumulus and large-scale moistening/drying. Notice that drying appears in the region of subsiding motion, and it is caused by an acceleration of the Hadley circulation in the warmer climate. Mid-tropospheric levels from the equator to 10° N show moistening of about 1 g/kg, which is a result of both large-scale and cumulus contributions. Drying of the boundary layer under the rising motion can also be detected, and it is a consequence of the cumulus model behavior.

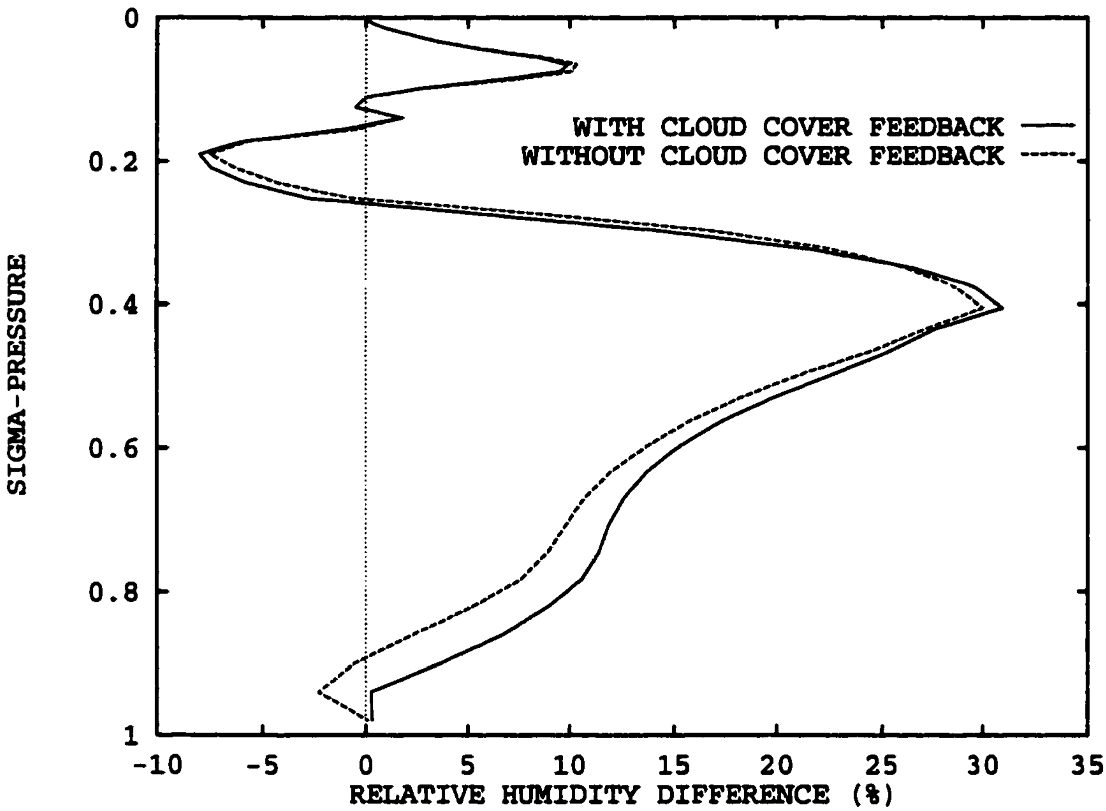

Figure 5.11: Profiles of zonally-averaged relative humidity differences between runs with surface temperatures of 299 K and 297 K using the ZM deep cumulus scheme.

The temperature difference plot (figure 5.18) shows a distinction in warming patterns meridionally about the 10 km level. This warming, as mentioned earlier, is a result of the slope reduction of the moist-adiabat when the SST is perturbed by +2 K. Since the subsiding motion promotes drying, the lapse-rate feedback becomes less operative beyond 15° N. Above the tropopause, radiative cooling dominates due to more water vapor diffusively transported from below in the warmer climate.

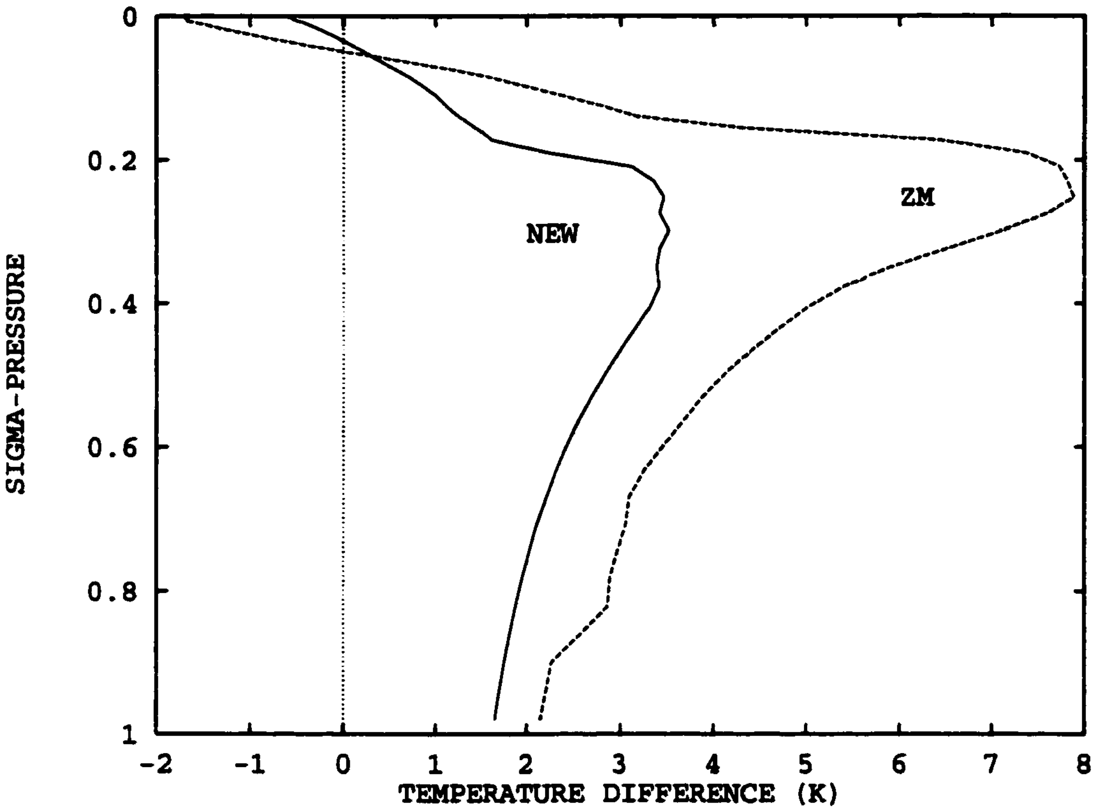

Figure 5.12: Profiles of zonally-averaged temperature differences between runs with surface temperatures of 299 K and 297 K. Results are shown with all feedback factors included.

With regard to the runs with the ZM scheme, figure 5.19 shows significant moistening of mid-tropospheric levels in the region of mean ascending motion of the Hadley cell. There is also boundary-layer drying until up to 5° N. The rest of the domain is subjected to slight moistening associated with increased evaporation from the surface diffusively transported upwards. In this case, the descending branch of the Hadley cell hardly affects the moisture distribution in the sub-tropics (data beyond about 23° N is ignored due to influence of the lateral boundary). There is some drying in the boundary

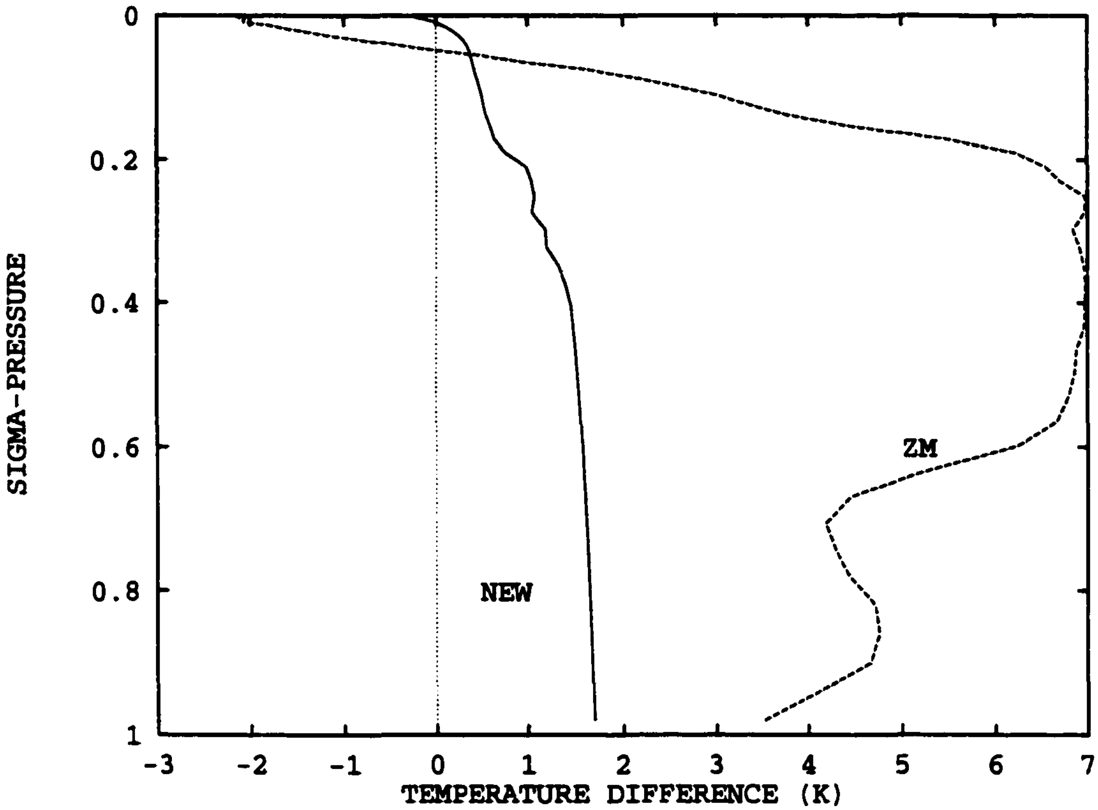

Figure 5.13: Profiles of zonally-averaged temperature differences between runs with surface temperatures of 299 K and 297 K. Results are shown with water vapor amount feedback factor only ($f_{h,T}$).

layer between 15° – 20° N that seems to be the only modification caused by the large-scale motion.

Two aspects of the results shown in figure 5.19 need to be explained in more detail: the strong mid-tropospheric moistening in the ascending branch region of the cell, and the drying in its boundary-layer. The drying is a consequence of the downdraft formulation in the ZM model. Zhang and McFarlane (1995) state that their downdraft formulation promotes drying of the sub-cloud layer. The reason for this effective drying is based on the fact that, in the warmer equilibrium climate, the height of updraft detrainment is *lower*

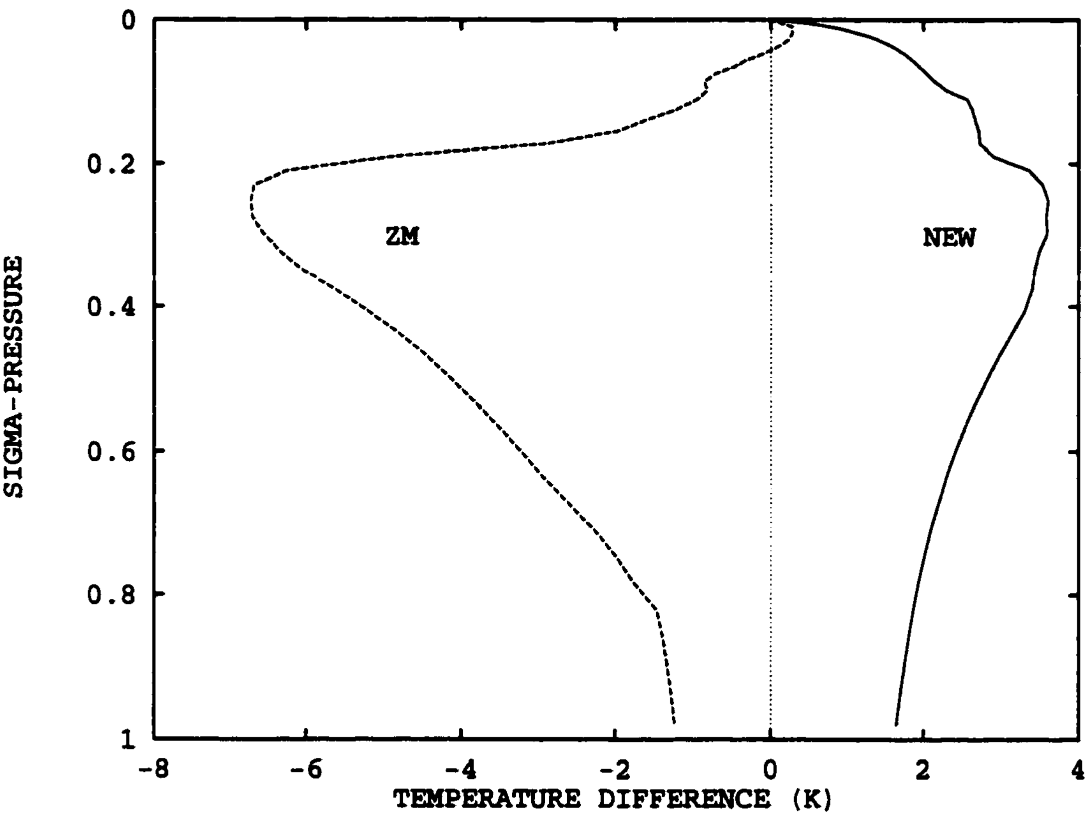

Figure 5.14: Profiles of zonally-averaged temperature differences between runs with surface temperatures of 299 K and 297 K. Results are shown with lapse-rate feedback factor only (f_r).

than the height in the equilibrium climate with SST = 297 K. The equation determining the cumulus ensemble downdraft mass flux is inversely proportional to this height. Accordingly, lower detrainment height implies larger downdraft mass flux and, in turn, more effective drying of the sub-cloud layer. The strong moistening of the cloud layer is also due to the reduction of cumulus heating depth when perturbing the SST by 2 K. The model behavior is such that the convective heating is shallower when the SST = 299 K, but stronger (that is, more warming). As a result, the saturation vapor pressure is increased in the shallower convective region, and the increased

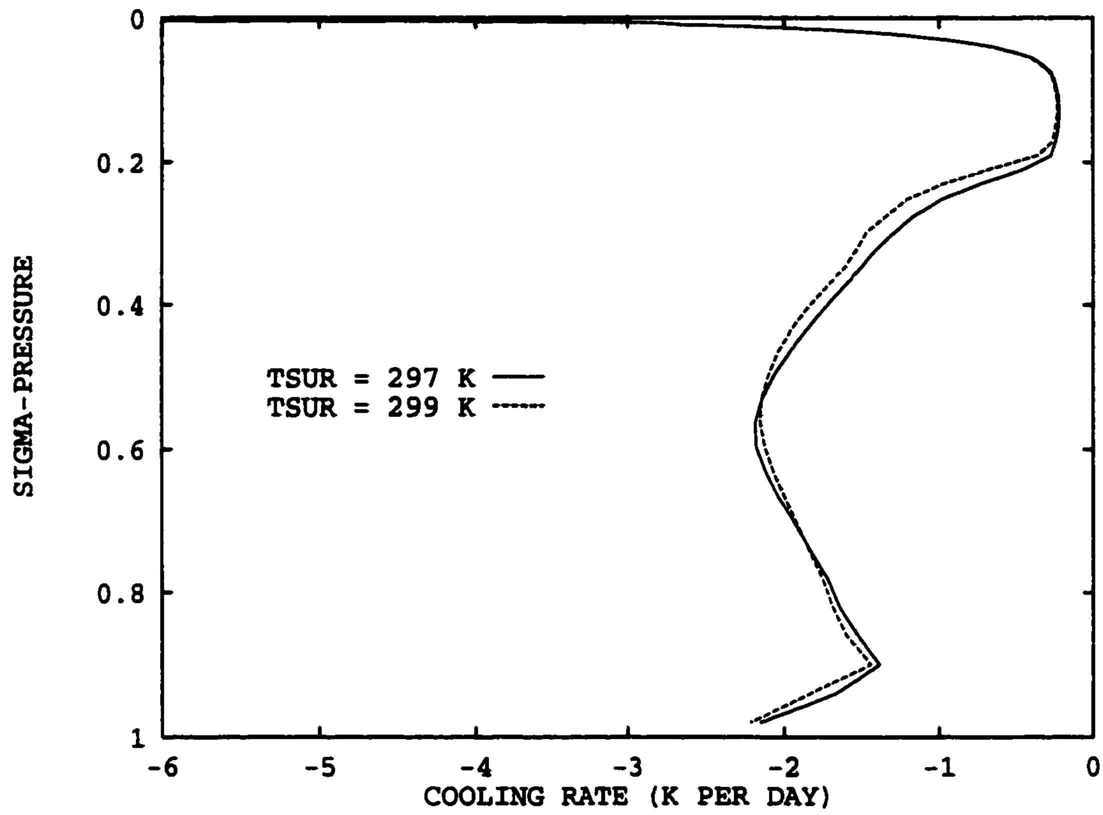

Figure 5.15: Profiles of zonally-averaged infrared cooling rates using the new deep cumulus scheme.

surface evaporation accommodates more water vapor in this warmer sector of the troposphere. In figure 5.17, the slight mid-tropospheric moistening is partially due to the same reason, although the warming shown in figure 5.18 is essentially a result of large-scale effects rather than due to cumulus processes. In brief, to explain the significant moistening with the ZM scheme, one needs to account for the interaction of the large-scale forcing (Hadley cell) and the convective heating behavior of the cumulus scheme. On the other hand, the sub-cloud layer drying is well explained by the behavior of the cumulus scheme only, i. e., by the cumulus downdraft mass flux effect.

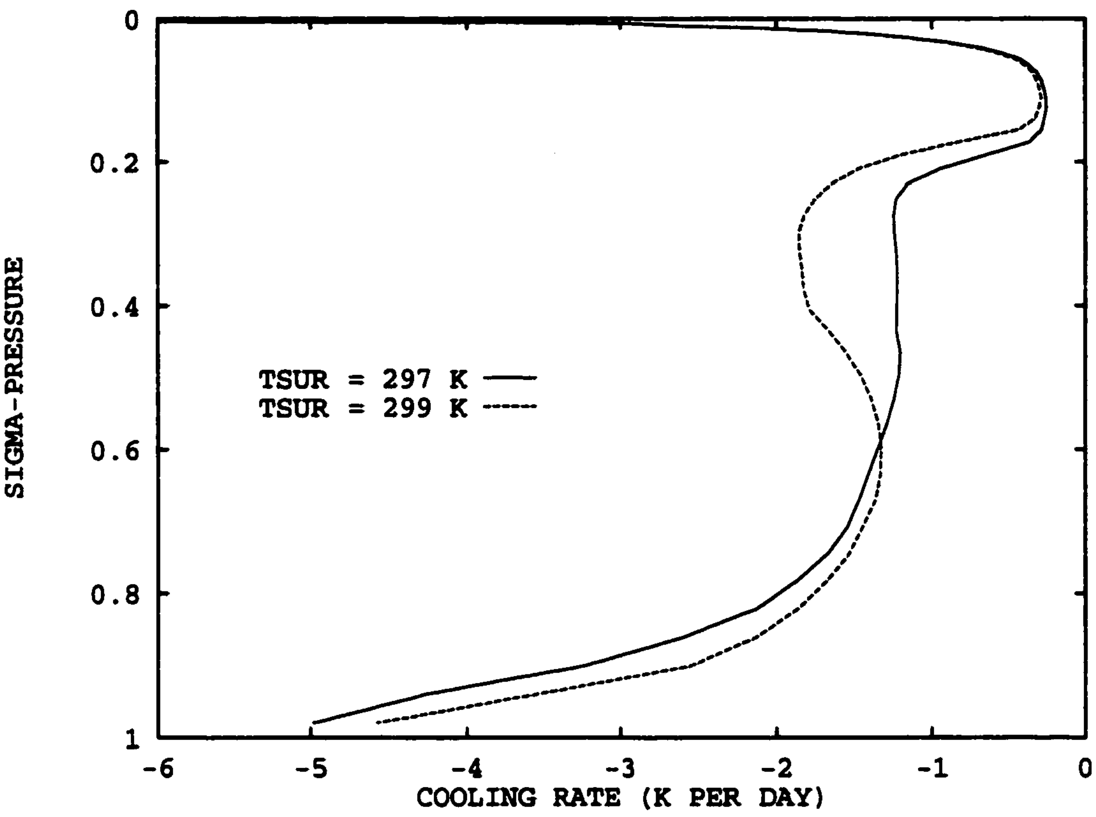

Figure 5.16: Profiles of zonally-averaged infrared cooling rates using the ZM deep cumulus scheme.

Figure 5.20 shows the temperature difference field. Overall, there is concentrated warming at upper-tropospheric levels and stratospheric cooling. The upper-tropospheric warming seems to be largely a consequence of the water vapor re-distribution feedback due to the lapse-rate adjustment. Essentially, in a warmer climate, the scale-height for water vapor is higher, which in turn makes the moist-adiabat less steeper in the moister depth. This behavior is associated with an elevation of the tropopause.

Let's now turn to a more quantitative analysis of the feedback factors and climate sensitivities. Figure 5.21 plots (2.13), indicating regions where the

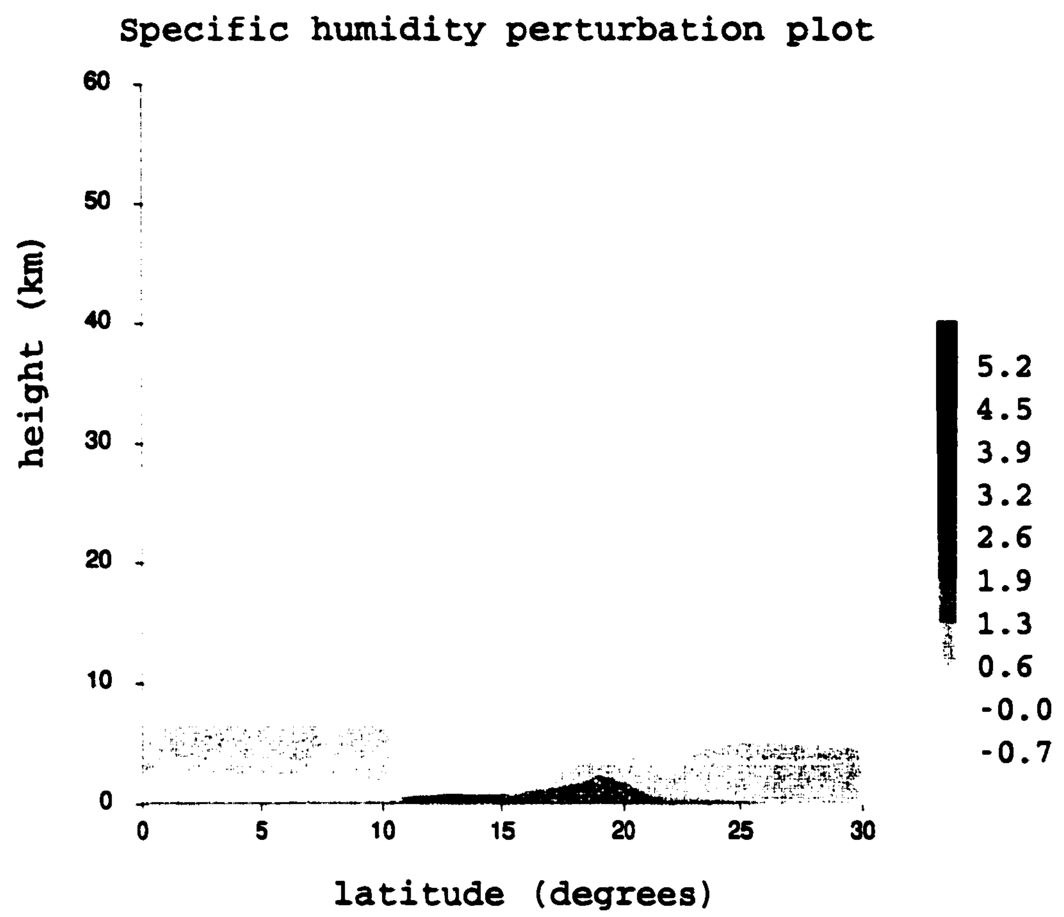

Figure 5.17: Specific humidity difference field between equilibrium climates with mean SSTs of 299 K and 297 K using new cumulus model. Color scale is in g/kg.

climate is stable/unstable, and, when stable, if effected by net positive or negative feedback. Also indicated in the figure is where the equilibrium climates lie. Peculiarly, when using the ZM scheme, the climate equilibrium is unstable. Table 5.3 shows the magnitude of each individual feedback factor that compounds the net result. By looking at figure 5.8 in conjunction with the feedback factor due to water vapor amount ($f_{h,T}$) given in table 5.3, it is concluded that upper-tropospheric relative humidity change is crucial in determining the sign of this feedback. Even though the new deep cumulus

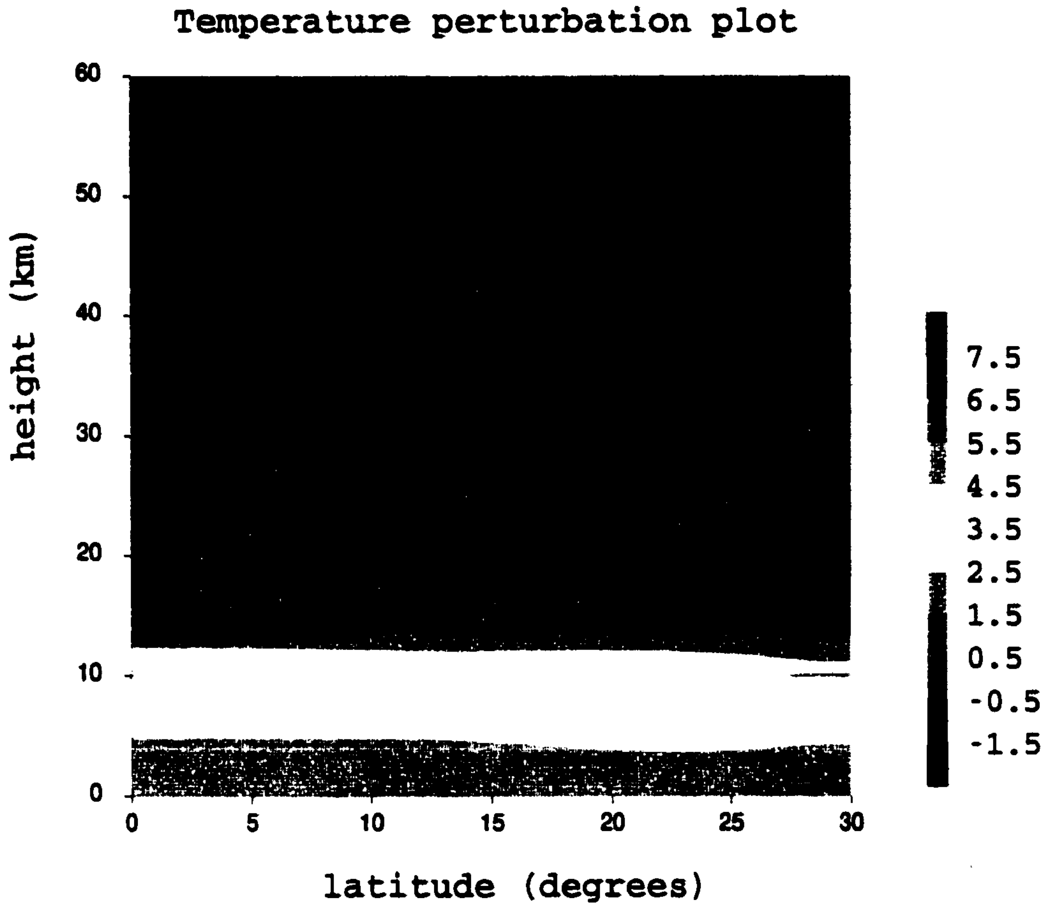

Figure 5.18: Temperature difference field between equilibrium climates with mean SSTs of 299 K and 297 K using new cumulus model. Color scale is in K.

model behaves as to dry the bulk of middle and low levels, the small moistening of about 5% in the upper-troposphere is enough to result in a positive water vapor feedback. The reverse is true when the ZM model is used. A significant drying at upper-levels causes this feedback to be strongly negative. The sign of the lapse-rate feedback factor (f_r), as given in table 5.3, is also consistent with the results shown in figure 5.9. The same consistency is apparent in figures 5.10 and 5.11. The small negative feedback factor due to cloud cover (f_a) with the new scheme is a result of more drying throughout

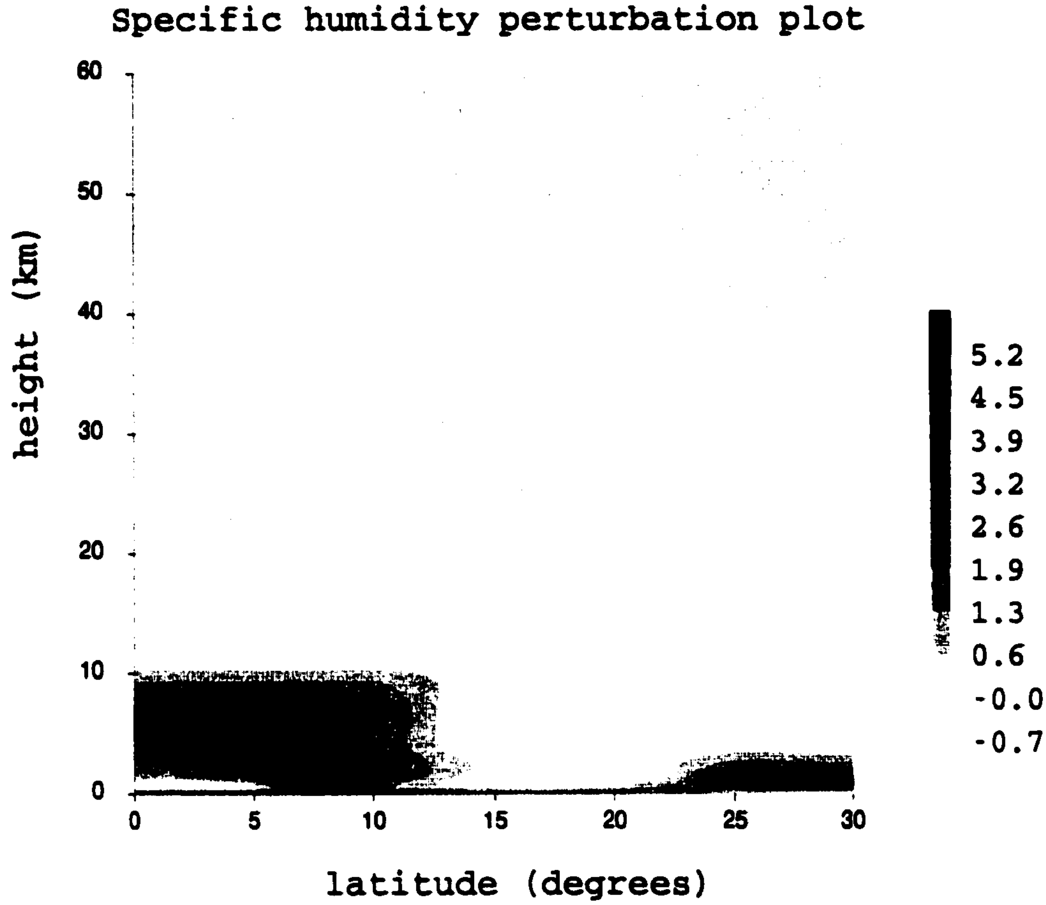

Figure 5.19: Specific humidity difference field between equilibrium climates with mean SSTs of 299 K and 297 K using ZM cumulus model. Color scale is in g/kg.

the bulk of the troposphere, as evidenced in figure 5.10. The higher relative humidity difference throughout low and mid-levels in figure 5.11 results in a positive feedback factor due to cloud cover with the ZM model. The stabilizing factor of the equilibrium climate using the new deep cumulus model is the lapse-rate behavior. With the ZM model, the water vapor amount feedback, $f_{h,T}$, attempts to stabilize the climate, but it is not enough to compensate for the strongly positive feedback factor due to water vapor distribution,

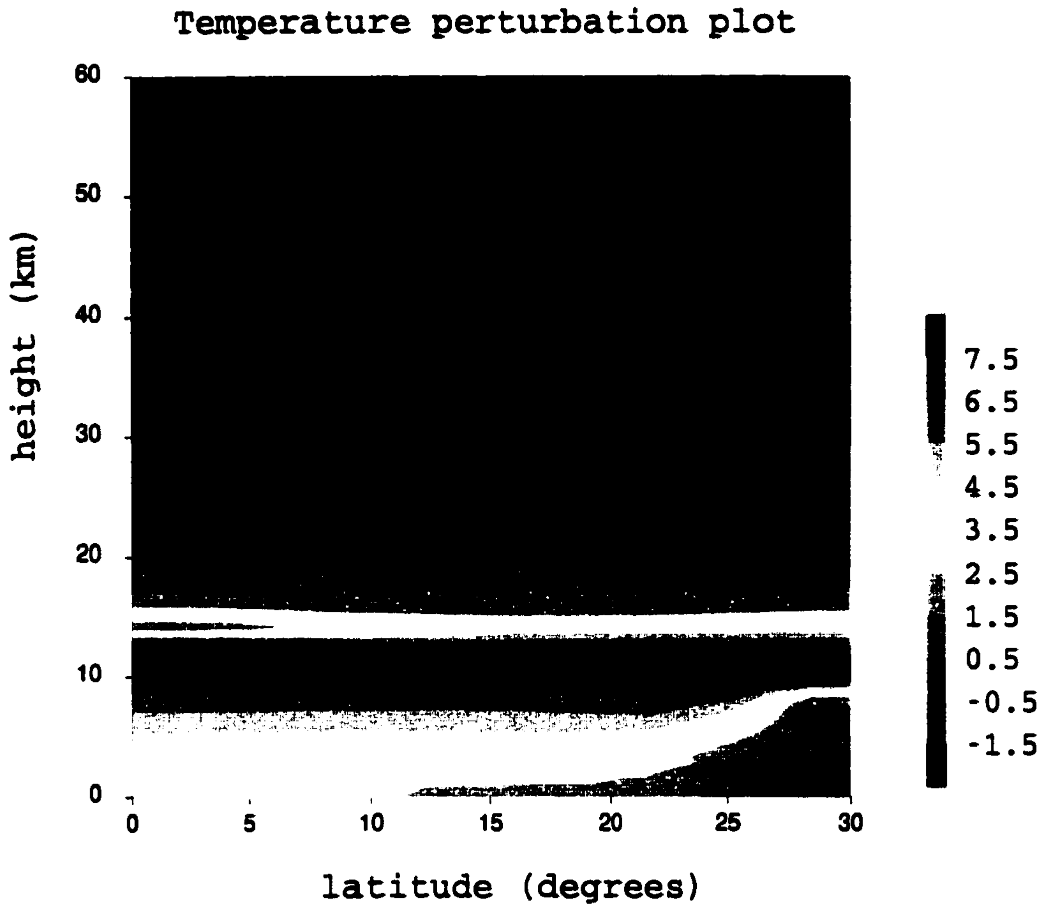

Figure 5.20: Temperature difference field between equilibrium climates with mean SSTs of 299 K and 297 K using ZM cumulus model. Color scale is in K.

$f_{h,r}$. These results show the importance of upper-tropospheric water vapor changes in determining the sign of the climatic feedbacks.

In closing, tables 5.4 and 5.5 present the values of F_{TOA}, as defined by (2.14), for the +2 K inverse experiments with the new and the ZM schemes, respectively. The tropical model sensitivity calculated with (2.18) is also shown in these tables. Previously, Fleischfresser (1999b) presented experiments with this same Hadley circulation model but utilizing a 6.5 K/km lapse-rate adjustment. Those results indicated that the tropical model sensitivity, λ_{TM}, lied

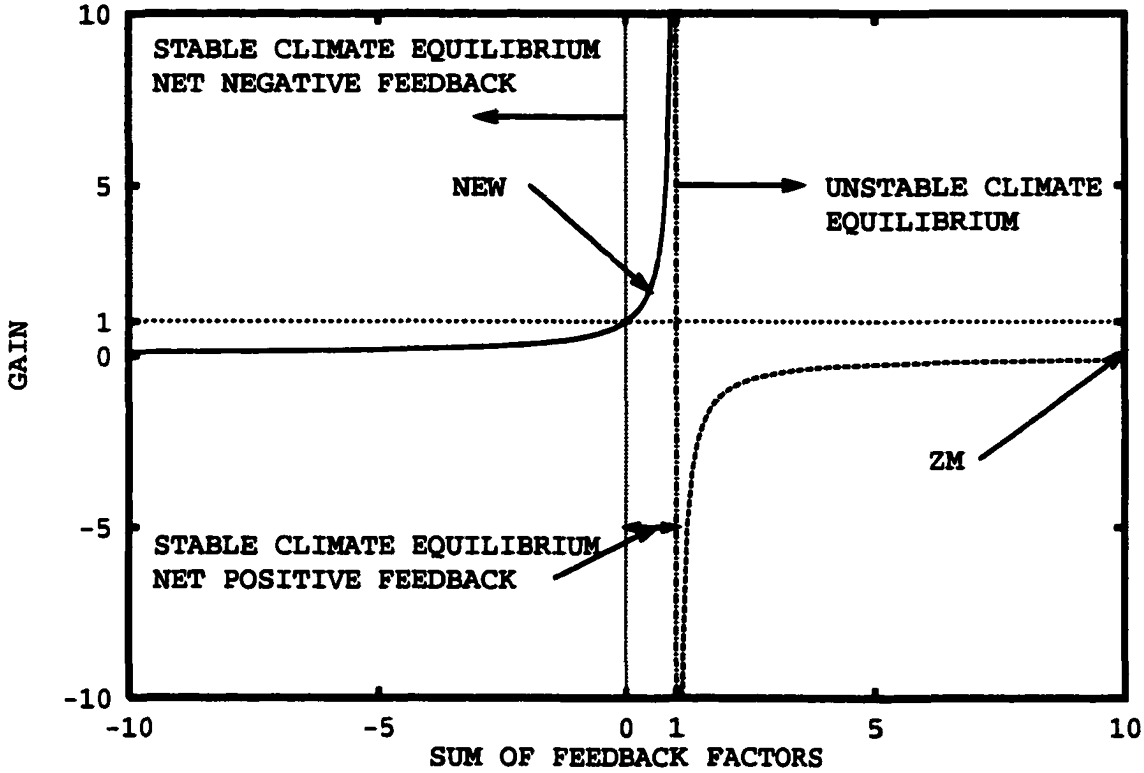

Figure 5.21: Gain as a function of feedback factor indicating where the equilibrium climates with each scheme lie.

within the typical range of equatorial sensitivities given by GCMs, which is generally known to be in between 0.5 K/Wm^{-2} and 1 K/Wm^{-2}. One now sees the effect of using a more internally consistent treatment of water vapor and deep cumulus clouds in the model. The λ_{TM} values shown in table 5.4 are consistently lower than those calculated without the deep cumulus model. This is a rewarding inference, since it is one of the crucial problems with current general circulation models — an equatorial climate sensitivity that is too high when compared to sensitivities calculated from data. The reductions of λ_{TM} are not too great, but they point in the right direction. The results with the ZM model (table 5.5) are shown for completeness, although their interpretation is not totally relevant since the equilibrium climate is unstable.

Table 5.3: Feedback factors comparison between new and ZM cumulus schemes. Symbols have been described previously.

FEEDBACK FACTOR	NEW	ZM
$f_{h,T}$	0.489	-30.348
$f_{h,r}$	0.311	33.153
f_r	-0.312	4.144
f_a	-0.01	4.968
$\sum f$	0.478	11.917
GAIN	1.916	-0.092

Table 5.4: Zonally-averaged top of atmosphere fluxes and climate sensitivities for new cumulus scheme. $[F]_{TOA}(297\,K) = -101.744\,W/m^2$. Symbols have been described previously.

FEEDBACKS	$[F]_{TOA}(299\,K)$ $[W/m^2]$	$\Delta[F]_{TOA}$ $[W/m^2]$	λ_{TM} $[K/Wm^{-2}]$
-	-93.820	7.924	0.252
$f_{h,T}$	-97.695	4.049	0.494
f_r	-91.350	10.394	0.192
$f_{h,T}$, $f_{h,r}$, f_r	-97.685	4.059	0.493
$f_{h,T}$, $f_{h,r}$, f_r, f_a	-97.610	4.134	0.484

Table 5.5: Zonally-averaged top of atmosphere fluxes and climate sensitivities for ZM cumulus scheme. $[F]_{TOA}(297\,K) = -77.372\,W/m^2$. Symbols have been described previously.

FEEDBACKS	$[F]_{TOA}(299\,K)$ $[W/m^2]$	$\Delta[F]_{TOA}$ $[W/m^2]$	λ_{TM} $[K/Wm^{-2}]$
-	-77.017	0.355	5.634
$f_{h,T}$	-66.242	11.130	0.179
f_r	-78.488	-1.116	-1.792
$f_{h,T}$, $f_{h,r}$, f_r	-79.484	-2.112	-0.947
$f_{h,T}$, $f_{h,r}$, f_r, f_a	-80.893	-3.521	-0.516

Chapter 6

Conclusions

The tropical climate stability of a wet planet was investigated using a Hadley circulation model. The analyses are relevant for climatic sensitivities associated with different climate regimes, where the determining factor is the equator to pole temperature gradient. It should be emphasized that this study does not apply to sensitivities associated with regional climate pattern rearrangements, as is the case with El Niño events, for example. The symmetric Hadley cell is relevant for annual mean conditions and it entails a rectification of the cumulus convection associated with the inter-tropical convergence zone. Accordingly, one must view these results as a first order scenario. It was also explained in section 2.3 that, due to the necessity of applying lateral boundaries in the model, the tropical model sensitivity given by (2.12) is a lower bound for the climate sensitivity of the open tropics in a warming equilibrium response. Yet, one should realize that the experiments here presented do not account for any latitudinal gradient changes of SST. The meridional heat flux changes would be minimal as a consequence. In fact, the results indicate that there is only a slight acceleration of the thermally direct circulation simulated by the symmetric model. Finally, it was still argued that the numerical approach is currently the best way to tackle the question of tropical climate stability due to the fact that pertinent data are limited in studying the issue from an observational standpoint.

The performance of two deep cumulus schemes were contrasted in the above-mentioned context: a mass flux parameterization, and a novel deep cumulus formulation developed for this study. The aim in developing this new cumulus model was to provide a more internally consistent representation of water vapor and deep cumulus clouds. But its deficiencies are still apparent. For example, the tropical troposphere is too moist, as evidenced in figure 5.7. This excessive moisturization may be attributed to two factors: a lack of efficient drying by the cumulus convection, and the limitation of closed lateral boundaries which do not allow the intrusion of drier air from mid-latitudes [Yang and Pierrehumbert (1994)]. On the other hand, the formulation of explicit downdrafts used in the ZM model demonstrated that its effect overcomes the modulation of the water vapor distribution by the Hadley circulation in the symmetric model. This effect is contrary to observed moisture distributions presented in Sun and Lindzen (1993). What is argued as a significant advantage of the new deep cumulus model is its property of accounting for phase transitions and the related latent heat release implicitly. The ZM scheme and, for that purpose, many other cumulus parameterizations in current use have an inherent limitation in this regard. The problem is due to explicit formulations of water vapor-cloud liquid water conversion, and precipitation efficiency specifications that invariably employ tuning parameters. It is a contention of this investigation that such formulations are major causes of model uncertainties related to greenhouse warming predictions.

The results with the ZM cumulus scheme yielded an unstable tropical climate equilibrium. This may seem odd in view of the many GCM simulations giving stable equilibriums with schemes that follow the same idea of the ZM model. Of course, the first distinction that one should be aware of is that GCMs are three-dimensional models that include many more details than the constrained two-dimensional simulations of a single thermally-direct circulation over an ocean surface. Another caution is that GCMs normally include cyclic and sometimes even evolutionary levels of complexity in modeling the climate system — both absent from the simulations presented in this study. A third and more subtle distinction is that the ZM code has been used as a "plug and play" program in the Hadley model: the interaction of two programs employing different design strategies affects the overall behavior of the simulations. Finally, the results with the ZM scheme must be taken at face value. This study attempted to interpret these results in view of the interaction of the cumulus model with the Hadley cell, and highlight potential deficiencies with similar formulations.

6.1 Prospects for Future Work

The new formulation has not been extensively compared against observed data. The only verification performed is the comparison of precipitation efficiencies presented in table 4.1, which is, admittedly, a very rudimentary indication of the model behavior. It is important to be able to perform more validations with pertinent observed data. In chapter 4, it was explained that the tuning of the scheme is done at the level of precipitation flux reaching the ground. This is where a comparison against observed data may begin.

Currently, there is a wealth of observational efforts attempting to quantify tropical precipitation. A suitable dataset might be, for example, the one being developed by the Surface Reference Data Center (SRDC) at the University of Oklahoma. Further developments in the theoretical framework should also be pursued. For example, the removal of "condensed" water vapor by the cumulus scheme is an important problem in future work. Concurrently, a more powerful approach to thermodynamics must be embraced to overcome the gaps between equilibrium thermodynamics and the fluid dynamics of wet planets. Finally, to account for a moving lower boundary in the model equations, one must await for further advances in mathematical fluid mechanics. With such tools in hand, the ability to develop a theory for precipitating clouds fully satisfying the continuum requirement becomes available.

6.2 Implications

Overall, there are some implications from this work that are believed to be important. First, it appears that there is no basis for the claim that higher model resolution will free the modeler from parameterizing precipitating convection. It is suggested here that, so long as fluid mechanical principles continue to be used in atmospheric models, precipitation will always imply discontinuities due to phase transitions and latent heat release. As a result, there will always be a need to parameterize them no matter how high the model resolution is. Second, from the experience developed in this study, it seems that progress in this area will be better achieved in accomplishing a more generalized formulation of cloud and radiative processes. In other words, an amalgamation of cloud and radiation schemes appears desirable, and this can more effectively be pursued with a solid theoretical understanding of the issues involved. Lastly, the results of this study indicate that the new deep cumulus formulation can effectively reduce the model sensitivity. Likewise, they suggest an approach to narrow the gap between modeled and observed tropical climate sensitivity.

Appendix A

Model Derivation

A.1 Conservation Laws

Let φ be the latitude, a_e be the radius of earth and Ω be the rotation rate. It is defined that

$$c \equiv \cos\varphi \tag{A.1}$$

$$\sigma \equiv \frac{p}{p_0} \tag{A.2}$$

The angular momentum is given by:

$$\overline{M} = \Omega a_e^2 c^2 + \overline{u} a_e c \tag{A.3}$$

$\overline{u}$ is the relative zonal velocity. Conservation of angular momentum is given by

$$\frac{\partial \overline{M}}{\partial t} = -\frac{1}{a_e c}\frac{\partial}{\partial \varphi}(\overline{v}\overline{M}c) - \frac{\partial}{\partial \sigma}(\overline{\omega}\overline{M}) - \frac{\partial(\overline{\omega' M'})}{\partial \sigma} \tag{A.4}$$

The meridional velocity $\bar{v}$ is governed by:

$$\frac{\partial \bar{v}}{\partial t} = -\frac{1}{a_e c}\frac{\partial}{\partial \varphi}(\bar{v}\bar{v}c) - \frac{\partial}{\partial \sigma}(\bar{\omega}\bar{v}) - f\bar{u} - \frac{\bar{u}^2 \tan\varphi}{a_e} - \frac{\partial \Phi}{a_e \partial \varphi} - \frac{\partial(\overline{\omega' v'})}{\partial \sigma} \quad \text{(A.5)}$$

The energy equation with implicit dissipative heating [Fiedler (2000)] is written as

$$\frac{\partial \bar{s}}{\partial t} = -\frac{1}{a_e c}\frac{\partial}{\partial \varphi}(\bar{v}\bar{s}c) - \frac{\partial}{\partial \sigma}(\bar{\omega}\bar{s}) - \frac{\partial(\overline{\omega' s'})}{\partial \sigma} + Q_{RAD} \quad \text{(A.6)}$$

With $\bar{s}$, the dry static energy, given by

$$\bar{s} = c_p T + gz \quad \text{(A.7)}$$

Q_{RAD} represents the radiative heating/cooling rates that are passed from the NCAR column radiation model. The water vapor conservation law is given by

$$\frac{\partial \bar{q}}{\partial t} = -\frac{1}{a_e c}\frac{\partial}{\partial \varphi}(\bar{v}\bar{q}c) - \frac{\partial}{\partial \sigma}(\bar{\omega}\bar{q}) - \frac{\partial(\overline{\omega' q'})}{\partial \sigma} - C_{grid} \quad \text{(A.8)}$$

The term $\partial(\overline{\omega' q'})/\partial\sigma$ includes the deep cumulus parameterization and the diffusion terms to be described ahead. C_{grid} represents the grid point saturation. The continuity equation is

$$\frac{1}{a_e c}\frac{\partial}{\partial \varphi}(\bar{v}c) + \frac{\partial \bar{\omega}}{\partial \sigma} = 0 \quad \text{(A.9)}$$

A.2 Sub-grid Terms

Sub-grid stresses are needed for the angular momentum and the meridional wind equations. For the angular momentum, it is assumed that:

$$\overline{\omega' M'} = (\frac{g}{p_0}) \cdot K \cdot \frac{\partial \overline{M}}{\partial z^*} \tag{A.10}$$

K is an eddy dynamic viscosity, and $z^* = -H_s \cdot \ln(\sigma)$. H_s, the scale height, is taken as 10 km. From (A.10) one obtains:

$$\overline{\omega' M'} = -a_e \cdot c \cdot \kappa \cdot \sigma \cdot \frac{\partial \overline{u}}{\partial \sigma} \tag{A.11}$$

With $\kappa = (g \cdot K)/(p_0 \cdot H_s)$. I use $\kappa = 10^{-7}\,s^{-1}$, which corresponds to an eddy dynamic viscosity $K = 10\ \mathrm{kg\,m^{-1}\,s^{-1}}$. Finally, the sub-grid stress divergence becomes:

$$-\frac{\partial}{\partial \sigma}(\overline{\omega' M'}) = a_e \cdot c \cdot \frac{\partial}{\partial \sigma}(\kappa \cdot \sigma \cdot \frac{\partial \overline{u}}{\partial \sigma}) \tag{A.12}$$

Similarly for the v-equation:

$$\overline{\omega' v'} = (\frac{g}{p_0}) \cdot K \cdot \frac{\partial \overline{v}}{\partial z^*} \tag{A.13}$$

The stress divergence becomes:

$$-\frac{\partial}{\partial \sigma}(\overline{\omega' v'}) = \frac{\partial}{\partial \sigma}(\kappa \cdot \sigma \cdot \frac{\partial \overline{v}}{\partial \sigma}) \tag{A.14}$$

At the surface, the usual phenomenological expression for the stress is assumed. Thus, the surface drag is given by:

$$\tau_0 = -C_D \cdot |U_0|^2 \qquad \text{(A.15)}$$

in both the angular momentum and the meridional wind equations. Formulations for the sub-grid heating due to the deep cumulus representation and the convective adjustment are included in the energy equation. Thus,

$$-\frac{\partial}{\partial\sigma}(\overline{\omega' s'}) = -\frac{\partial}{\partial\sigma}(\overline{\omega' s'})|_{DEEP} - \frac{\partial}{\partial\sigma}(\overline{\omega' s'})|_{ADJ} \qquad \text{(A.16)}$$

Or,

$$-\frac{\partial}{\partial\sigma}(\overline{\omega' s'}) = Q_{DEEP} + Q_{ADJ} \qquad \text{(A.17)}$$

With $Q_{DEEP} = \frac{a^2}{(1-a)} \cdot Q_{SOLAR}$ *only in the conditionally unstable layer*, and zero elsewhere. The terms appearing in this equation have been introduced before. At the surface, the convective heat flux is given by the bulk aerodynamic formula:

$$\overline{\omega' s'}|_{\sigma=1} = -(\frac{g}{p_0}) \cdot \rho \cdot C_h \cdot |U_0| \cdot c_P \cdot (T_S - T_0) \qquad \text{(A.18)}$$

The water vapor conservation equation employs an *eddy* diffusion as well as the deep cumulus representation in the sub-grid divergence term. Thus,

$$-\frac{\partial}{\partial\sigma}(\overline{\omega' q'}) = -\frac{\partial}{\partial\sigma}(\overline{\omega' q'})|_{DEEP} - \frac{\partial}{\partial\sigma}(\overline{\omega' q'})|_{DIF} \qquad \text{(A.19)}$$

The diffusion flux term is given by:

$$\overline{\omega' q'}|_{DIF} = (\frac{g}{p_0}) \cdot K_v \cdot \frac{\partial \overline{q}}{\partial z^*} \qquad \text{(A.20)}$$

And, after proper manipulations one obtains:

$$-\frac{\partial}{\partial\sigma}(\overline{\omega' q'})|_{DIF} = \frac{\partial}{\partial\sigma}(\kappa_v \cdot \sigma \cdot \frac{\partial\overline{q}}{\partial\sigma}) \quad \text{(A.21)}$$

With $\kappa_v = (g \cdot K_v)/(p_0 \cdot H_s)$. The deep cumulus sub-grid term formulation follows the top-hat method as described in the text. At the surface, the sub-grid flux term becomes:

$$\overline{\omega' q'}|_{\sigma=1} = -(\frac{g}{p_0}) \cdot \rho \cdot C_q \cdot |U_0| \cdot (\overline{q}_{SAT} - \overline{q}_0) \quad \text{(A.22)}$$

A.3 Pressure Solver

The hydrostatic equation is given by

$$\frac{\partial\Phi}{\partial p} = -\frac{RT}{p} = -\frac{R}{\sigma c_p} \cdot (\overline{s} - \Phi) \quad \text{(A.23)}$$

This can be written as

$$\frac{\partial\Phi}{\partial\sigma} - \frac{R \cdot \Phi}{\sigma \cdot c_p} = -\frac{R \cdot \overline{s}}{\sigma \cdot c_p} \quad \text{(A.24)}$$

Or,

$$\frac{\partial}{\partial\sigma}(\sigma^{-R/c_p} \cdot \Phi) = \frac{\partial}{\partial\sigma}(\sigma^{-R/c_p}) \cdot \overline{s} \quad \text{(A.25)}$$

$\Phi(\sigma, \varphi)$ is obtained with

$$\sigma^{-R/c_p} \cdot \Phi - \Phi_s = \int_1^{\sigma} \overline{s} \cdot d\sigma^{-R/c_p} \quad \text{(A.26)}$$

Or,

$$\Phi = \sigma^{R/c_p} \cdot \Phi_s + \Phi_b \tag{A.27}$$

Where

$$\Phi_b = \sigma^{R/c_p} \cdot \int_1^{\sigma} \bar{s} \cdot d\sigma^{-R/c_p} \tag{A.28}$$

$\Phi_s(\varphi)$ is determined so that the continuity equation is enforced. This enforcement is explained as follows. All the accelerations of $\bar{v}$, except for the pressure gradient force, are accumulated in a term $\partial\bar{v}'/\partial t$. The meridional momentum equation can be written as

$$\frac{\partial \bar{v}}{\partial t} = \frac{\partial \bar{v}'}{\partial t} - \frac{\partial \Phi_s}{a_e \partial \varphi} \cdot \sigma^{R/c_p} - \frac{\partial \Phi_b}{a_e \partial \varphi} \tag{A.29}$$

The term $\partial\Phi_b/a_e\partial\varphi$ is then added to the acceleration, stored as $\partial\bar{v}^*/\partial t$. One last acceleration is needed to compute $\partial\bar{v}/\partial t$:

$$\frac{\partial \bar{v}}{\partial t} = \frac{\partial \bar{v}^*}{\partial t} - \frac{\partial \Phi_s}{a_e \partial \varphi} \cdot \sigma^{R/c_p} \tag{A.30}$$

And Φ_s is chosen so that

$$\int_{\sigma=0}^{\sigma=1} \frac{\partial \bar{v}}{\partial t} \cdot d\sigma = 0 \tag{A.31}$$

Therefore

$$\frac{\partial \Phi_s}{a_e \partial \varphi} = \frac{1}{\int_{\sigma=0}^{\sigma=1} \sigma^{R/c_p} \cdot d\sigma} \cdot \int_{\sigma=0}^{\sigma=1} \frac{\partial \bar{v}^*}{\partial t} \cdot d\sigma \tag{A.32}$$

A.4 Volume Integrals

In this section the volume integrals of the model equations are derived. A few definitions are set first:

$$d\Pi = a_e \cdot c \cdot \partial\varphi \cdot \partial\sigma \tag{A.33}$$

$d\Pi$ is the differential volume over which the integration is performed. Consequently:

$$d\Sigma = a_e \cdot c \cdot \partial\varphi \tag{A.34}$$

$d\Sigma$ is the differential area. The divergence theorem will be frequently used, so we state it here for clarity (refer to figure A.1):

$$\int_{\Pi} (\vec{\nabla} \cdot \vec{X}) \cdot d\Pi = \int_{\Sigma} (\vec{X} \cdot \mathbf{n}) \cdot d\Sigma \tag{A.35}$$

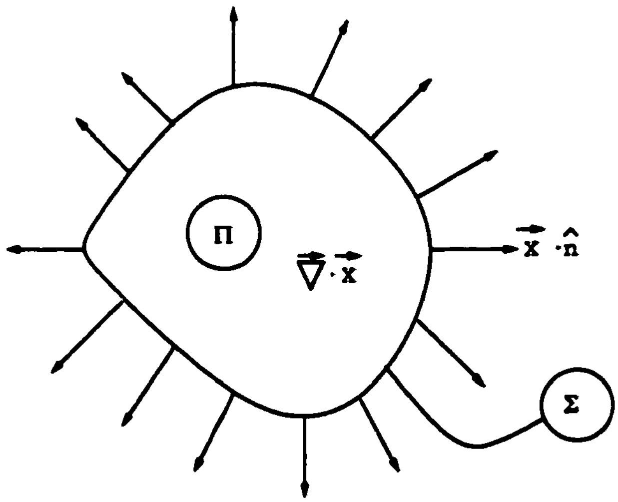

Figure A.1: Schematic figure illustrating the divergence theorem.

Refer to any textbook on fluid mechanics for a more comprehensive explanation of the divergence theorem [e.g., Kundu (1990)]. The following definition is made to simplify the notation:

$$[X] \equiv \int_{\varphi=0}^{\varphi=\pi/6} \overline{X} \cdot c \cdot \partial\varphi \tag{A.36}$$

φ is latitude ranging from the equator to 30° N. X is a generic tensor and the other symbols have already been described. The volume integral for the angular momentum equation is written as:

$$\begin{aligned}
\int_{\sigma=0}^{\sigma=1}\int_{\varphi=0}^{\varphi=\pi/6} \frac{\partial\overline{M}}{\partial t} \cdot a_e \cdot c \cdot \partial\varphi \cdot \partial\sigma \;=\; & -\int_{\sigma=0}^{\sigma=1}\int_{\varphi=0}^{\varphi=\pi/6} \frac{1}{a_e c} \cdot \frac{\partial}{\partial\varphi}(\overline{v}\overline{M}c) \cdot a_e \cdot c \cdot \partial\varphi \cdot \partial\sigma \\
& -\int_{\sigma=0}^{\sigma=1}\int_{\varphi=0}^{\varphi=\pi/6} \frac{\partial}{\partial\sigma}(\overline{\omega}\overline{M}) \cdot a_e \cdot c \cdot \partial\varphi \cdot \partial\sigma \\
& -\int_{\sigma=0}^{\sigma=1}\int_{\varphi=0}^{\varphi=\pi/6} \frac{\partial}{\partial\sigma}(\overline{\omega'M'}) \cdot a_e \cdot c \cdot \partial\varphi \cdot \partial\sigma
\end{aligned} \tag{A.37}$$

Or,

$$\begin{aligned}
\int_{\sigma=0}^{\sigma=1}\int_{\varphi=0}^{\varphi=\pi/6} \frac{\partial\overline{M}}{\partial t} \cdot a_e \cdot c \cdot \partial\varphi \cdot \partial\sigma \;=\; & -\int_{\sigma=0}^{\sigma=1} (\overline{v}\overline{M}c|_{\varphi=\pi/6} - \overline{v}\overline{M}c|_{\varphi=0}) \cdot d\sigma \\
& -\int_{\varphi=0}^{\varphi=\pi/6} (\overline{\omega}\overline{M}|_{\sigma=1} - \overline{\omega}\overline{M}|_{\sigma=0}) \cdot a_e \cdot c \cdot d\varphi \\
& -\int_{\varphi=0}^{\varphi=\pi/6} (\overline{\omega'M'}|_{\sigma=1} - \overline{\omega'M'}|_{\sigma=0}) \cdot a_e \cdot c \cdot d\varphi
\end{aligned} \tag{A.38}$$

The first two integrals on the right-hand side are zero since $\overline{v}(\varphi = 0) = \overline{v}(\varphi = \pi/6) = 0$ and $\overline{\omega}(\sigma = 0) = \overline{\omega}(\sigma = 1) = 0$. On the last integral, the term $\overline{\omega' M'}|_{\sigma=0} = 0$ as well, since the model upper boundary is stress-free. We are left with:

$$\int_{\sigma=0}^{\sigma=1} \int_{\varphi=0}^{\varphi=\pi/6} \frac{\partial \overline{M}}{\partial t} \cdot a_e \cdot c \cdot \partial\varphi \cdot \partial\sigma = -a_e \cdot \int_{\varphi=0}^{\varphi=\pi/6} \overline{\omega' M'}|_{\sigma=1} \cdot c \cdot d\varphi \tag{A.39}$$

Using the definition given by (A.36):

$$\int_{\sigma=0}^{\sigma=1} \int_{\varphi=0}^{\varphi=\pi/6} \frac{\partial \overline{M}}{\partial t} \cdot a_e \cdot c \cdot \partial\varphi \cdot \partial\sigma = -a_e \cdot [\overline{\omega' M'}|_{\sigma=1}] \tag{A.40}$$

In steady-state:

$$\frac{d}{dt}[\overline{M}] = -[\overline{\omega' M'}|_{\sigma=1}] = 0 \tag{A.41}$$

Or,

$$[\overline{\omega' M'}|_{\sigma=1}] = 0 \tag{A.42}$$

Similarly for dry-static energy:

$$\begin{aligned} \int_{\sigma=0}^{\sigma=1} \int_{\varphi=0}^{\varphi=\pi/6} \frac{\partial \overline{s}}{\partial t} \cdot a_e \cdot c \cdot \partial\varphi \cdot \partial\sigma \; = \; & -\int_{\sigma=0}^{\sigma=1} \int_{\varphi=0}^{\varphi=\pi/6} \frac{1}{a_e c} \cdot \frac{\partial}{\partial \varphi}(\overline{v}\,\overline{s}\, c) \cdot a_e \cdot c \cdot \partial\varphi \cdot \partial\sigma \\ & -\int_{\sigma=0}^{\sigma=1} \int_{\varphi=0}^{\varphi=\pi/6} \frac{\partial}{\partial \sigma}(\overline{\omega}\,\overline{s}) \cdot a_e \cdot c \cdot \partial\varphi \cdot \partial\sigma \\ & -\int_{\sigma=0}^{\sigma=1} \int_{\varphi=0}^{\varphi=\pi/6} \frac{\partial}{\partial \sigma}(\overline{\omega' s'}) \cdot a_e \cdot c \cdot \partial\varphi \cdot \partial\sigma \end{aligned}$$

$$+\int_{\sigma=0}^{\sigma=1}\int_{\varphi=0}^{\varphi=\pi/6} Q_{RAD}\cdot a_e\cdot c\cdot\partial\varphi\cdot\partial\sigma \quad (A.43)$$

The first two integrals of the right-hand side are zero as before. Thus:

$$\int_{\sigma=0}^{\sigma=1}\int_{\varphi=0}^{\varphi=\pi/6}\frac{\partial\overline{s}}{\partial t}\cdot a_e\cdot c\cdot\partial\varphi\cdot\partial\sigma = -\int_{\sigma=0}^{\sigma=1}\int_{\varphi=0}^{\varphi=\pi/6}\frac{\partial}{\partial\sigma}(\overline{\omega' s'})\cdot a_e\cdot c\cdot\partial\varphi\cdot\partial\sigma + \int_{\sigma=0}^{\sigma=1}\int_{\varphi=0}^{\varphi=\pi/6} Q_{RAD}\cdot a_e\cdot c\cdot\partial\varphi\cdot\partial\sigma \quad (A.44)$$

Or,

$$\int_{\sigma=0}^{\sigma=1}\int_{\varphi=0}^{\varphi=\pi/6}\frac{\partial\overline{s}}{\partial t}\cdot a_e\cdot c\cdot\partial\varphi\cdot\partial\sigma = -\int_{\sigma=0}^{\sigma=1}\int_{\varphi=0}^{\varphi=\pi/6}\frac{\partial}{\partial\sigma}(\overline{\omega' s'})|_{DEEP}\cdot a_e\cdot c\cdot\partial\varphi\cdot\partial\sigma - \int_{\sigma=0}^{\sigma=1}\int_{\varphi=0}^{\varphi=\pi/6}\frac{\partial}{\partial\sigma}(\overline{\omega' s'})|_{ADJ}\cdot a_e\cdot c\cdot\partial\varphi\cdot\partial\sigma - \int_{\sigma=0}^{\sigma=1}\int_{\varphi=0}^{\varphi=\pi/6}\frac{\partial F_{RAD}}{\partial\sigma}\cdot a_e\cdot c\cdot\partial\varphi\cdot\partial\sigma \quad (A.45)$$

Equivalently,

$$\int_{\sigma=0}^{\sigma=1}\int_{\varphi=0}^{\varphi=\pi/6}\frac{\partial\overline{s}}{\partial t}\cdot a_e\cdot c\cdot\partial\varphi\cdot\partial\sigma = -\int_{\varphi=0}^{\varphi=\pi/6}(\overline{\omega' s'}|_{DEEP_{(\sigma=1)}} - \overline{\omega' s'}|_{DEEP_{(\sigma=0)}})\cdot a_e\cdot c\cdot\partial\varphi - \int_{\varphi=0}^{\varphi=\pi/6}(\overline{\omega' s'}|_{ADJ_{(\sigma=1)}} - \overline{\omega' s'}|_{ADJ_{(\sigma=0)}})\cdot a_e\cdot c\cdot d\varphi - \int_{\varphi=0}^{\varphi=\pi/6}(F_{RAD}|_{\sigma=1} - F_{RAD}|_{\sigma=0})\cdot a_e\cdot c\cdot\partial\varphi \quad (A.46)$$

The only convective flux left is $\overline{\omega' s'}|_{ADJ_{(\sigma=1)}} = \overline{\omega' s'}|_{\sigma=1}$:

$$\int_{\sigma=0}^{\sigma=1}\int_{\varphi=0}^{\varphi=\pi/6}\frac{\partial\overline{s}}{\partial t}\cdot a_e\cdot c\cdot\partial\varphi\cdot\partial\sigma = -\int_{\varphi=0}^{\varphi=\pi/6}\overline{\omega's'}|_{\sigma=1}\cdot a_e\cdot c\cdot d\varphi - \int_{\varphi=0}^{\varphi=\pi/6}(F_{RAD}|_{\sigma=1} - F_{RAD}|_{\sigma=0})\cdot a_e\cdot c\cdot d\varphi \quad (A.47)$$

Finally:

$$\int_{\sigma=0}^{\sigma=1}\int_{\varphi=0}^{\varphi=\pi/6}\frac{\partial\overline{s}}{\partial t}\cdot a_e\cdot c\cdot\partial\varphi\cdot\partial\sigma = -a_e\cdot[\overline{\omega's'}|_{\sigma=1}] - a_e\cdot([F_{RAD}|_{\sigma=1}] - [F_{RAD}|_{\sigma=0}]) \quad (A.48)$$

With $F_{RAD} = F_{LW} - F_{SW}$, where F_{LW} is the infrared (longwave) radiative flux and F_{SW} is the solar (shortwave) radiative flux. In steady-state:

$$\frac{d}{dt}[s] = -[\overline{\omega's'}|_{\sigma=1}] - ([F_{RAD}|_{\sigma=1}] - [F_{RAD}|_{\sigma=0}]) = 0 \quad (A.49)$$

Or:

$$[\overline{\omega's'}|_{\sigma=1}] + [F_{LW}|_{\sigma=1}] - [F_{SW}|_{\sigma=1}] = [F_{LW}|_{\sigma=0}] - [F_{SW}|_{\sigma=0}] \quad (A.50)$$

And for the specific humidity equation now:

$$\int_{\sigma=0}^{\sigma=1}\int_{\varphi=0}^{\varphi=\pi/6}\frac{\partial\overline{q}}{\partial t}\cdot a_e\cdot c\cdot\partial\varphi\cdot\partial\sigma = -\int_{\sigma=0}^{\sigma=1}\int_{\varphi=0}^{\varphi=\pi/6}\frac{1}{a_e c}\cdot\frac{\partial}{\partial\varphi}(\overline{v}\,\overline{q}c)\cdot a_e\cdot c\cdot\partial\varphi\cdot\partial\sigma - \int_{\sigma=0}^{\sigma=1}\int_{\varphi=0}^{\varphi=\pi/6}\frac{\partial}{\partial\sigma}(\overline{\omega}\,\overline{q})\cdot a_e\cdot c\cdot\partial\varphi\cdot\partial\sigma$$

$$-\int_{\sigma=0}^{\sigma=1}\int_{\varphi=0}^{\varphi=\pi/6}\frac{\partial}{\partial\sigma}(\overline{\omega'q'})\cdot a_e\cdot c\cdot\partial\varphi\cdot\partial\sigma$$
$$-\int_{\sigma=0}^{\sigma=1}\int_{\varphi=0}^{\varphi=\pi/6}C_{grid}\cdot a_e\cdot c\cdot\partial\varphi\cdot\partial\sigma \quad (A.51)$$

Following the same logic as for the two previous derivations, one gets:

$$\int_{\sigma=0}^{\sigma=1}\int_{\varphi=0}^{\varphi=\pi/6}\frac{\partial\overline{q}}{\partial t}\cdot a_e\cdot c\cdot\partial\varphi\cdot\partial\sigma=-\int_{\varphi=0}^{\varphi=\pi/6}\overline{\omega'q'}|_{\sigma=1}\cdot a_e\cdot c\cdot\partial\varphi-\int_{\sigma=0}^{\sigma=1}a_e\cdot[C_{grid}]\cdot\partial\sigma \quad (A.52)$$

And,

$$\int_{\sigma=0}^{\sigma=1}\int_{\varphi=0}^{\varphi=\pi/6}\frac{\partial\overline{q}}{\partial t}\cdot a_e\cdot c\cdot\partial\varphi\cdot\partial\sigma=-a_e\cdot[\overline{\omega'q'}]-a_e\cdot\int_{\sigma=0}^{\sigma=1}[C_{grid}]\cdot\partial\sigma \quad (A.53)$$

In steady-state:

$$\frac{d}{dt}[q]=-[\overline{\omega'q'}]-[P]=0 \quad (A.54)$$

P is the precipitation removed from the water vapor budget. Thus,

$$[E]=[P] \quad (A.55)$$

In closing, the application of Gauss theorem to the continuity equation is trivially solved for:

$$\int_{\sigma=0}^{\sigma=1}\int_{\varphi=0}^{\varphi=\pi/6}\frac{1}{a_e c}\cdot\frac{\partial}{\partial\varphi}(vc)\cdot a_e\cdot c\cdot\partial\varphi\cdot\partial\sigma=-\int_{\sigma=0}^{\sigma=1}\int_{\varphi=0}^{\varphi=\pi/6}\frac{\partial\omega}{\partial\sigma}\cdot a_e\cdot c\cdot\partial\varphi\cdot\partial\sigma \quad (A.56)$$

which can easily be shown to be zero.

Appendix B

Numerical Schemes

B.1 Advection Schemes

The model has the capability of using odd-order, upstream-biased advection schemes, in either pure advection form or in flux form. To derive the third-order scheme, one seeks a four-point approximation of form:[1]

$$\frac{\partial}{\partial x} s(x,z,t) \simeq \frac{1}{\delta}[A\, s(x-\delta,z,t)+B\, s(x,z,t)+C\, s(x+\delta,z,t)+D\, s(x+2\delta,z,t)] \quad \text{(B.1)}$$

A, B, C and D are chosen to make (B.1) as accurate as possible. If one expands (B.1) with a Taylor series:

$$\begin{aligned} s' \simeq\ & \frac{A}{\delta}(s-\delta s' + \frac{\delta^2}{2}s'' - \frac{\delta^3}{6}s''' + \ldots)+ \\ & \frac{B}{\delta}s + \\ & \frac{C}{\delta}(s+\delta s' + \frac{\delta^2}{2}s'' + \frac{\delta^3}{6}s''' + \ldots) + \end{aligned}$$

[1]From now on, the derivations are presented in Cartesian coordinates for simplicity.

$$\frac{D}{\delta}(s + 2\delta s' + 2\delta^2 s'' + \frac{4\delta^3}{3} s''' + \ldots) \tag{B.2}$$

Where

$$s' = \frac{\partial}{\partial x} s(x, z, t) \tag{B.3}$$

It is easy to show that (B.2) is satisfied to $O(\delta^3)$ if $A = -1/3$, $B = -1/2$, $C = 1$ and $D = 1/6$. Thus one approximates:

$$\frac{\partial s}{\partial x} \simeq \frac{1}{6\delta}[-2\ s(x - \delta) - 3\ s(x) + 6\ s(x + \delta) - s(x + 2\delta)] \tag{B.4}$$

Conversely,

$$\frac{\partial s}{\partial x} \simeq \frac{1}{6\delta}[s(x - 2\delta) - 6\ s(x - \delta) + 3\ s(x) + 2\ s(x + \delta)] \tag{B.5}$$

When combined with advection, the "upstream" derivatives should be used: (B.4) is preferable when $u \leq 0$ and (B.5) is preferable when $u \geq 0$. Needless to say, the third-order approximations for $\partial s/\partial z$ are similar to (B.4) and (B.5). The use of third-order derivatives is sometimes not possible at one grid point away from the boundary; in that case second-order derivatives are used.

The flux form of the advection terms is desirable for some quantities. Instead of:

$$\frac{\partial s}{\partial t} = -u\frac{\partial s}{\partial x} - w\frac{\partial s}{\partial z} \tag{B.6}$$

One may want to use:

$$\frac{\partial s}{\partial t} = -\frac{\partial}{\partial x}(us) - \frac{\partial}{\partial z}(wz) \tag{B.7}$$

Or,

$$\frac{\partial s}{\partial t} = -\frac{\partial f}{\partial x} - \frac{\partial g}{\partial z} \tag{B.8}$$

The flux divergence is calculated by centered second-order schemes, for example:

$$\frac{\partial f}{\partial x} = \frac{f(x+\delta/2, z, t) - f(x-\delta/2, z, t)}{\delta} \tag{B.9}$$

This guarantees that a volume integral would show the only source of s coming from the boundaries. The flux itself is given by:

$$\begin{aligned} f(x-\delta/2, z, t) = {} & \frac{1}{2}[u(x-\delta, z, t) + u(x, z, t)] \times \\ & \frac{1}{6}[-s(x-2\delta, z, t) + 5s(x-\delta, z, t) + 2s(x, z, t)] \end{aligned} \tag{B.10}$$

When $u \geq 0$ and:

$$\begin{aligned} f(x-\delta/2, z, t) = {} & \frac{1}{2}[u(x-\delta, z, t) + u(x, z, t)] \times \\ & \frac{1}{6}[-s(x+\delta, z, t) + 5s(x, z, t) + 2s(x-\delta, z, t)] \end{aligned} \tag{B.11}$$

When $u \leq 0$. The goal here is that, for the special case of constant u, the flux form would be the same as the advection form, or:

$$\frac{\partial f}{\partial x} = u\frac{\partial s}{\partial x} \tag{B.12}$$

With $\partial s/\partial x$ given either by (B.4) or by (B.5).

In general, the flux form has greater amplitude and phase errors than the advective form, but still may be desirable because of the global conservation properties.

B.2 Time Integration Scheme

After the spatial derivatives are approximated with finite differences, the model consists of coupled ordinary differential equations, with the grid point values of the fields now serving as the independent variables in the model. For example, the time-derivative of a value of s at a grid point is coupled to the values of s, u, and w at neighboring grid points that are in the finite difference schemes for the spatial derivatives. Consider a value $q(t)$ of a variable s at a certain grid point, for example:

$$q(t) = s(x_i, z_j, t) \tag{B.13}$$

For notational convenience one writes:

$$\frac{d\,q(t)}{d\,t} = F(t) \tag{B.14}$$

F(t) is the sum of all the terms on the r.h.s. of (B.1). The simplest finite-difference scheme for integrating (B.14) is the first-order Euler scheme:

$$q(t+\delta) \simeq q(t) + \delta F(t) \tag{B.15}$$

In which the error is $O(\delta^2)$. A more accurate scheme would retain higher derivatives of F:

$$q(t+\delta) = q(t) + \delta F(t) + \frac{\delta^2}{2} F'(t) + \frac{\delta^3}{6} F''(t) + \ldots \tag{B.16}$$

The higher derivatives of F are not readily available from the model. Alternatively, one can obtain greater accuracy by proposing:

$$q(t+\delta) \simeq q(t) + \delta[A\, F(t) + B\, F(t-\delta) + C\, F(t-2\delta)] \tag{B.17}$$

Which to $O(\delta^3)$ is:

$$q(t+\delta) \simeq q(t) + \delta A\, F(t) + \delta B[F(t) - \delta F'(t) + \frac{\delta^2}{2} F''(t)] + \delta C[F(t) - 2\delta F'(t) + 2\delta^2 F''(t)] \tag{B.18}$$

If $A = 23/12$, $B = -16/12$ and $C = 5/12$ are chosen, then (B.18) is the same as (B.16) through $O(\delta^3)$. The third-order Adams-Bashforth scheme is thus:

$$q(t+\delta) \simeq q(t) + \frac{\delta}{12}[23\, F(t) - 16\, F(t-\delta) + 5\, F(t-2\delta)] \tag{B.19}$$

The virtues of this scheme are discussed in Durran (1991). At the initial time, $F(t-\delta)$ and $F(t-2\delta)$ are unknown, so the Euler scheme is used. At the second time-step, the second-order Adams-Bashforth scheme is used:

$$q(t+\delta) \simeq q(t) + \frac{\delta}{2}[3\, F(t) - F(t-\delta)] \tag{B.20}$$

Bibliography

Anthes, R. A., 1977: A Cumulus Parameterization Scheme Utilizing a One-Dimensional Cloud Model. *Mon. Wea. Rev.*, **105**, 270–286.

Arakawa, A., 1993: Closure Assumptions in Cumulus Parameterization, *The Representation of Cumulus Convection in Numerical Models*, K. A. Emanuel and D. J. Raymond, eds., Amer. Meteor. Soc., vol. 24, chap. 1, 1–16.

Arakawa, A. and W. H. Schubert, 1974: Interaction of a Cumulus Cloud Ensemble with the Large-Scale Environment, Part I. *J. Atmos. Sci.*, **31**, 674–701.

Aris, R., 1962: *Vectors, Tensors, and the Basic Equations of Fluid Mechanics*, Prentice-Hall Inc., 286pp.

Bjerknes, J., 1938: Saturated Adiabatic Ascent of Air Through Dry Adiabatically Descending Environment. *Quart. J. Roy. Meteor. Soc.*, **64**, 325–330.

Briegleb, B. P., 1992: Delta-Eddington Approximation for Solar Radiation in the NCAR Community Climate Model. *J. of Geophys. Res.*, **97**, 7603–7612.

Cess, R. D. et al., 1999: Absorption of Solar Radiation by the Cloudy Atmosphere: Further Interpretations of Collocated Aircraft Measurements. *J. of Geophys. Res.*, **104**, 2059–2066.

Cess, R. D. and G. L. Potter, 1988: A Methodology for Understanding and Intercomparing Atmospheric Climate Feedback Processes in General Circulation Models. *J. of Geophys. Res.*, **93**, 8305–8314.

Cessi, P., 1998: Angular Momentum and Temperature Homogenization in the Symmetric Circulation of the Atmosphere. *J. Atmos. Sci.*, **55**, 1997–2015.

Durran, D. R., 1991: The Third-Order Adams-Bashfort Method: An Attractive Alternative to Leapfrog Time Differencing. *Mon. Wea. Rev.*, **119**, 702–720.

Eliassen, A., 1951: Slow Thermally or Frictionally Controlled Meridional Circulation in a Circular Vortex. *Astrophys. Norvegica*, **5**, 19–60.

Ellsaesser, H. W., 1990: A Different View of the climatic effect of CO_2 – Updated. *Atmósfera*, **3**, 3–29.

Emanuel, K. A., 1991: A Scheme for Representing Cumulus Convection in Large-Scale Models. *J. Atmos. Sci.*, **48**, 2313–2335.

Emanuel, K. A., 1994: *Atmospheric Convection*, Oxford University Press, 580pp., New York, Oxford.

Fang, M., 1995: *On the Axisymmetric Circulation of the Atmosphere*, Ph.D. thesis, University of Washington, 162 pp., Seattle, WA, *Available from UMI Dissertation Services*.

Fiedler, B. H., 2000: Dissipative Heating in Climate Models. *Quart. J. Roy. Meteor. Soc.*, **126**, 925–939.

Fleischfresser, L., 1999a: Representing Deep Cumulus Convection in a Hadley Circulation Model. *12th AMS Conference on Atmospheric and Oceanic Fluid Dynamics*, 32–35.

Fleischfresser, L., 1999b: Studying Tropical Climate Equilibrium with a Hadley Circulation Model. *10th AMS Symposium on Global Change Studies*, 374–377.

Goody, R. et al., 1998: Testing Climate Models: An Approach. *Bull. of the Amer. Met. Soc.*, **79**, 2541–2549.

Gregory, D., 1997: The mass flux approach to the parameterization of deep convection, *The Physics and Parameterization of Moist Atmospheric Convection*, R. K. Smith, ed., Kluwer Academic Publishers, vol. 505 of *NATO ASI Series C: Mathematical and Physical Sciences*, chap. 12, 297–320.

Held, I. M., 1978: The Tropospheric Lapse Rate and Climatic Sensitivity: Experiments with a Two-Level Atmospheric Model. *J. Atmos. Sci.*, **35**, 2083–2098.

Held, I. M. and A. Y. Hou, 1980: Nonlinear Axially Symmetric Circulations in a Nearly Inviscid Atmosphere. *J. Atmos. Sci.*, **37**, 515–533.

Kiehl, J. T. et al., 1996: Description of the NCAR Community Climate Model (CCM3), Tech. rep., National Center for Atmospheric Research, Climate and Global Dynamics Division.

Krishnamurti, T. N., Y. Ramanathan, H.-L. Pan, R. J. Pasch, and J. Molinari, 1980: Cumulus Parameterization and Rainfall Rates I. *Mon. Wea. Rev.*, **108**, 465–472.

Kundu, P. K., 1990: *Fluid Mechanics*, Academic Press, 638pp.

Kuo, H. L., 1965: On Formation and Intensification of Tropical Cyclones through Latent Heat Release by Cumulus Convection. *J. Atmos. Sci.*, **22**, 40–63.

Kuo, H. L., 1974: Further Studies of the Parameterization of the Influence of Cumulus Convection on Large-Scale Flow. *J. Atmos. Sci.*, **31**, 1232–1240.

Lewis, J. S. and R. G. Prinn, 1984: *Planets and Their Atmospheres*, Academic Press, New York, London.

Lindzen, R. S., 1990: *Dynamics in Atmospheric Physics*, Cambridge University Press, 310 pp., Cambridge, New York.

Lindzen, R. S., 1991: Prospects for Tropical Modeling. *ECMWF Seminar Proceedings on Tropical extra-tropical interactions*, 13, 419–439.

Lindzen, R. S., 1994: Climate Dynamics and Global Change. *Annu. Rev. of Fluid Mech.*, **26**, 353–378.

Lindzen, R. S., 1997: Can Increasing Carbon Dioxide Cause Climate Change? *Proc. Natl. Acad. Sci., USA*, **94**, 8335–8342.

Lindzen, R. S., A. Y. Hou, and B. F. Farrell, 1982: The Role of Convective Model Choice in Calculating the Climate Impact of Doubling CO_2. *J. Atmos. Sci.*, **39**, 1189–1205.

Lord, S. J., 1982: Interaction of a Cumulus Cloud Ensemble with the Large-Scale Environment, Part III: Semi-Prognostic Test of the Arakawa-Schubert cumulus parameterization. *J. Atmos. Sci.*, **39**, 88–103.

Magalhães, J. A., 1985: *Hadley Circulation in Planetary Atmospheres*, Ph.D. thesis, Cornell University, 145 pp., Ithaca, NY, *Available from UMI Dissertation Services.*

McClatchey, R. A. et al., 1972: Optical Properties of the Atmosphere, Tech. rep., Air Force Cambridge Research Laboratories, Third Edition. *(Available from NTIS).*

Molinari, J., 1982: A Method for Calculating the Effects of Deep Cumulus Convection in Numerical Models. *Mon. Wea. Rev.*, **110**, 1527–1534.

Moorthi, S. and M. J. Suarez, 1992: Relaxed Arakawa-Schubert: A Parameterization of Moist Convection for General Circulation Models. *Mon. Wea. Rev.*, **120**, 978–1002.

United States, Senate Committee on Energy and Natural Resources. Hearing on U.S. Global Climate Change Policy, 104th Congress, second session, 1996:

Pan, D.-M. and D. A. Randall, 1998: A Cumulus Parametrization with a Prognostic Closure. *Quart. J. Roy. Meteor. Soc.*, **124**, 949–981.

Peixoto, J. P. and A. H. Oort, 1992: *Physics of Climate*, American Institute of Physics, 520 pp., New York, NY.

Pierrehumbert, R. T., 1995: Thermostats, Radiator Fins, and the Local Runaway Greenhouse. *J. Atmos. Sci.*, **52**, 1784–1806.

Ramanathan, V. et al., 1995: Warm Pool Heat Budget and Shortwave Cloud Forcing: A Missing Physics? *Science*, **267**, 499–503.

Ramanathan, V. and P. Downey, 1986: A Nonisothermal Emissivity and Absorptivity Formulation for Water Vapor. *J. of Geophys. Res.*, **97**, 8649–8666.

Raymond, D. J. and K. A. Emanuel, 1993: The Kuo Cumulus Parameterization, *The Representation of Cumulus Convection in Numerical Models. Meteor. Mono.*, K. A. Emanuel and D. J. Raymond, eds., Amer. Meteor. Soc., vol. 24, chap. 11, 145–147.

Riehl, H. and J. S. Malkus, 1958: On the Heat Balance in the Equatorial Trough Zone. *Geophys.*, **6**, 503–537.

Satoh, M., 1994: Hadley Circulations in Radiative-Convective Equilibrium in an Axially Symmetric Atmosphere. *J. Atmos. Sci.*, **51**, 1947–1968.

Satoh, M., 1995: Hadley Circulations and Large-Scale Motions of Moist Convection in the Two-Dimensional Numerical Model. *J. Met. Soc. Japan*, **73**, 1059–1078.

Schneider, E. K., 1977: Axially Symmetric Steady-State Models of the Basic State for Instability and Climate Studies. Part II: Nonlinear Calculations. *J. Atmos. Sci.*, **34**, 280–296.

Schneider, E. K. and R. S. Lindzen, 1977: Axially Symmetric Steady-State Models of the Basic State for Instability and Climate Studies. Part I: Linearized Calculations. *J. Atmos. Sci.*, **34**, 263–279.

Sellers, W. D., 1965: *Physical Climatology*, University of Chicago Press, 272 pp., Chicago, London.

Sinha, A. and M. R. Allen, 1994: Climate Sensitivity and Tropical Moisture Distribution. *J. of Geophys. Res.*, **99**, 3707–3716.

Slingo, A., 1989: A GCM Parameterization for the Shortwave Radiative Properties of Water Clouds. *J. Atmos. Sci.*, **46**, 1419–1427.

Soden, B. J. and R. Fu, 1995: A Satellite Analysis of Deep Convection, Upper-Tropospheric Humidity, and the Greenhouse Effect. *J. of Climate*, 8, 2333–2351.

Spencer, R. W. and W. D. Braswell, 1997: How Dry is the Tropical Free Troposphere? Implications for Global Warming Theory. *Bull. of the Amer. Met. Soc.*, **94**, 8335–8342.

Sun, D.-Z. and I. M. Held, 1996: A Comparison of Modeled and Observed Relationships Between Interannual Variations of Water Vapor and Temperature. *J. of Climate*, **9**, 665–675.

Sun, D.-Z. and R. S. Lindzen, 1993: Distribution of Tropical Tropospheric Water Vapor. *J. Atmos. Sci.*, **50**, 1643–1660.

Tiedtke, M., 1989: A Comprehensive Mass Flux Scheme for Cumulus Parameterization in Large-Scale Models. *Mon. Wea. Rev.*, **117**, 1779–1800.

Townsend, A. A., 1998: *The structure of turbulent shear flow*, Cambridge University Press, 429 pp., Cambridge, New York.

Wallace, J. M. and P. V. Hobbs, 1977: *Atmospheric Science: An Introductory Survey*, Academic Press, 467 pp., New York, London.

Wigley, T. M. L. et al., 1997: The Observed Global Warming Record: What Does It Tell Us? *Proc. Natl. Acad. Sci., USA*, **94**, 8314–8320.

Yanai, M., 1973: Determination of Bulk Properties of Cloud Clusters from the Large-Scale Budgets of Energy and Moisture. *J. Atmos. Sci.*, **30**, 674–701.

Yang, H. and R. T. Pierrehumbert, 1994: Production of Dry Air by Isentropic Mixing. *J. Atmos. Sci.*, **51**, 3437–3454.

Yang, H. and K. K. Tung, 1998: Water Vapor, Surface Temperature, and the Greenhouse Effect – A Statistical Analysis of Tropical-Mean Data. *J. of Climate*, **11**, 2686–2697.

Zhang, G. J. and N. A. McFarlane, 1995: Sensitivity of Climate Simulations to the Parameterization of Cumulus Convection in the Canadian Climate Centre General Circulation Model. *Atmos.-Ocean*, **33**, 407–446.

Index